Mon. Not. R. Astron. Soc. **305,** 259–296 (1999)

# The peculiar motions of early-type galaxies in two distant regions – II. The spectroscopic data

Gary Wegner,[1] Matthew Colless,[2] R. P. Saglia,[3] Robert K. McMahan, Jr,[4,5] Roger L. Davies,[6] David Burstein[7] and Glenn Baggley[6]

[1]*Department of Physics and Astronomy, 6127 Wilder Laboratory, Dartmouth College, Hanover, NH 03755-3528, USA*
[2]*Research School of Astronomy and Astrophysics, The Australian National University, Weston Creek, ACT 2611, Australia*
[3]*Universitäts-Sternwarte München, Scheinerstraße 1, D-81679 München, Germany*
[4]*Department of Physics and Astronomy, University of North Carolina, CB 3255 Phillips Hall, Chapel Hill, NC 27599-3255, USA*
[5]*PO Box 14026, McMahan Research Laboratories, 79 Alexander Drive, Research Triangle, NC 27709, USA*
[6]*Department of Physics, University of Durham, South Road, Durham DH1 3LE*
[7]*Department of Physics and Astronomy, Box 871054, Arizona State University, Tempe, AZ 85287-1504, USA*

Accepted 1998 November 26. Received 1998 September 23; in original form 1998 July 17

**ABSTRACT**

We present the spectroscopic data for the galaxies studied in the EFAR project, which is designed to measure the properties and peculiar motions of early-type galaxies in two distant regions. We have obtained 1319 spectra of 714 early-type galaxies over 33 observing runs on 10 different telescopes. We describe the observations and data reductions used to measure redshifts, velocity dispersions and the Mg$b$ and $Mg_2$ Lick linestrength indices. Detailed simulations and intercomparison of the large number of repeat observations lead to reliable error estimates for all quantities. The measurements from different observing runs are calibrated to a common zero-point or scale before being combined, yielding a total of 706 redshifts, 676 velocity dispersions, 676 Mg$b$ linestrengths and 582 $Mg_2$ linestrengths. The median estimated errors in the combined measurements are $\Delta cz = 20\,\mathrm{km\,s^{-1}}$, $\Delta\sigma/\sigma = 9.1$ per cent, $\Delta\mathrm{Mg}b/\mathrm{Mg}b = 7.2$ per cent and $\Delta\mathrm{Mg}_2 = 0.015$ mag. Comparison of our measurements with published data sets shows no systematic errors in the redshifts or velocity dispersions, and only small zero-point corrections to bring our linestrengths on to the standard Lick system. We have assigned galaxies to physical clusters by examining the line-of-sight velocity distributions based on EFAR and ZCAT redshifts, together with the projected distributions on the sky. We derive mean redshifts and velocity dispersions for these clusters, which will be used in estimating distances and peculiar velocities and to test for trends in the galaxy population with cluster mass. The spectroscopic parameters presented here for 706 galaxies combine high-quality data, uniform reduction and measurement procedures, and detailed error analysis. They form the largest single set of velocity dispersions and linestrengths for early-type galaxies published to date.

**Key words:** surveys – galaxies: clusters: general – galaxies: distances and redshifts – galaxies: elliptical and lenticular, cD – large-scale structure of Universe.

## 1 INTRODUCTION

We are measuring the peculiar motions of galaxy clusters in the Hercules–Corona Borealis (HCB) and Perseus–Pisces–Cetus (PPC) regions at distances between 6000 and 15 000 $\mathrm{km\,s^{-1}}$ using the global properties of elliptical galaxies. This study (the EFAR project) has as primary goals: (i) characterizing the intrinsic properties of elliptical galaxies in clusters by compiling a large and homogeneous sample with high-quality photometric and spectroscopic data; (ii) testing possible systematic errors, such as environmental dependence, in existing elliptical galaxy distance estimators; (iii) deriving improved distance estimators based on a more comprehensive understanding of the properties of ellipticals and how these are affected by the cluster environment; and (iv) determining the peculiar velocity field in regions that are dynamically independent of the mass distribution within $5000\,\mathrm{km\,s^{-1}}$ of our Galaxy in order to test whether the large-amplitude coherent flows seen locally are typical of bulk motions in the Universe.

The background and motivation of this work are discussed in

Paper I of this series (Wegner et al. 1996), which also describes in detail the choice of regions to study, the sample of clusters and groups, and the selection procedure and selection functions of the programme galaxies. In earlier papers we reported the photoelectric photometry for 352 programme galaxies which underpins the transformation of our CCD data to the standard $R$ magnitude system (Colless et al. 1993), and described our technique for correcting for the effects of seeing on our estimates of length-scales and surface brightnesses (Saglia et al. 1993). This paper (Paper II) describes the spectroscopic observations and gives redshifts, velocity dispersions and linestrength indices for the programme galaxies. The CCD imaging observations of these galaxies, and their photometric parameters, are described in Paper III (Saglia et al. 1997a), while descriptions of the profile fitting techniques used to determine these parameters (along with detailed simulations establishing the uncertainties and characterizing the systematic errors) are given in Paper IV (Saglia et al. 1997b). The Mg–$\sigma$ relation and its implications are discussed in Paper V (Colless et al. 1999). Subsequent papers in the series will explore other intrinsic properties of the galaxies and their dependence on environment, derive an optimal distance estimator, and discuss the peculiar motions of the clusters in each of our survey regions and their significance for models of the large-scale structure of the Universe.

The structure of the present paper is as follows. In Section 2 we describe the observations and reductions used in obtaining the 1319 spectra in our data set (1250 spectra for 666 programme galaxies, and 69 spectra for 48 calibration galaxies), and discuss the quality of the data. We explain the techniques by which redshifts, velocity dispersions and linestrength indices were estimated from the spectra in Section 3, including the various corrections applied to the raw values. In Section 4 we describe the method used to combine data from different runs and evaluate the internal precision of our results using the large number of repeat measurements in our data set. We then give the final values of the spectroscopic parameters for each galaxy in our sample: we have redshifts for 706 galaxies, dispersions and Mg$b$ linestrengths for 676 galaxies and $Mg_2$ linestrengths for 582 galaxies. We compare our results with previous studies in the literature to obtain external estimates of our random and systematic errors. In Section 5 we combine our redshifts with those from ZCAT in order to assign sample galaxies to physical clusters, and to estimate the mean redshifts and velocity dispersions of these clusters. Our conclusions are summarized in Section 6.

This paper presents the largest and most homogeneous sample of velocity dispersions and linestrengths for elliptical galaxies ever obtained. The precision of our measurements is sufficiently good to achieve the goal of measuring distances via the Fundamental Plane out to 15 000 km s$^{-1}$.

## 2 OBSERVATIONS

The spectroscopic observations for the EFAR project were obtained over a period of seven years from 1986 to 1993 in a total of 33 observing runs on 10 different telescopes. In this section we describe the spectroscopic setups, the observing procedures, the quality of the spectra and the data reduction techniques. Further detail on these points is given by Baggley (1996).

### 2.1 Spectroscopic setups

Table 1 gives the spectroscopic setup for each run, including the run number, date, telescope, spectrograph and detector, wavelength range, spectral dispersion (in Å pixel$^{-1}$), effective resolution (in km s$^{-1}$), effective aperture size and number of spectra taken in the run. Note that two runs (116 and 130) produced no useful data and are included in Table 1 only for completeness. Three runs utilized fibre spectrographs: runs 127 and 133 used Argus on the Cerro Tololo Inter-american Observatory (CTIO) 4-m, and run 131 used MEFOS on the European Southern Observatory (ESO) 3.6-m. All the other runs employed long-slit spectrographs, mostly on 2-m-class telescopes [Michigan–Dartmouth–MIT (MDM) Hiltner 2.4-m, Isaac Newton 2.5-m, Kitt Peak 2.1-m, Siding Spring 2.3-m, Calar Alto 2.2-m], although some 4-m-class telescopes were also used [Kitt Peak 4-m, William Herschel 4.2 m, the Multiple Mirror Telescope (MMT)].

The spectra from almost all runs span at least the wavelength range 5126–5603 Å, encompassing the Mg I $b$ 5174-Å band and the Fe I 5207- and 5269-Å features in the rest frame for galaxies over the sample redshift range $cz \approx 6000$–$15\,000$ km s$^{-1}$. The exceptions are the spectra from runs 115 and 131. Run 115 comprises eight spectra obtained at the WHT with the blue channel of the ISIS spectrograph which have a red wavelength limit of 4970 Å (i.e. including H$\beta$ but not Mg$b$). Since we have spectra for all these galaxies from other runs, we do *not* use the redshifts and dispersions from run 115. Run 131 comprises 128 spectra obtained at the ESO 3.6-m with the MEFOS fibre spectrograph to a red limit of 5468 Å, including Mg$b$ and Fe I 5207 Å over the redshift range of interest, but not Fe I 5269 Å beyond $cz \approx 11\,000$ km s$^{-1}$. For most of the runs the spectra also encompass H$\beta$, and several span the whole range from Ca I H+K 3933+3969 Å to Na I D 5892 Å.

The effective instrumental resolution of the spectra, $\sigma_i$, was measured from the autocorrelation of stellar template spectra (see Section 3.1 below), and ranged from 80 to 170 km s$^{-1}$, with a median value of 125 km s$^{-1}$. Both long-slit and circular entrance apertures were used. Slits were typically 1.7–2.0 arcsec wide and the spectra were extracted to the point where the galaxy fell to about 10 per cent of its peak value. Circular apertures (in the fibre spectrographs and the MMT Big Blue spectrograph) were between 1.9 and 2.6 arcsec in diameter. Further details of the observing setup for each telescope/instrument combination are given in Appendix A.

### 2.2 Observing procedures

The total integration times on programme galaxies varied considerably, depending on telescope aperture, observing conditions and the magnitude and surface brightness of the target (our programme galaxies have $R$-band total magnitudes in the range 10–16). On 2-m-class telescopes (with which the bulk of the spectroscopy was done), exposure times were usually in the range 30–60 min, with a median of 40 min; on 4-m-class telescopes, exposure times were generally 15–20 min (up to 60 min for the faintest galaxies) with single-object slit spectrographs, but 60 or 120 min with the fibre spectrographs [where the aim was high signal-to-noise ratio (S/N) and completeness]. Slit orientations were not generally aligned with galaxy axes. The nominal goal in all cases was to obtain around 500 photon Å$^{-1}$ at Mg$b$, corresponding to a S/N per 100 km s$^{-1}$ resolution element of about 30. In fact our spectra have a median of 370 photon Å$^{-1}$ at Mg$b$, corresponding to a S/N per 100 km s$^{-1}$ of 26 (see Section 2.4).

In each run several G8 to K5 giant stars with known heliocentric velocities were observed. These 'velocity standard stars' are used as spectral templates for determining redshifts and velocity dispersions. In observing these standards, care was taken to ensure that the illumination across the slit was uniform, in order both to remove

**Table 1.** The spectroscopic observing runs.

| Run # | Date | Telescope[a] | Spectrograph + grating | Detector | λλ (Å) | Δλ[b] (Å pixel$^{-1}$) | $\sigma_i$[c] (km s$^{-1}$) | Aperture[d] (arcsec) | $N$[e] |
|---|---|---|---|---|---|---|---|---|---|
| 101 | 86/12 | MG24 | MarkIIIa + 600B | GEC | 4912–6219 | 2.27 | 145 | 1.9×10% | 22 |
| 102 | 87/03 | MG24 | MarkIIIa + 600B | RCA | 4787–6360 | 3.10 | 145 | 1.9×10% | 58 |
| 103 | 87/05 | MG24 | MarkIIIa + 600B | RCA | 4809–6364 | 3.07 | 145 | 1.9×10% | 37 |
| 104 | 88/04 | MG24 | MarkIIIa + 600V | RCA | 5025–6500 | 2.90 | 125 | 1.9×10% | 12 |
| 105 | 88/06 | MG24 | MarkIIIa + 600V | RCA | 5055–6529 | 2.90 | 125 | 1.9×10% | 37 |
| 106 | 88/09 | MG24 | MarkIIIa + 600V | Thompson | 5041–6303 | 2.21 | 130 | 1.9×10% | 23 |
| 107 | 88/10 | MG24 | MarkIIIa + 600V | RCA | 5048–6522 | 2.90 | 130 | 1.9×10% | 27 |
| 108 | 88/07 | MMTB | BigBlue + 300B | Reticon | 3700–7200 | 1.14 | 135 | 2.5 | 10 |
| 109 | 88/11 | KP4M | RC + UV-Fast + 17B | TI2 | 4890–5738 | 1.07 | 100 | 2.0×3.9 | 104 |
| 110 | 88/11 | KP2M | GoldCam + #240 | TI5 | 4760–5879 | 1.52 | 105 | 2.0×3.9 | 72 |
| 111 | 88/11 | MMTB | BigBlue + 300B | Reticon | 3890–7500 | 1.34 | 135 | 2.5 | 20 |
| 112 | 89/04 | MG24 | MarkIIIb + 600V | RCA | 5066–6534 | 2.91 | 130 | 1.7×10% | 34 |
| 113 | 89/06 | MG24 | MarkIIIb + 600V | TI4849 | 5126–6393 | 2.18 | 150 | 2.4×10% | 23 |
| 114 | 89/06 | MMTB | BigBlue + 300B | Reticon | 3890–7500 | 1.34 | 135 | 2.5 | 12 |
| 115 | 89/08 | WHT4 | ISIS-Blue + R600B | CCD-IPCS | 4330–4970 | 0.45 | 095 | 2.0×3.9 | 8 |
| 116[f] | 89/10 | MMTR | RedChannel + 600B | TI | 4750–5950 | 1.50 | 125 | 1.5×10% | 7 |
| 117 | 89/10 | MG24 | MarkIIIb + 600V | Thompson | 5031–6300 | 2.21 | 130 | 1.7×10% | 61 |
| 118 | 89/11 | MG24 | MarkIIIb + 600V | RCA | 5018–6499 | 2.89 | 170 | 1.7×10% | 14 |
| 119 | 90/05 | MMTR | RedChannel + 600B | TI | 4750–5950 | 1.50 | 125 | 1.5×10% | 17 |
| 120 | 90/10 | IN25 | IDS + 235mm + R632V | GEC6 | 4806–5606 | 1.46 | 100 | 1.9×7.2 | 40 |
| 121 | 91/05 | IN25 | IDS + 235mm + R632V | GEC3 | 4806–5603 | 1.46 | 100 | 1.9×7.2 | 87 |
| 122 | 91/10 | MG24 | MarkIIIb + 600V | Thompson | 5018–6278 | 2.20 | 125 | 1.7×10% | 43 |
| 123 | 91/11 | IN25 | IDS + 235mm + R632V | GEC3 | 4806–5603 | 1.46 | 100 | 1.9×7.2 | 29 |
| 124 | 92/01 | MG24 | MarkIIIb + 600V | Thompson | 5038–6267 | 2.15 | 125 | 1.7×10% | 35 |
| 125 | 92/06 | MG24 | MarkIIIb + 600V | Loral | 4358–7033 | 1.31 | 125 | 1.7×10% | 57 |
| 126 | 92/06 | CA22 | B&C spec + #7 | TEK6 | 4800–6150 | 1.40 | 100 | 5.0×4.2 | 39 |
| 127[g] | 92/09 | CT4M | Argus + KPGL#3 | Reticon II | 3877–6493 | 2.19 | 145 | 1.9 | 199 |
| 128 | 93/05 | MG24 | MarkIIIb + 600V | Loral | 5090–7050 | 1.40 | 105 | 1.7×10% | 24 |
| 129 | 93/06 | MG24 | MarkIIIb + 600V | TEK | 4358–6717 | 2.31 | 135 | 1.7×10% | 3 |
| 130[f] | 93/06 | SS23 | DBS-blue + 600B | PCA | 5015–5555 | 0.80 | 085 | 2.0×10% | 0 |
| 131[g] | 93/10 | ES36 | MEFOS + B&C + #26 | TEK512CB | 4850–5468 | 1.22 | 105 | 2.6 | 128 |
| 132 | 93/10 | SS23 | DBS-blue + 600B | Loral | 4820–5910 | 1.10 | 080 | 2.0×10% | 14 |
| 133[g] | 93/10 | CT4M | Argus + KPGL#3 | Reticon II | 3879–6485 | 2.19 | 145 | 1.9 | 193 |

[a] Telescopes: MG24 = MDM 2.4-m; KP4M/KP2M = KPNO 4-m/2.1-m; WHT4 = William Herschel 4.2-m (La Palma Observatory); IN25 = Isaac Newton 2.5-m (LPO); MMTB/MMTR = MMT (blue/red); CA22 = Calar Alto 2.2-m; CT4M = Cerro Tololo 4-m; SS23 = Siding Spring 2.3-m; ES36 = ESO 3.6-m.
[b] Spectral dispersion in Å pixel$^{-1}$.
[c] Instrumental resolution ($\sigma$, not FWHM) in km s$^{-1}$, as determined from the cross-correlation analysis calibration curves (see Section 3.1).
[d] The aperture over which the galaxy spectrum was extracted: diameter for circular apertures and fibres, width × length for rectangular slits (10 per cent means that the spectrum was extracted out to the point where the luminosity had fallen to 10 per cent of its peak value).
[e] The number of spectra taken in the run.
[f] These runs produced no useful data.
[g] These runs used fibre spectrographs.

redshift zero-point errors and to mimic the illumination produced by a galaxy, thereby minimizing systematic errors in velocity dispersion estimates. This was achieved in various ways: by defocusing the telescope slightly, by moving the star back and forth across the slit several times, or by trailing it up and down the slit. Such procedures were not necessary for standards obtained with fibre spectrographs, as internal reflections in the fibres ensure even illumination of the spectrograph for all sources. Very high S/Ns (typically >10 000 photon Å$^{-1}$) were obtained in order that the stellar templates did not contribute to the noise in the subsequent analysis.

The normal calibration exposures were also obtained: bias frames, flat-fields (using continuum lamps internal to the spectrographs or illuminating the dome) and spectra of wavelength calibration lamps before and/or after each galaxy or star exposure. In general we did not make use of spectrophotometric standards, as fluxed spectra were not necessary and we wished to minimize overheads as much as possible.

The calibration procedures were slightly different for the three large data sets taken using fibre-fed spectrographs at CTIO (runs 127 and 133) and ESO (run 131). Because of the need to calibrate the relative throughput of the fibres in order to perform sky subtraction, fibre observations always included several twilight sky flat-field exposures. Each velocity standard star was observed through several fibres by moving the fibres sequentially to accept the starlight.

### 2.3 Reductions

The reductions of both the long-slit and fibre observations followed standard procedures as implemented in the IRAF, MIDAS and Starlink FIGARO software packages. We briefly summarize the main steps in

the reduction of our long-slit and fibre data below; further details can be found in Baggley (1996).

The first stage of the reductions, common to all observations, was to remove the CCD bias using a series of bias frames taken at the start or end of the night. These frames were median-filtered and the result, scaled to the mean level of the CCD overscan strip, was subtracted from each frame in order to remove both the spatial structure in the bias pedestal and temporal variations in its overall level. We also took long dark exposures to check for dark current, but in no case did it prove significant. Subsequent reductions differed somewhat for long-slit and fibre observations.

For long-slit data, the next step was the removal of pixel-to-pixel sensitivity variations in the CCD by dividing by a sensitivity map. This map was produced by median-filtering the flat-field exposures (of an internal calibration lamp or dome lamp) and dividing this by a smoothed version of itself (achieved by direct smoothing or two-dimensional surface fitting) in order to remove illumination variations in the 'flat'-field. If necessary (because of a long exposure time or a susceptible CCD), cosmic ray events were identified and interpolated over in the two-dimensional image using either algorithmic or manual methods (or both).

The transformation between wavelength and pixel position in long-slit data was mapped using the emission lines in the comparison lamp spectra. The typical precision achieved in wavelength calibration, as indicated by the residuals of the fit to the calibration line positions, was $\lesssim 0.1$ pixel, corresponding to 0.1–0.3 Å or 5–15 km s$^{-1}$, depending on the spectrograph setup (see Table 1). The spectra were then rebinned into equal intervals of $\log\lambda$ so that each pixel corresponded to a fixed velocity interval, $\Delta v \equiv c\Delta z = c(10^{\Delta \log \lambda} - 1)$, chosen to preserve the full velocity resolution of the data.

The final steps in obtaining long-slit spectra are sky subtraction and extraction. The sky level was measured from two or more regions along the slit sufficiently far from the target object to be uncontaminated by its light. To account for variations in transmission along the slit, the sky under the object was interpolated using a low-order curve fitted to the slit illumination profile. A galaxy spectrum was then extracted by summing along the profile, usually over the range where the luminosity of the object was greater than $\sim$10 per cent of its peak value, but sometimes over a fixed width in arcsec (see Table 1). Standard star spectra were simply summed over the range along the slit that they had been trailed or defocused to cover.

For the fibre runs the individual object and sky spectra were extracted first, using a centroid-following algorithm to map the position of the spectrum along the CCD. The extraction algorithm fitted the spatial profile of the fibre, in order to remove cosmic ray events and pixel defects, and then performed a weighted sum over this fit out to the points where the flux fell to $\sim$5 per cent of the peak value. Next, the dome illumination flat-field spectra were median-combined and a sensitivity map for each fibre constructed by dividing the flat-field spectrum of each fibre by the average over all fibres and normalizing the mean of the result to unity. The pixel-to-pixel variations in the CCD response were then removed by dividing all other spectra from that fibre by this sensitivity map. Wavelength calibration was accomplished using the extracted comparison lamp spectra, giving similar precision to the long-slit calibrations, and the object spectra were rebinned to a $\log\lambda$ scale. Using the total counts through each fibre from the twilight sky flat-field to give the relative throughputs, the several sky spectra obtained in each fibre exposure were median-combined (after manually removing 'sky' fibres which were inadvertently placed on faint objects). The resulting high-S/N sky spectrum, suitably normalized to the throughput of each fibre, was then subtracted from each galaxy or standard star spectrum.

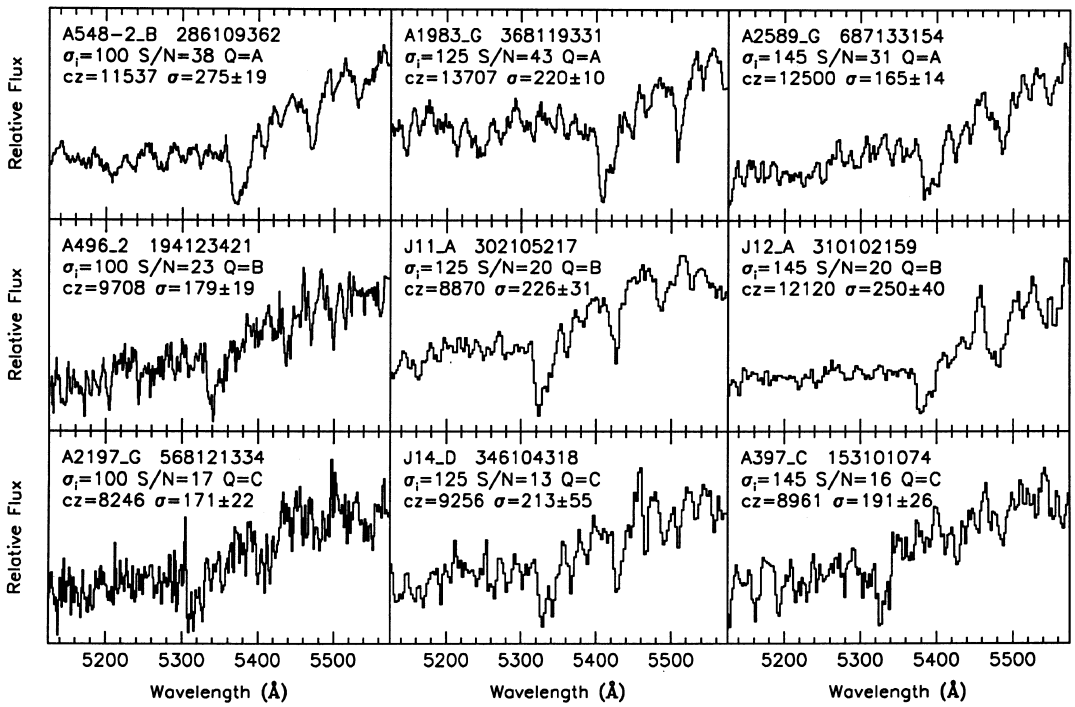


**Figure 1.** Examples of spectra covering a range of quality classes and instrumental resolutions: the top, middle and bottom rows are spectra with quality classes A, B and C respectively; the left, central and right columns are spectra with resolutions 100, 125 and 145 km s$^{-1}$ respectively. The label for each spectrum gives the galaxy name, the GINRUNSEQ spectrum identifier, the instrumental resolution, the S/N and quality class of the spectrum, the redshift, the dispersion and its estimated error. Note that the panels show relative flux and have a false zero for viewing convenience.

The final step in the reductions for both long-slit and fibre data was manually to clean all the one-dimensional spectra of remaining cosmic ray events or residual sky lines (usually only the 5577-Å line) by linearly interpolating over affected wavelengths.

### 2.4 Spectrum quality

We have two methods for characterizing the quality of our spectra. One is a classification of the spectra into five quality classes, based on our experience in reducing and analysing such data. Classes A and B indicate that both the redshift and the velocity dispersion are reliable (with class A giving smaller errors than class B); class C spectra have reliable redshifts and marginally reliable dispersions; class D spectra have marginally reliable redshifts but unreliable dispersions; class E spectra have neither redshifts nor dispersions. The second method is based on the S/N per $100\,\mathrm{km\,s^{-1}}$ bin, estimated approximately from the mean flux over the rest-frame wavelength range used to determine the redshifts and dispersions (see Section 3.1) under the assumption that the spectrum is shot-noise-dominated. These two measures of spectral quality are complementary: the S/N estimate is objective but cannot take into account qualitative problems which are readily incorporated in the subjective classifications. Fig. 1 shows example spectra covering a range of quality classes and instrumental resolutions.

Fig. 2 shows the S/N distribution for the whole sample and for each quality class individually, and gives the total number of objects, the fraction of the sample and the median S/N in each class. For the whole sample, 39 per cent of the spectra have S/N > 30, 70 per cent have S/N > 20, and 96 per cent have S/N > 10. The two quality measures are clearly correlated, in the sense that better-classed spectra tend to have higher S/N. However there is also considerable overlap in the S/N range spanned by the different classes. This overlap has various sources: (i) factors other than S/N that affect the quality of the redshift and dispersion estimates, notably the available rest-frame spectral range (which depends on both the spectrograph setup and the redshift of the target) and whether the object has emission lines; (ii) errors in estimating the S/N [e.g. owing to sky subtraction errors, the neglect of the sky contribution in computing the S/N for fainter galaxies, or uncertainties in the CCD gain (affecting the conversion from counts to photons)]; (iii) subjective uncertainties in the quality classification, particularly in determining the reliability of dispersion estimates (i.e. between classes B and C). Both ways of determining spectral quality are therefore needed in order to estimate the

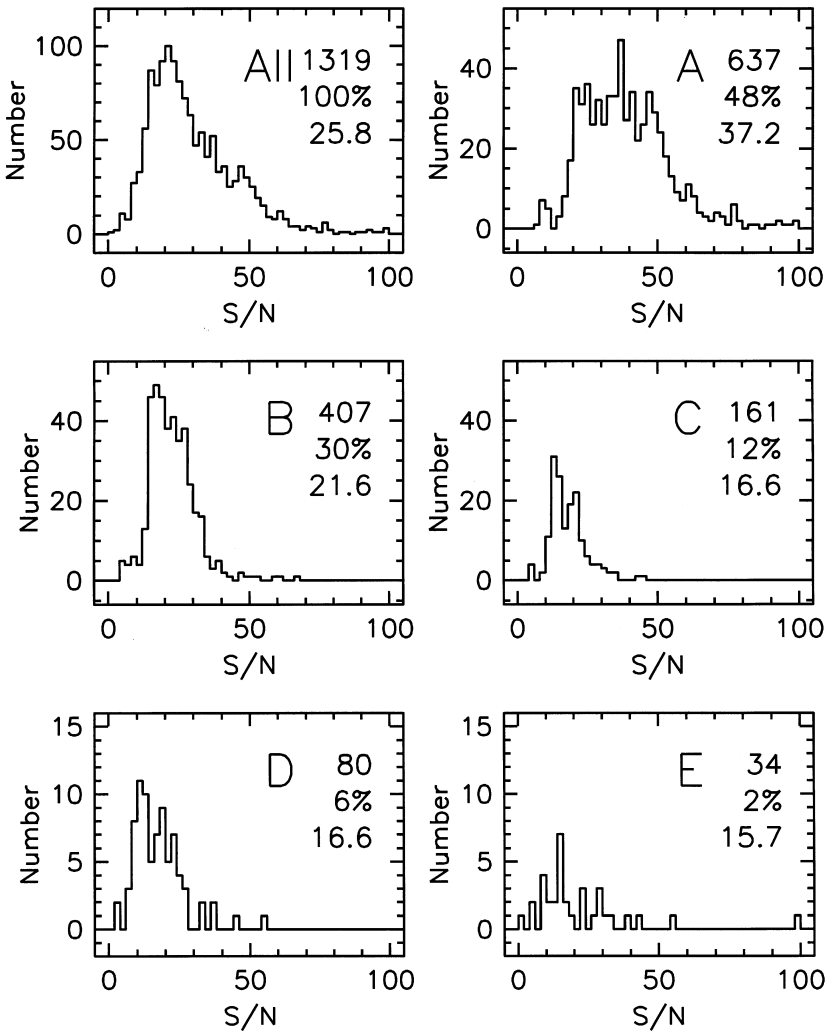


**Figure 2.** The distribution of S/N with quality class. For each class the panels give the total number of spectra, the percentage of the whole sample and the median S/N.

reliability and precision of the spectroscopic parameters that we measure.

## 3 ANALYSIS

### 3.1 Redshifts and dispersions

We derived redshifts and velocity dispersions from our spectra using the FXCOR utility in IRAF, which is based on the cross-correlation method of Tonry & Davis (1979). We preferred this straightforward and robust method to more elaborate techniques since it is well-suited to the relatively modest S/N of our spectra. We used a two-step procedure, obtaining an initial estimate of the redshift using the whole available spectrum and then using a fixed rest-frame wavelength range for the final estimates of redshift and velocity dispersion. The procedure was applied in a completely uniform manner to all the spectra in our sample as far as differences in wavelength range and resolution would allow.

The first step in the cross-correlation analysis is to fit and subtract the continuum of each spectrum in order to avoid the numerical difficulties associated with a dominant low-frequency spike in the Fourier transform. In the first pass through FXCOR the continuum shape was fitted with a cubic spline, with the number of segments along the spectrum chosen so that each segment corresponded to about 8000 km s$^{-1}$. Each iteration of the fit excluded points more than $1.5\sigma$ below or $3\sigma$ above the previous fit. In this way we achieved a good continuum fit without following broad spectral features. We then apodized 10 per cent of the spectrum at each end with a cosine bell before padding the spectrum to 2048 pixels with zeros.

This continuum-subtracted, apodized spectrum was then Fourier transformed and a standard 'ramp' filter applied. This filter is described by four wavenumbers $(k_1, k_2, k_3, k_4)$, rising linearly from 0 to 1 between $k_1$ and $k_2$ and then falling linearly from 1 to 0 between $k_3$ and $k_4$. In the first pass these wavenumbers were chosen to be $k_1 = 4$–$8$ and $k_2 = 9$–$12$ (tailored to remove residual power from the continuum without affecting broad spectral features), and $k_3 = N_{\rm pix}/3$ and $k_4 = N_{\rm pix}/2$ ($N_{\rm pix}$ is the number of pixels in original spectrum before it is padded to 2048 pixels; these choices attenuate high-frequency noise and eliminate power beyond the Nyquist limit at $N_{\rm pix}/2$). The same procedures were also applied to the spectrum of the stellar velocity standard to be used as a template. The cross-correlation of the galaxy and stellar template was then computed, and the top 90 per cent of the highest cross-correlation peak fitted with a Gaussian in order to obtain a redshift estimate.

This procedure was repeated for every template from that run, and the redshifts corrected to the heliocentric frame. Offsets in the velocity zero-point between templates, measured as the mean difference in the redshifts measured with different templates for all the galaxies in the run, were typically found to be $\lesssim$30 km s$^{-1}$. These were brought into relative agreement within each run by choosing the best-observed K0 template as defining the fiducial velocity zero-point. Applying these offsets brought the galaxy redshifts estimated from different templates into agreement to within $\lesssim$3 km s$^{-1}$. (The removal of run-to-run velocity offsets is described below.) The mean over all templates then gave the initial redshift estimate for the galaxy.

This initial redshift was then used to determine the wavelength range corresponding to the rest-frame range $\lambda_{\rm min} = 4770$ Å to $\lambda_{\rm max} = 5770$ Å. This range was chosen for use in the second pass through FXCOR because: (i) it contains the Mg I *b* 5174-Å band, H$\beta$ 4861 Å and the Fe I 5207- and 5269-Å lines, but excludes the Na I D line at 5892 Å, which gives larger velocity dispersions than the lines in the region of Mg*b* (Faber & Jackson 1976); (ii) for redshifts up to our sample limit of $cz = 15\,000$ km s$^{-1}$ this rest-frame wavelength range is included in the great majority of our spectra. The input for the second pass was thus the available spectrum within the range corresponding to rest-frame 4770–5770 Å. All but two of our runs cover the rest frame out to at least 5330 Å for $cz = 15\,000$ km s$^{-1}$; the exceptions are run 115 (which is not used for measuring dispersions) and run 131 (which reaches rest-frame 5207 Å).

In the second pass through FXCOR we employed only minimal continuum subtraction based on a one- or two-segment cubic spline fit, preferring the better control over continuum suppression afforded by more stringent filtering at low wavenumbers. After considerable experimentation and simulation, we found that the best filter for recovering velocity dispersions was a ramp with the same $k_3$ and $k_4$ values as in the first pass, but with $k_2 = 0.01(N_{\rm max} - N_{\rm min})$, where $N_{\rm min}$ and $N_{\rm max}$ are the pixels corresponding to $\lambda_{\rm min}$ and $\lambda_{\rm max}$, and $k_1 = 0.75k_2$. Again, the top 90 per cent of the highest cross-correlation peak was fitted with a Gaussian. The position of this peak, corrected for the motion of the template star and the heliocentric motion of the Earth relative to both the template and the galaxy, gave the final redshift estimate.

The velocity dispersion of the galaxy, $\sigma_{\rm g}$, is in principle related to the dispersion of the Gaussian fitted to the cross-correlation peak, $\sigma_{\rm x}$, by $\sigma_{\rm x}^2 = \sigma_{\rm g}^2 + 2\sigma_{\rm i}^2$ (where $\sigma_{\rm i}$ is the instrumental resolution: Tonry & Davis 1979). In practice this relationship needs to be calibrated empirically because of the imperfect match between the spectra of a broadened stellar template and a galaxy and the effects of the filter applied to both spectra. The calibration relation between $\sigma_{\rm x}$ and $\sigma_{\rm g}$ for a typical case is shown in Fig. 3 (see the caption for more details). We estimate the instrumental resolution for a given run from the mean value of the calibration curve intercepts for all the templates in the run ($\sigma_{\rm i} \approx \sigma_{\rm x}/\sqrt{2}$ when $\sigma_{\rm g} = 0$); these are the values listed in Table 1.

The values of heliocentric radial velocity and velocity dispersion were determined in this second pass through FXCOR for each galaxy spectrum using all the templates in the same run. The final step is then to combine the redshift and dispersion estimates from each template, as summarized below.

For the redshifts the steps involved were as follows. (i) Cases in which the ratio of cross-correlation function peak height to noise [the *R* parameter defined by Tonry & Davis (1979)] was less than 2 were rejected, as were cases that differed from the median by more than a few hundred km s$^{-1}$. (ii) The mean offset between the redshifts from a fiducial K0 template and each other template was used to shift all the redshifts from the other template to the velocity zero-point of the fiducial. These offsets were typically $\lesssim$ 50 km s$^{-1}$. (iii) A mean redshift for each galaxy was then computed from all the unrejected cases using two-pass $2\sigma$ clipping. (iv) Any template that gave consistently discrepant results was rejected and the entire procedure repeated. The scatter in the redshift estimates from different templates after this procedure was typically a few km s$^{-1}$.

A very similar procedure was followed in combining velocity dispersions, except that a scalefactor rather than an offset was applied between templates. (i) Cases with $R < 4$ were rejected. (ii) The mean ratio between the dispersions from a fiducial K0 template and each other template was used to scale all the dispersions from the other template to the dispersion scale of the fiducial. These dispersion scales differed by less than 5 per cent for 90 per cent of the templates. (iii) A mean dispersion for each galaxy was then computed from all the unrejected cases using two-pass $2\sigma$ clipping. (iv) Any template with a scale differing by more than 10 per cent from the mean was rejected as being a poor match to the

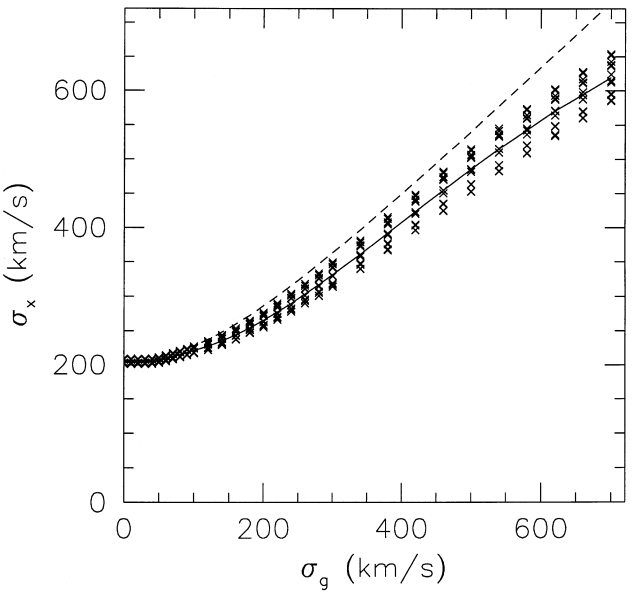


**Figure 3.** A typical calibration curve showing the relation between the width of the cross-correlation peak, $\sigma_x$, and the true velocity dispersion of the galaxy, $\sigma_g$. The crosses are the individual calibrations obtained by broadening each of the other templates in the run and cross-correlating with the template being calibrated. The solid curve is the calibration curve used, a series of linear segments joining the median value of $\sigma_x$ at each calibrated value of $\sigma_g$. The dashed curve is the theoretical relation when no filtering is applied, $\sigma_x^2 = \sigma_g^2 + 2\sigma_i^2$, where $\sigma_i$ is the instrumental resolution, in this case $145\,\mathrm{km\,s^{-1}}$. Note that the calibration curve flattens for $\sigma_g < \sigma_i$, indicating that the true dispersion becomes increasingly difficult to recover as it drops below the instrumental resolution.

programme galaxies, and the entire procedure was then repeated. (Note that no significant correlation was found between scalefactor and spectral type over the range G8 to K5 spanned by our templates.) The scatter in the dispersion estimates from different templates after this procedure was typically 3–4 per cent.

Two corrections need to be applied to the velocity dispersions before they are fully calibrated: (i) an aperture correction to account for different effective apertures sampling different parts of the galaxy velocity dispersion profile; and (ii) a run correction to remove systematic scale errors between different observing setups. The latter type of correction is also applied to the redshifts to give them a common zero-point. These two corrections are discussed below in Sections 3.4 and 3.5 respectively.

### 3.2 Linestrength indices

Once redshifts and velocity dispersions were determined, linestrength indices could also be measured using the prescription given by González (1993). This is a refinement of the original 'Lick' system in which a standard set of bands was defined for measuring linestrength indices for 11 features in the spectra of spheroidal systems (Burstein et al. 1984). González (1993), Worthey (1993) and Worthey et al. (1994) describe how this system has been updated and expanded to a set of 21 indices. Here we measure both the Mg*b* and $Mg_2$ indices.

The feature bandpass for Mg*b* index is 5160.1–5192.6 Å, encompassing the Mg I triplet with components at 5166.6, 5172.0 and 5183.2 Å. The continuum on either side of the absorption feature is defined in bands covering 5142.6–5161.4 and 5191.4–5206.4 Å. Mg*b* is an *atomic* index, and so is defined as the equivalent width of the feature in ångstroms,

$$\mathrm{Mg}b = \int \left[1 - \frac{S(\lambda)}{C(\lambda)}\right] \mathrm{d}\lambda, \qquad (1)$$

where the integral is over the feature bandpass, $S(\lambda)$ is the object spectrum and $C(\lambda)$ is the linear pseudo-continuum defined by interpolating between two continuum estimates, taken at the midpoints of the blue and red continuum bands to be the mean values of the observed spectrum in those bands.

Closely related to Mg*b* is the $Mg_2$ index, for which the feature bandpass is 5154.1–5196.6 Å and the continuum bands are 4895.1–4957.6 and 5301.1–5366.1 Å. This index measures both the Mg I atomic absorption and the broader MgH molecular absorption feature. $Mg_2$ is a *molecular* index, and so is defined as the mean ratio of flux to local continuum in magnitudes,

$$\mathrm{Mg2} = -2.5 \log_{10} \left[ \frac{\int S(\lambda)/C(\lambda)\,\mathrm{d}\lambda}{\Delta\lambda} \right], \qquad (2)$$

where the integral is over the $Mg_2$ feature bandpass, $\Delta\lambda = 42.5$ Å is the width of that bandpass, and the pseudo-continuum is interpolated from the $Mg_2$ continuum bands.

In fact we will often find it convenient to express the Mg*b* index in magnitudes rather than as an equivalent width. By analogy with the $Mg_2$ index, we therefore define Mg$b'$ to be

$$\mathrm{Mg}b' = -2.5 \log_{10}\left(1 - \frac{\mathrm{Mgb}}{\Delta\lambda}\right), \qquad (3)$$

where in this case $\Delta\lambda = 32.5$ Å, the width of the Mg*b* feature bandpass.

In passing it should be noted that a different definition of linestrength indices has sometimes been used (e.g. Worthey 1994, equations 4 and 5), in which the integral of the ratio of the object spectrum and the continuum in equations (1) and (2) is replaced by the ratio of the integrals. This alternative definition has merits (such as simplifying the error properties of measured indices), but it is not mathematically equivalent to the standard definition. In practice, however, the two definitions generally give linestrengths with negligibly different numerical values.

It is usual in studies of this sort to employ the $Mg_2$ index as the main indicator of metallicity and star formation history. However, we find it useful for operational reasons also to measure the Mg*b* index. One problem is that the limited wavelength coverage of the spectra from some runs means that in a number of cases we cannot measure the $Mg_2$ index (requiring as it does a wider wavelength range), although we can measure the Mg*b* index. We obtain Mg*b* for 676 objects (with 299 having repeat measurements) and $Mg_2$ for 582 objects (with 206 having repeat measurements). Another problem with $Mg_2$ is that the widely separated continuum bands make it more susceptible than Mg*b* to variations in the non-linear continuum shape of our unfluxed spectra, which result from using a variety of different instruments and observing galaxies over a wide range in redshift. We therefore present measurements of both Mg*b* and $Mg_2$: the former because it is better determined and available for more sample galaxies; the latter for comparison with previous work. As previously demonstrated (Gorgas, Efstathiou & Salamanca 1990; Jørgensen 1997) and confirmed here, Mg*b* and $Mg_2$ are strongly correlated, and so can to some extent be used interchangeably.

Several corrections must be applied to obtain a linestrength measurement that is calibrated to the standard Lick system. The

first correction allows for the fact that the measured linestrength depends on the instrumental resolution. Since all our spectra were obtained at higher resolution than the spectra on which the Lick system was defined, we simply convolve our spectra with a Gaussian of dispersion $(\sigma^2_{\rm Lick} - \sigma^2_{\rm i})^{1/2}$ in order to broaden our instrumental resolution $\sigma_{\rm i}$ (see Table 1) to the Lick resolution of 200 km s$^{-1}$.

The second correction allows for the fact that the measured linestrength depends on the internal velocity dispersion of the galaxy – a galaxy with high enough velocity dispersion $\sigma_{\rm g}$ will have features broadened to the point that they extend outside their index bandpasses, and so their linestrengths will be underestimated. Moreover, if an absorption feature is broadened into the neighbouring continuum bands then the estimated continuum will be depressed and the linestrength will be further reduced. The '$\sigma$-correction' needed to calibrate out this effect can be obtained either by measuring linestrength as a function of velocity broadening for a set of suitable stellar spectra (such as the templates obtained for measuring redshifts and dispersions) or by modelling the feature in question.

Although most previous studies have adopted the former approach, we prefer to use a model to calibrate our indices, since we observe a dependence of the Mg*b* profile shape on $\sigma$ that is not taken into account by simply broadening stellar templates. Our simple model assumes Mg*b* to be composed of three Gaussians centred on the three Mg I lines at $\lambda_{\rm b} = 5166.6$ Å, $\lambda_{\rm c} = 5172.0$ Å and $\lambda_{\rm r} = 5183.2$ Å with corresponding relative strengths varying linearly with dispersion from 1.0 : 1.0 : 1.0 at $\sigma = 100$ km s$^{-1}$ to 0.2 : 1.0 : 0.7 at $\sigma = 300$ km s$^{-1}$. This dependence on dispersion is empirically determined and approximate (the relative strengths of the individual lines are not tightly constrained), but it does significantly improve the profile fits compared with assuming any fixed set of relative weights. Such variation of the Mg*b* profile shape reflects changes, as a function of velocity dispersion, in the stellar population mix and relative abundances (particularly of Mg, C, Fe and Cr), which each affect the profile in complex ways (Tripicco & Bell 1995).

Using the estimated value of the index to normalize the model profile and the effective dispersion $(\sigma^2_{\rm g} + \sigma^2_{\rm Lick})^{1/2}$ to give the broadening, we can estimate both the profile flux that is broadened out of the feature bandpass and the resulting depression of the continuum. Correcting for both these effects gives an improved estimate for the linestrength. Iterating leads rapidly to convergence and an accurate $\sigma$-correction for the Mg*b* and $\rm Mg_2$ indices. We find that the Mg*b* $\sigma$-correction is typically +4 per cent at 100 km s$^{-1}$ and increases approximately linearly to +16 per cent at 400 km s$^{-1}$; the $\rm Mg_2$ $\sigma$-correction is typically 0.000 mag up to 200 km s$^{-1}$ and increases approximately linearly to 0.004 mag at 400 km s$^{-1}$.

Note that the usual method of determining the $\sigma$-correction by broadening standard stars ignores the dependence of profile shape on changes in the stellar population mix as a function of luminosity or velocity dispersion. Our tests indicate that, by doing so, the usual method tends to overestimate Mg*b* for galaxies with large dispersions: by 2 per cent at 200 km s$^{-1}$, 6 per cent at 300 km s$^{-1}$ and 14 per cent at 400 km s$^{-1}$. The two methods give essentially identical results for $\rm Mg_2$, since it has much smaller $\sigma$-corrections owing to its wider feature bandpass and well-separated continuum bands.

The other corrections that need to be applied to the linestrength estimates are: (i) an aperture correction to account for different effective apertures sampling different parts of the galaxy (Section 3.4); (ii) a run correction to remove systematic scale errors between different observing setups (Section 3.5); and (iii) an overall calibration to the Lick system determined by comparisons with literature data (Section 4.3).

### 3.3 Error estimates

Error estimates for our redshifts, velocity dispersions and linestrengths come from detailed Monte Carlo simulations of the measurement process for each observing run. By calibrating the errors estimated from these simulations against the rms errors obtained from the repeat measurements that are available for many of the objects (see Section 3.6), we can obtain precise and reliable error estimates for each measurement of every object in our sample.

The procedure for estimating the uncertainties in our redshifts and velocity dispersions was as follows. For each stellar template in each observing run, we constructed a grid of simulated spectra with Gaussian broadenings of 100–300 km s$^{-1}$ in 20 km s$^{-1}$ steps and continuum counts corresponding to S/N ratios of 10–90 in steps of 10. For each spectrum in this grid we generated 16 realizations assuming Poisson noise. These simulated spectra were then cross-correlated against all the other templates from the run in order to derive redshifts and velocity dispersions in the standard manner. The simulations do not account for spectral mismatch between the galaxy spectra and the stellar templates, but for well-chosen templates this effect is only significant at higher S/N than is typically found in our data.

Fig. 4 shows the random error in redshift and the systematic and random errors in dispersion as functions of input dispersion and S/N for four of the larger runs. The systematic errors in redshift are not shown as they are negligibly small ($\sim$1 km s$^{-1}$), although the simulations do not include possible zero-point errors. The systematic errors in dispersion are generally small (a few per cent or less) for S/N > 20, but become rapidly larger at lower S/N. The random errors in redshift increase for lower S/N and higher dispersion, while the random errors in dispersion increase for lower S/N but have a broad minimum at around twice the instrumental dispersion. These curves have the general form predicted for the random errors from the cross-correlation method (Tonry & Davis 1979; Colless 1987).

Given the dispersion and S/N measured for a spectrum, we interpolated the error estimates from the simulation for that particular observing run to obtain the systematic and random errors in each measured quantity. We used the results of these simulations to correct the systematic errors in the velocity dispersions and to estimate the uncertainties in individual measurements of redshift and dispersion. For quality class D measurements of redshifts, where the spectra are too poor to estimate a dispersion and hence a reliable redshift error, we take a conservative redshift error of 50 km s$^{-1}$.

The linestrength error estimates were obtained by generating 50 Monte Carlo realizations of the object spectrum with Poisson noise appropriate to the S/N level of the spectrum. The Mg*b* and $\rm Mg_2$ linestrengths were then measured for each of these realizations and the error estimated as the rms error of these measurements about the observed value. The error estimate obtained in this fashion thus takes into account the noise level of the spectrum, but does not account for errors in the linestrength owing to errors in the redshift and dispersion estimates, nor for systematic run-to-run differences in the underlying continuum shape.

The estimated errors in the spectroscopic parameters are compared with, and calibrated to, the rms errors derived from repeat observations in Section 3.6.

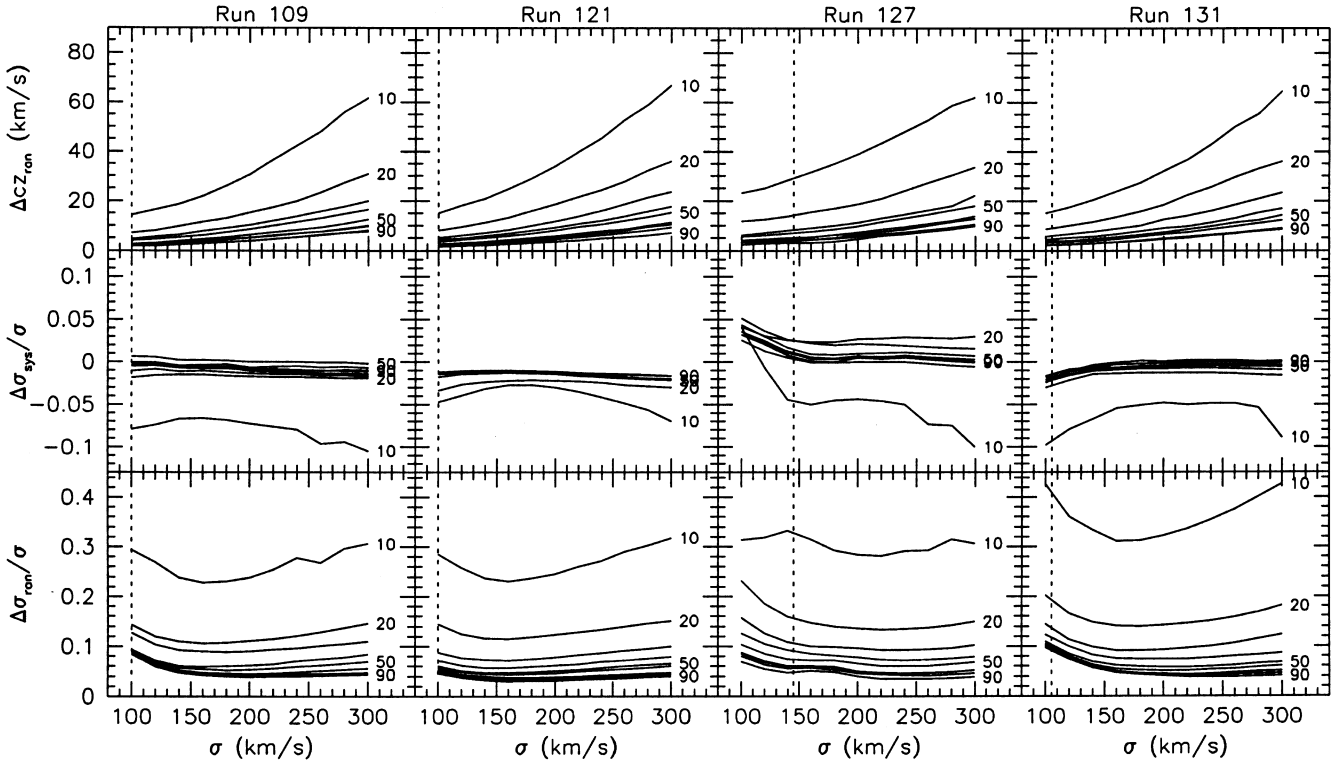


**Figure 4.** Redshift and dispersion errors as functions of input dispersion and S/N (labelling the curves) from the simulations of four of the larger runs. The top panels show the random error in the redshift, and the centre and bottom panels show the systematic and random errors in the dispersion. The vertical dotted lines indicate the instrumental dispersion of each run.

### 3.4 Aperture corrections

The velocity dispersion measured for a galaxy is the luminosity-weighted velocity dispersion integrated over the region of the galaxy covered by the spectrograph aperture. It therefore depends on: (i) the velocity dispersion profile; (ii) the luminosity profile; (iii) the distance of the galaxy; (iv) the size and shape of the spectrograph aperture; and (v) the seeing in which the observations were made. In order to intercompare dispersion measurements it is therefore necessary to convert them to a standard scale. The 'aperture correction' that this requires has often been neglected because it depends in a complex manner on a variety of quantities, some of which are poorly known. The neglect of such corrections may account in part for the difficulties often found in reconciling dispersion measurements from different sources.

The aperture correction applied by Davies et al. (1987) was derived by measuring dispersions for a set of nearby galaxies through apertures of $4\times4$ arcsec$^2$ and $16\times16$ arcsec$^2$. In this way they used their nearby galaxies to define the velocity dispersion profile and obtained a relation between the corrected value, $\sigma_{\rm cor}$, and the observed one, $\sigma_{\rm obs}$. This turned out to be an approximately linear relation amounting to a 5 per cent correction over the distance range between Virgo and Coma.

More recently Jørgensen, Franx & Kjærgaard (1995) have derived an aperture correction from kinematic models based on data in the literature. Published photometry and kinematics for 51 galaxies were used to construct two-dimensional models of the surface brightness, velocity dispersion, and rotational velocity projected on the sky. They found that the position angle only gave rise to 0.5 per cent variations in the derived dispersions and could thus be ignored. They converted rectangular apertures into an 'equivalent circular aperture' of radius $r_{\rm ap}$ which the models predicted would give the same dispersion as the rectangular slit. They found that to an accuracy of 4 per cent one could take $r_{\rm ap} = 1.025(xy/\pi)^{1/2}$, where $x$ and $y$ are the width and length of the slit.

From their models they then calculated the correction factor from the observed dispersion to the dispersion in some standard aperture. For a standard *metric* aperture, they found this aperture correction to be well approximated by a power law of the form

$$\frac{\sigma_{\rm cor}}{\sigma_{\rm obs}} = \left[\left(\frac{r_{\rm ap}}{r_0}\right)\left(\frac{cz}{cz_0}\right)\right]^{0.04}, \qquad (4)$$

where $\sigma_{\rm obs}$ and $\sigma_{\rm cor}$ are the observed and corrected dispersions, $r_0$ is a standard aperture radius, defined to be 1.7 arcsec, and $cz_0$ is a standard redshift, defined as the redshift of Coma. The standard metric aperture is thus $0.54\,h^{-1}$ kpc in radius. Alternatively, one can correct to a standard *relative* aperture (defined to be $R_{\rm e}/8$) using the same power-law relation,

$$\frac{\sigma_{\rm cor}}{\sigma_{\rm obs}} = \left(\frac{r_{\rm ap}}{R_{\rm e}/8}\right)^{0.04}. \qquad (5)$$

This power law approximates the true relation to within 1 per cent over the observed range of effective apertures [compare the distribution metric aperture sizes in Fig. 5(a) with fig. 4(c) of Jørgensen et al.].

We also apply an aperture correction to our linestrengths. Jørgensen et al. noted that the radial gradient in the $\rm Mg_2$ index is similar to the radial gradient in $\log\sigma$, and so applied the same aperture correction for $\rm Mg_2$ as for $\log\sigma$. We adopt this procedure for $\rm Mg_2$. For Mg$b$ we convert to Mg$b'$ (equation 3) and, assuming that the radial profile of Mg$b'$ is similar to that of $\rm Mg_2$ (and hence $\log\sigma$),

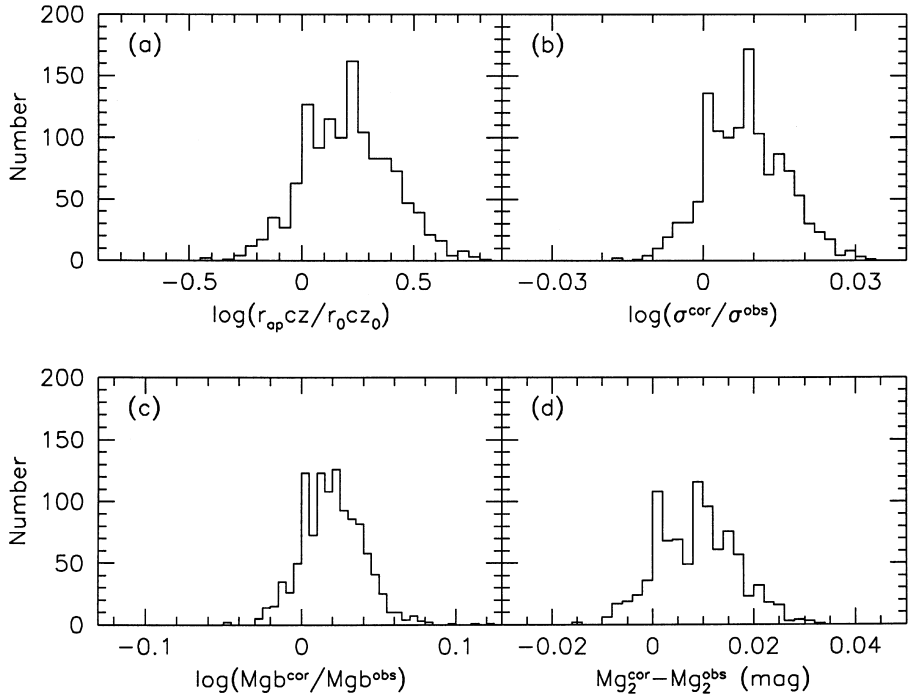


**Figure 5.** The distribution of aperture corrections to a standard metric aperture. (a) The distribution of the ratio of the observed metric apertures to the standard metric aperture (corresponding to 1.7 arcsec at the redshift of Coma). (b)–(d) The aperture corrections to this standard metric aperture for the dispersion, Mg$b$ and $Mg_2$ measurements. Note that $\sigma^{cor}$ is the aperture-corrected dispersion and $\sigma^{obs}$ is the raw observed dispersion; likewise for the linestrengths.

we apply the $\log\sigma$ aperture correction to Mg$b'$ before converting back to Mg$b$.

The distributions of corrections to the standard metric aperture for the dispersions and linestrengths are shown in Figs 5(b)–(d). These corrections are generally positive, as most objects in our sample are observed through larger effective apertures and are further away than Jørgensen et al.'s standard aperture and redshift. The corrections to standard relative apertures are quite similar, although having slightly greater amplitude and range. We choose to adopt the correction to a standard metric aperture in order to minimize the size and range of the corrections and to facilitate comparisons with dispersions and linestrengths in the literature.

### 3.5 Combining different runs

In comparing the redshifts, dispersions and linestrengths obtained from different runs, we found some significant systematic offsets. The origin of these run-to-run offsets is not fully understood. For the redshifts, the use of different velocity standard stars as the fiducials in different runs clearly contributes some systematic errors. For the dispersions, the calibration procedure that we use should in principle remove instrumental systematics; in practice, scale differences are common, as is shown by the range of scalefactors needed to reconcile velocity dispersions from various sources in the compilation by McElroy (1995; see Table 2).

We cannot directly calibrate the measurements from each run to the system defined by a chosen fiducial run, as there is no run with objects in common with all other runs to serve as the fiducial. Instead, we use the mean offset, $\Delta$, between the measurements from any particular run and *all* the other runs. To compute this offset we separately compute, for each galaxy $i$, the error-weighted mean value of the measurements obtained from the run in question, $x_{ij}$, and from all other runs, $y_{ik}$:

$$\langle x_i\rangle = \frac{\sum_j x_{ij}/\delta_{ij}^2}{\sum_j 1/\delta_{ij}^2}, \langle y_i\rangle = \frac{\sum_k y_{ik}/\delta_{ik}^2}{\sum_k 1/\delta_{ik}^2}. \quad (6)$$

Here $j$ runs over the $m_i$ observations of galaxy $i$ in the target run and $k$ runs over the $n_i$ observations of galaxy $i$ in all other runs; $\delta_{ij}$ and $\delta_{ik}$ are the estimated errors in $x_{ij}$ and $y_{ik}$. We then take the average over all galaxies, weighting by the number of comparison pairs, to arrive at an estimate for the offset of the target run:

$$\Delta = \frac{\sum_i m_i n_i(\langle x_i\rangle - \langle y_i\rangle)}{\sum_i m_i n_i}. \quad (7)$$

Here $i$ runs over the $l$ galaxies in the sample. We can reject outliers at this point by excluding galaxies for which the difference $\langle x_i\rangle - \langle y_i\rangle$ is larger than some cut-off: for $cz$, $\log\sigma$, Mg$b'$ and $Mg_2$ we required differences of less than $300\,km\,s^{-1}$, 0.2 dex, 0.1 mag and 0.1 mag respectively. The uncertainty, $\epsilon$, in this estimate of the run offset is given by

$$\epsilon^2 = \frac{\sum_i (m_i n_i)^2(\delta\langle x_i\rangle^2 + \delta\langle y_i\rangle^2)}{\left(\sum_i m_i n_i\right)^2}, \quad (8)$$

where $\delta\langle x_i\rangle$ and $\delta\langle y_i\rangle$ are the error-weighted uncertainties in $\langle x_i\rangle$ and $\langle y_i\rangle$ given by

$$\delta\langle x_i\rangle^2 = \left(\sum_j \delta_{ij}^{-2}\right)^{-1}, \delta\langle y_i\rangle^2 = \left(\sum_k \delta_{ik}^{-2}\right)^{-1}. \quad (9)$$

We subtract the offset determined in this manner from each run and then iterate the whole procedure until there are no runs with residual offsets larger than $0.5\epsilon$. As a final step, we place the entire data set (now corrected to a common zero-point) on to a fiducial system by subtracting from all runs the offset of the fiducial system. Note that the run corrections for dispersion and Mg$b$ are determined in terms of offsets in $\log\sigma$ and Mg$b'$.

In order to maximize the number of objects with multiple

measurements, we included the data set from the 'Streaming Motions of Abell Clusters' project (SMAC: Hudson, private communication; see also Smith et al. 1997) in this analysis. There is a considerable overlap between the SMAC and EFAR samples which significantly increases the number of comparison observations and reduces the uncertainties in the run offsets. We chose to use the 'Lick' system of Davies et al. (1987; included in the SMAC data set) as our fiducial, in order to bring the 7 Samurai, EFAR and SMAC data sets on to a single common system. This is not possible with Mg*b*, which is not measured in most previous work or by SMAC. We therefore chose run 109 (the Kitt Peak 4-m run of 1988 November) as the Mg*b* fiducial because it had a large number of high-quality observations and the systematics of the slit spectrograph are believed to be well understood.

We checked that this procedure gives relative run corrections consistent with those obtained by directly comparing runs in those cases where there *are* sufficient objects in common. We have also compared our method with a slightly different method used by the SMAC collaboration to determine the run corrections for their own data, and found good agreement (Hudson, private communication). We carried out Monte Carlo simulations of the whole procedure in order to check the uncertainties in the offsets computed according to equation (8). We found that this equation in general provides a good estimate of the uncertainties, although when the number of comparisons is small or they involve a small number of other runs it can underestimate the uncertainties by up to 30 per cent. Our final estimates of the uncertainties are therefore derived as the rms of the offsets from 100 Monte Carlo simulations.

Table 2 lists the offsets for each run computed according to the above procedure, their uncertainties based on Monte Carlo simulations, the number of individual measurements ($N$) and the number of comparison pairs ($N^{\rm c}$). Note that to correct our observed measurements to the fiducial system we *subtract* the appropriate run offset in Table 2 from each individual measurement. Of the 31 spectroscopic runs with usable data, only runs 104 and 129 have no objects in common with other runs and hence no run corrections; run 118 has no $\rm Mg_2$ measurements in common and so no run correction for $\rm Mg_2$.

Weighting by the number of individual measurements in each run, the mean amplitude of the corrections and their uncertainties are $28\pm8\,{\rm km\,s^{-1}}$ in $cz$, $0.023\pm0.015$ dex in $\log\sigma$, $0.008\pm0.006$ mag in Mg$b'$ and $0.015\pm0.006$ mag in $\rm Mg_2$. The significance of the individual run corrections (in terms of the ratio of the amplitude of the offset to its uncertainty) varies; however, over all runs the reduced $\chi^2$ is highly significant: 15.7, 4.0, 3.3 and 11.4 for the corrections to the redshifts, dispersions, Mg*b* and $\rm Mg_2$ respectively. Application of the run corrections reduces the median rms error amongst those objects with repeat measurements from 18 to

**Table 2.** Calibration of observing runs to a common system.

| Run | $\Delta cz$ ($\rm km\,s^{-1}$) | $N_z$ | $N_z^{\rm c}$ | $\Delta\log\sigma$ (dex) | $N_\sigma$ | $N_\sigma^{\rm c}$ | $\Delta{\rm Mg}b'$ (mag) | $N_b$ | $N_b^{\rm c}$ | $\Delta{\rm Mg_2}$ (mag) | $N_2$ | $N_2^{\rm c}$ |
|---|---|---|---|---|---|---|---|---|---|---|---|---|
| 101 | $-9\pm9$ | 19 | 62 | $+0.014\pm0.016$ | 18 | 65 | $+0.009\pm0.009$ | 18 | 32 | $-0.008\pm0.007$ | 16 | 30 |
| 102 | $+62\pm10$ | 56 | 57 | $+0.034\pm0.023$ | 56 | 56 | $+0.012\pm0.011$ | 56 | 24 | $-0.013\pm0.010$ | 56 | 12 |
| 103 | $-43\pm10$ | 36 | 53 | $-0.034\pm0.028$ | 34 | 48 | $-0.002\pm0.011$ | 34 | 27 | $-0.025\pm0.009$ | 34 | 20 |
| 104[b] | $+0$ | 11 | 0 | $+0.000$ | 11 | 0 | $+0.000$ | 11 | 0 | $+0.000$ | 11 | 0 |
| 105 | $+16\pm9$ | 36 | 54 | $+0.018\pm0.019$ | 36 | 55 | $+0.020\pm0.007$ | 36 | 37 | $+0.008\pm0.009$ | 21 | 14 |
| 106 | $-17\pm14$ | 23 | 61 | $+0.024\pm0.029$ | 22 | 54 | $+0.009\pm0.007$ | 22 | 41 | $+0.001\pm0.014$ | 14 | 13 |
| 107 | $-19\pm10$ | 27 | 61 | $+0.060\pm0.033$ | 27 | 64 | $+0.000\pm0.009$ | 27 | 33 | $-0.003\pm0.008$ | 21 | 24 |
| 108 | $-71\pm23$ | 9 | 35 | $-0.055\pm0.035$ | 9 | 34 | $-0.005\pm0.008$ | 9 | 12 | $+0.032\pm0.008$ | 9 | 11 |
| 109[a] | $+1\pm4$ | 93 | 222 | $-0.015\pm0.005$ | 92 | 220 | $+0.000\pm0.000$ | 92 | 167 | $+0.008\pm0.002$ | 92 | 126 |
| 110 | $+3\pm6$ | 71 | 186 | $-0.010\pm0.008$ | 61 | 171 | $+0.004\pm0.004$ | 61 | 78 | $-0.009\pm0.004$ | 61 | 50 |
| 111 | $-10\pm14$ | 19 | 72 | $-0.024\pm0.024$ | 19 | 76 | $-0.005\pm0.006$ | 19 | 33 | $+0.046\pm0.006$ | 19 | 25 |
| 112 | $+45\pm8$ | 31 | 82 | $-0.006\pm0.008$ | 31 | 103 | $+0.001\pm0.009$ | 31 | 16 | $-0.027\pm0.013$ | 16 | 7 |
| 113 | $+154\pm15$ | 20 | 9 | $+0.041\pm0.038$ | 20 | 9 | $+0.025\pm0.012$ | 20 | 7 | $-0.015\pm0.026$ | 2 | 1 |
| 114 | $-9\pm11$ | 12 | 22 | $-0.059\pm0.024$ | 12 | 22 | $-0.012\pm0.009$ | 12 | 20 | $+0.032\pm0.007$ | 12 | 15 |
| 115 | $+9\pm10$ | 8 | 24 | $+0.024\pm0.022$ | 8 | 23 | $-0.069\pm0.026$ | 1 | 2 | $-0.087\pm0.034$ | 1 | 2 |
| 116[d] | — | — | — | — | — | — | — | — | — | — | — | — |
| 117 | $-2\pm7$ | 59 | 132 | $+0.005\pm0.021$ | 55 | 121 | $+0.016\pm0.007$ | 55 | 90 | $+0.028\pm0.007$ | 41 | 51 |
| 118[c] | $+120\pm22$ | 14 | 4 | $-0.018\pm0.066$ | 13 | 4 | $-0.011\pm0.029$ | 13 | 3 | $+0.000$ | 5 | 0 |
| 119 | $-20\pm9$ | 17 | 20 | $-0.004\pm0.015$ | 17 | 19 | $+0.003\pm0.007$ | 17 | 19 | $-0.013\pm0.009$ | 17 | 8 |
| 120 | $-39\pm7$ | 38 | 47 | $+0.009\pm0.011$ | 34 | 44 | $+0.005\pm0.005$ | 33 | 25 | $+0.059\pm0.008$ | 26 | 14 |
| 121 | $-66\pm8$ | 86 | 177 | $+0.038\pm0.010$ | 82 | 181 | $+0.002\pm0.008$ | 82 | 23 | $+0.008\pm0.008$ | 54 | 17 |
| 122 | $-28\pm8$ | 41 | 70 | $+0.001\pm0.012$ | 37 | 58 | $+0.020\pm0.006$ | 37 | 32 | $+0.033\pm0.008$ | 31 | 24 |
| 123 | $-22\pm8$ | 22 | 41 | $+0.022\pm0.017$ | 17 | 34 | $+0.005\pm0.006$ | 16 | 26 | $+0.010\pm0.006$ | 13 | 16 |
| 124 | $+14\pm17$ | 22 | 49 | $+0.020\pm0.044$ | 14 | 40 | $+0.029\pm0.012$ | 14 | 8 | $+0.012\pm0.022$ | 11 | 1 |
| 125 | $-48\pm14$ | 57 | 62 | $+0.037\pm0.010$ | 55 | 64 | $+0.007\pm0.008$ | 55 | 8 | $-0.018\pm0.011$ | 55 | 7 |
| 126 | $+57\pm14$ | 36 | 43 | $-0.004\pm0.039$ | 33 | 40 | $+0.029\pm0.023$ | 33 | 9 | $+0.008\pm0.023$ | 33 | 6 |
| 127 | $-3\pm4$ | 131 | 187 | $+0.002\pm0.007$ | 127 | 167 | $-0.007\pm0.003$ | 127 | 136 | $-0.007\pm0.003$ | 127 | 83 |
| 128 | $+6\pm12$ | 24 | 29 | $-0.042\pm0.010$ | 23 | 29 | $+0.010\pm0.015$ | 23 | 7 | $-0.055\pm0.013$ | 9 | 4 |
| 129[b] | $+0$ | 3 | 0 | $+0.000$ | 3 | 0 | $+0.000$ | 3 | 0 | $+0.000$ | 3 | 0 |
| 130[d] | — | — | — | — | — | — | — | — | — | — | — | — |
| 131[e] | $+35\pm5$ | 123 | 174 | $-0.078\pm0.014$ | 99 | 152 | $+0.002\pm0.004$ | 98 | 136 | — | — | — |
| 132 | $-24\pm19$ | 12 | 7 | $-0.025\pm0.026$ | 12 | 6 | $-0.032\pm0.008$ | 12 | 4 | $+0.005\pm0.016$ | 12 | 4 |
| 133 | $-11\pm4$ | 128 | 247 | $-0.009\pm0.006$ | 128 | 241 | $-0.009\pm0.002$ | 128 | 183 | $-0.014\pm0.002$ | 128 | 151 |

[a] Run 109 is the fiducial run for Mg$b'$, defined to have zero offset. [b] Runs 104 and 129 have no objects in common with other runs. [c] Run 118 has no $\rm Mg_2$ measurements in common with other runs. [d] Runs 116 and 130 have no usable data. [e] Run 131 has no $\rm Mg_2$ measurements.

14 km s$^{-1}$ in redshift, 6.3 to 5.6 per cent in dispersion, 4.9 to 4.4 per cent in Mg*b* and 0.012 to 0.009 mag in $Mg_2$. We also checked to see whether applying the run corrections reduced the scatter in external comparisons between our data and measurements in the literature (see Section 4.3). We found that, although the scatter is dominated by the combined random errors, the corrections did reduce the scatter slightly in all cases.

As another test of the run corrections for Mg$b'$ and $Mg_2$ (and also, more weakly, for $\log\sigma$), we compared the Mg$b'-\sigma$ and $Mg_2-\sigma$ distributions for each run (after applying the run corrections) with the global Mg$b'-\sigma$ and $Mg_2-\sigma$ relations derived in Paper V. Using the $\chi^2$ goodness-of-fit statistic to account both for measurement errors in the dispersions and linestrengths and for the intrinsic scatter about the Mg$-\sigma$ relations, we find that for Mg$b'-\sigma$ there were two runs (113 and 132) with reduced $\chi^2$ greater than 3, while for $Mg_2-\sigma$ there was one such run (122). In all three cases the removal of one or two obvious outliers decreased the reduced $\chi^2$ to a non-significant level.

### 3.6 Calibrating the estimated errors

Obtaining precise error estimates is particularly important because we will make extensive use of them in applying maximum likelihood methods to deriving the Fundamental Plane and relative cluster distances for our sample. Although we have estimated the measurement errors as carefully as possible, simulating the noise in the observations and the measurement procedures, some sources of error are likely to remain unaccounted for and we may be systematically mis-estimating the errors. We therefore autocalibrate our errors by scaling the estimated errors in the combined measurements (the *internal* error estimate, based on the individual measurement errors derived from simulations; see Sections 3.3 and 4.2) to match the rms errors from objects with repeat measurements (an *external* error estimate).

Fig. 6 shows the differential and cumulative distributions of the ratio of the rms error to the estimated error for each galaxy with repeat measurements of redshift, dispersion, Mg*b* and $Mg_2$. The smooth curves are the predicted differential and cumulative distributions of this ratio assuming that the estimated errors are the true errors. The top panel shows the comparison using the estimated errors (including all the corrections discussed above). For the redshifts and linestrengths, the estimated errors are generally underestimates of the true errors, since the ratio of rms and estimated errors tends to be larger than predicted. For the dispersions the estimated errors are generally overestimates of the true errors, since this ratio tends to be smaller than predicted. For all quantities the assumption that the estimated errors are consistent with the true errors is ruled out with high confidence by a Kolmogorov–Smirnov (KS) test applied to the observed and predicted cumulative distributions. These differences between the estimated errors from the simulations and the rms errors from repeat measurements reflect the approximate nature of the S/N estimates and systematic measurement errors not accounted for in the simulations.

In order to bring our estimated errors into line with the rms errors from the repeat measurements, we found it necessary to add 15 km s$^{-1}$ in quadrature to the estimated redshift errors, to scale the dispersion and Mg*b* errors by factors of 0.85 and 1.15 respectively, and to add 0.005 mag to the $Mg_2$ errors. These corrections were determined by maximizing the agreement of the observed and predicted distributions of the ratio of rms and estimated errors under a KS test (excluding outliers with values of this ratio >3.5). The corrections are quite well determined: to within a couple of km s$^{-1}$ for the redshift correction, a few per cent for the dispersion and Mg*b* corrections, and 0.001 mag for the $Mg_2$ correction. Applying these corrections, and repeating the comparison of rms and estimated errors, gives the lower panels of Fig. 6, which show the good agreement between the rms errors from repeat measurements and the calibrated error estimates for the redshifts, dispersions and Mg linestrengths.

The need for such a correction to the redshift errors may be due in part to the residual zero-point uncertainties in the redshifts, and in part to a tendency for the simulations to underestimate the errors for high S/N spectra. The origin of the overestimation of the dispersion errors is uncertain, although it may result from slightly different prescriptions for estimating the S/N in the observations and the simulations. The underestimation of the linestrength errors may be due to neglecting the effects of errors in the redshift and dispersion

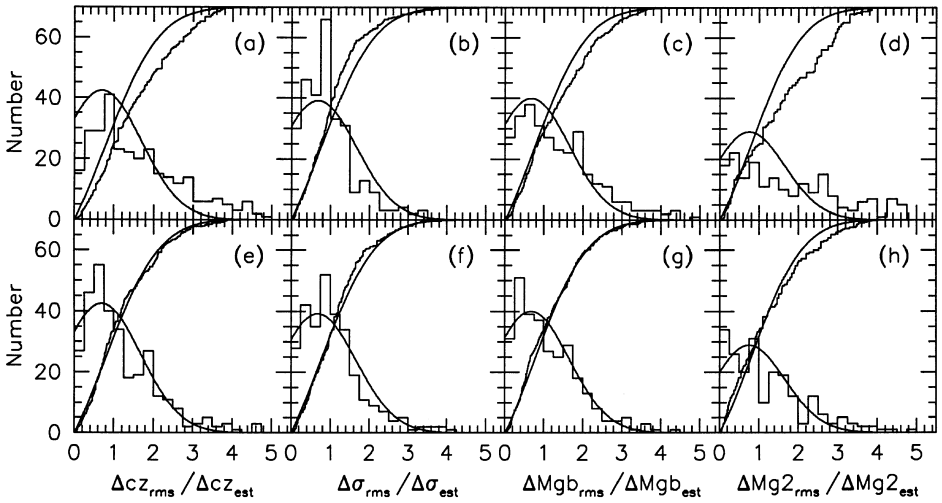


**Figure 6.** Comparison of the estimated errors derived from simulations and the rms errors for galaxies with repeat measurements of redshift, dispersion, Mg*b* and $Mg_2$. Each panel shows the differential and cumulative distributions of the ratio of rms error to estimated error. The stepped curves are the observed distributions, while the smooth curves are the predicted distributions. The upper panels show the comparisons using the original estimated errors; the lower panels show the comparisons after correcting the estimated errors as described in the text.

**Table 3.** Individual spectroscopic measurements (abridged). The full table is available electronically.

| (1) GINRUNSEQ | (2) Galaxy Name | (3) Telescope | (4) Obsvn Date | (5) $Q$ | (6) S/N | (7) $cz$ ($\mathrm{km\,s^{-1}}$) | (8) | (9) $\sigma$ ($\mathrm{km\,s^{-1}}$) | (10) | (11) Mg$b$ (Å) | (12) | (13) $\mathrm{Mg_2}$ (mag) | (14) | (15) Notes |
|---|---|---|---|---|---|---|---|---|---|---|---|---|---|---|
| 001106215 | A76 A | MG24 | 880914 | A | 21.4 | 11296 | 51 | 262 | 50 | 5.20 | 0.54 | 0.353 | 0.020 | |
| 002106221 | A76 B | MG24 | 880914 | B | 18.8 | 11317 | 47 | 225 | 47 | 4.76 | 0.59 | 0.326 | 0.019 | |
| 003106218 | A76 C | MG24 | 880914 | A | 17.8 | 11973 | 49 | 217 | 48 | 5.17 | 0.68 | 0.392 | 0.021 | |
| 004107095 | A76 D | MG24 | 881011 | C | 14.8 | 12184 | 31 | 316 | 103 | 6.18 | 0.83 | 0.326 | 0.028 | |
| 005120504 | A76 E | IN25 | 901016 | B | 33.2 | 12241 | 19 | 217 | 16 | 6.35 | 0.22 | 0.312 | 0.011 | |
| 005120505 | A76 E | IN25 | 901017 | B | 32.8 | 12147 | 17 | 169 | 11 | 6.16 | 0.23 | 0.275 | 0.012 | |
| 006107098 | A76 F | MG24 | 881011 | B | 17.6 | 12371 | 28 | 307 | 82 | 5.29 | 0.83 | 0.331 | 0.027 | |
| 008122534 | A85 A | MG24 | 911016 | B | 18.7 | 16577 | 39 | 290 | 52 | 5.14 | 0.59 | 0.344 | 0.021 | |
| 008123319 | A85 A | IN25 | 911201 | D | 21.4 | 16692 | 50 | — | — | — | — | — | — | |
| 009120626 | A85 B | IN25 | 901017 | A | 37.6 | 17349 | 34 | 436 | 46 | 5.74 | 0.22 | — | — | |
| 010120628 | A85 C | IN25 | 901017 | D | 33.9 | 22837 | 50 | — | — | — | — | — | — | Mg$b$ at sky |
| 011122540 | A85 1 | MG24 | 911016 | B | 25.8 | 15112 | 20 | 195 | 18 | 3.82 | 0.39 | 0.253 | 0.016 | |
| 012132001 | A85 2 | SS2B | 931022 | B | 28.3 | 16264 | 25 | 294 | 32 | 5.86 | 0.31 | 0.337 | 0.011 | |
| 013101059 | A119 A | MG24 | 861202 | B | 16.5 | 11516 | 49 | 299 | 48 | 6.06 | 0.51 | 0.294 | 0.022 | |
| 013109339 | A119 A | KP4M | 881107 | A | 44.2 | 11457 | 19 | 289 | 18 | 5.00 | 0.20 | 0.320 | 0.010 | |
| 013131330 | A119 A | ES36 | 931008 | A | 30.9 | 11451 | 24 | 320 | 29 | 4.86 | 0.26 | — | — | |
| 014101063 | A119 B | MG24 | 861202 | C | 14.4 | 13205 | 63 | 323 | 65 | 5.90 | 0.72 | 0.320 | 0.025 | |
| 014109339 | A119 B | KP4M | 881107 | A | 35.0 | 13345 | 21 | 276 | 21 | 4.86 | 0.22 | 0.361 | 0.010 | |
| 015109343 | A119 C | KP4M | 881107 | A | 33.2 | 13508 | 19 | 250 | 19 | 5.51 | 0.22 | 0.295 | 0.011 | |
| 015131330 | A119 C | ES36 | 931008 | B | 19.5 | 13484 | 28 | 265 | 35 | 5.88 | 0.48 | — | — | |
| 016109346 | A119 D | KP4M | 881107 | C* | 20.8 | 14980 | 16 | 104 | 13 | 3.30 | 0.37 | 0.151 | 0.016 | H$\beta$ |
| 016110611 | A119 D | KP2M | 881114 | D* | 15.6 | 15022 | 50 | — | — | — | — | — | — | H$\beta$ |
| 016131330 | A119 D | ES36 | 931008 | D* | 16.1 | 14996 | 50 | — | — | — | — | — | — | H$\beta$ |
| 017109347 | A119 E | KP4M | 881107 | A | 36.1 | 12807 | 19 | 251 | 17 | 5.18 | 0.18 | 0.326 | 0.010 | |
| 017131330 | A119 E | ES36 | 931008 | A | 27.0 | 12788 | 21 | 243 | 22 | 6.01 | 0.32 | — | — | |
| 018109342 | A119 F | KP4M | 881107 | B | 28.4 | 13034 | 18 | 193 | 15 | 4.95 | 0.32 | 0.245 | 0.013 | |
| 018131330 | A119 F | ES36 | 931008 | C | 21.1 | 13006 | 16 | 112 | 20 | 4.69 | 0.37 | — | — | |
| 019109342 | A119 G | KP4M | 881107 | E | 32.7 | — | — | — | — | — | — | — | — | mis-ID |
| 019131330 | A119 G | ES36 | 931008 | A | 36.7 | 13457 | 19 | 267 | 19 | 4.78 | 0.20 | — | — | |
| 021122654 | A119 I | MG24 | 911018 | A | 31.0 | 13271 | 20 | 225 | 19 | 4.85 | 0.38 | 0.326 | 0.014 | |
| 022131330 | A119 J | ES36 | 931008 | B | 22.3 | 13520 | 21 | 219 | 24 | 4.55 | 0.33 | — | — | |
| 023131330 | A119 1 | ES36 | 931008 | C* | 11.5 | 4127 | 18 | 92 | 38 | 0.50 | 0.78 | — | — | H$\beta$ |
| 024122657 | A119 2 | MG24 | 911018 | E | 28.9 | — | — | — | — | — | — | — | — | mis-ID |
| 024131330 | A119 2 | ES36 | 931008 | B | 20.4 | 12346 | 16 | 100 | 20 | 5.13 | 0.38 | — | — | |
| 025107103 | J3 A | MG24 | 881011 | B | 15.2 | 14453 | 32 | 333 | 111 | 6.25 | 0.74 | 0.329 | 0.025 | |
| 026120714 | J3 B | IN25 | 901018 | A | 39.5 | 13520 | 18 | 231 | 15 | 4.93 | 0.23 | — | — | |
| 027107106 | J3 C | MG24 | 881011 | C | 15.8 | 13771 | 21 | 163 | 38 | 4.33 | 0.86 | 0.224 | 0.027 | |
| 028120712 | J3 D | IN25 | 901017 | A | 36.3 | 14316 | 22 | 287 | 23 | 5.45 | 0.24 | — | — | double |
| 028120713 | J3 D | IN25 | 901017 | B | 30.8 | 14837 | 19 | 207 | 15 | 4.87 | 0.26 | — | — | double |
| 031107190 | J4 A | MG24 | 881012 | C | 13.2 | 12074 | 24 | 185 | 51 | 5.35 | 0.75 | 0.387 | 0.029 | |
| 032107189 | J4 B | MG24 | 881012 | C | 13.3 | 12090 | 31 | 302 | 102 | 4.11 | 1.08 | 0.261 | 0.032 | |
| 033132002 | J4 C | SS2B | 931021 | A | 30.0 | 17154 | 30 | 358 | 43 | 6.20 | 0.26 | 0.355 | 0.010 | |
| 036107195 | A147 A | MG24 | 881012 | C | 12.2 | 12811 | 26 | 208 | 62 | 3.96 | 1.16 | 0.288 | 0.034 | |
| 036117298 | A147 A | MG24 | 891015 | B | 19.0 | 12741 | 35 | 281 | 49 | 4.84 | 0.60 | 0.314 | 0.022 | |
| 036133157 | A147 A | CT4M | 931019 | A | 61.4 | 12760 | 17 | 235 | 12 | 4.77 | 0.17 | 0.285 | 0.010 | |
| 036133158 | A147 A | CT4M | 931019 | A | 62.3 | 12776 | 17 | 253 | 13 | 5.01 | 0.18 | 0.289 | 0.010 | |

The columns of this table give: (1) observation identifier (GINRUNSEQ); (2) galaxy name; (3) telescope used; (4) date of observation; (5) quality parameter; (6) signal-to-noise ratio; (7)–(8) redshift and estimated error; (9)–(10) velocity dispersion and estimated error; (11)–(12) Mg$b$ linestrength and estimated error; (13)–(14) $\mathrm{Mg_2}$ linestrength and estimated error; and (15) notes on each observation. In the notes, 'double' means that the EFAR galaxy is double; 'star' means that the EFAR object is a star, not a galaxy; 'mis-ID' means that the spectrum is for some galaxy other than the nominated EFAR object; 'mis-ID*' means that the spectrum is for a nearby star rather than the EFAR object; 'Mg$b$ at sky' means that the object is at a redshift that puts Mg$b$ on the 5577-Å sky line; 'number = number' notes the duplicated pairs in the EFAR sample (see Paper I; only the first of the two GINs is used); emission-line objects (with an asterisk on $Q$) have the emission features listed; 'H$\beta$ abs' or 'H$\beta$ abs, [OIII]' means that the redshift is based on the H$\beta$ absorption feature (and [OIII] if present), as the spectrum stops short of Mg$b$ (no dispersion or Mg$b$ index is given for these objects). The objects for which we have no spectrum have GINs 7, 20, 29, 30, 34, 35, 55, 62, 64, 67, 82, 83, 91, 104, 121, 131, 133, 134, 161, 181, 191, 214, 225, 228, 231, 234, 256, 265, 309, 327, 391, 405, 407, 417, 434, 435, 442, 450, 451, 452, 458, 463, 464, 465, 470, 475, 477, 483, 484, 486, 494, 516, 520, 521, 522, 523, 526, 544, 551, 553, 567, 569, 570, 575, 576, 577, 587, 594, 597, 603, 605, 624, 625, 644, 671, 727, 760, 793, 798, 801, 901. This is an abridged version of this table; the full table is available on Synergy, from NASA's Astrophysical Data Center (ADC); (URL http://adc.gsfc.nasa.gov, table ID number J/MNRAS/305/259) and the Centre de Données astronomiques de Strasbourg (CDS); (URL http://cdsweb.u-strasbg.fr, table ID number J/MNRAS/305/259).

estimates and the different continuum shapes of spectra from different runs when measuring linestrengths.

## 4 RESULTS

### 4.1 Individual measurements

The previous two sections describe the observations and analysis of our spectroscopic data. Table 3 (full version available electronically) lists the observational details for each spectrum and the fully corrected measurements of redshift, dispersion, Mg*b* and $Mg_2$, together with their calibrated error estimates. Note that these error estimates are the individual measurement errors, and must be combined in quadrature with the run correction uncertainties given in Table 2 to give the total error estimate. We list the measurement errors rather than the total errors because the total errors are not independent, being correlated for objects in the same run. The version of the table presented here is abridged; the full table is available from NASA's Astrophysical Data Center (ADC) and from the Centre de Données astronomiques de Strasbourg (CDS).

The entries in Table 3 are as follows: column 1 gives GINRUNSEQ, a unique nine-digit identifier for each spectrum, composed of the galaxy identification number (GIN) as given in the master list of EFAR sample galaxies (table 3 of Paper I), the run number (RUN) as given in Table 1, and a sequence number (SEQ) which uniquely specifies the observation within the run; column 2 gives the galaxy name, as in the master list of Paper I; column 3 is the telescope code, as in Table 1; column 4 is the UT date of the observation; columns 5 and 6 are the quality parameter (with an asterisk if the spectrum shows emission features) and S/N of the spectrum (see Section 2.4); columns 7 and 8 are the fully corrected heliocentric redshift $cz$ (in $\mathrm{km\,s^{-1}}$) and its measurement error; columns 9 and 10 are the fully corrected velocity dispersion $\sigma$ (in $\mathrm{km\,s^{-1}}$) and its measurement error; columns 11 and 12 are the fully corrected Mg*b* linestrength index and its measurement error (in Å); columns 13 and 14 are the fully corrected $Mg_2$ linestrength index and its measurement error (in mag); column 15 provides comments, the full meanings of which are described in the notes to the table.

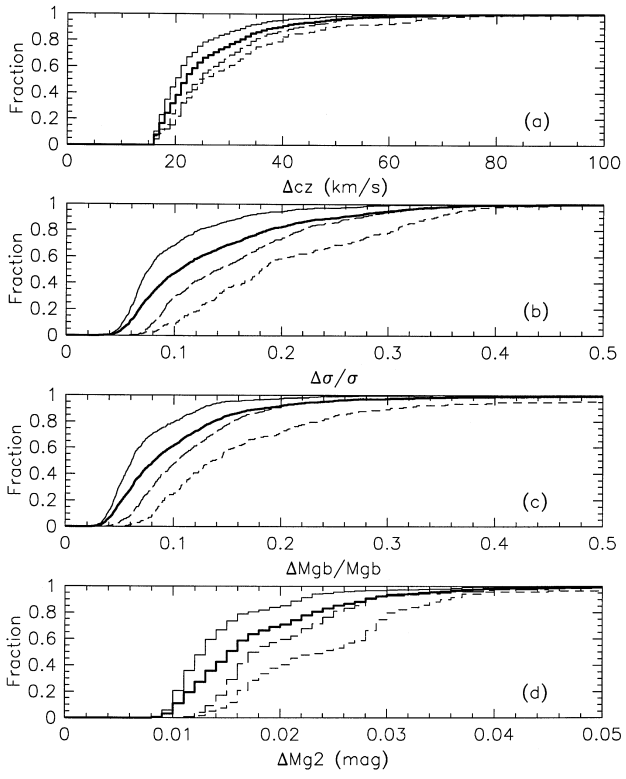


**Figure 7.** The cumulative distributions of estimated errors for individual measurements of redshift, velocity dispersion and Mg*b* linestrength. The distributions for quality classes A, B and C are shown as full, long-dashed and short-dashed lines respectively; the overall distribution is the thick full line. (a) The distribution of estimated errors in $cz$; (b) estimated relative errors in $\sigma$; (c) estimated relative errors in Mg*b*; (d) estimated errors in $Mg_2$.

There are 1319 spectra in this table. Note that 81 objects from our original sample do not have spectroscopic observations and do not appear in the table (see the list of missing GINs in the table notes). Three of these are the duplicate objects (GINs 55, 435, 476) and three are known stars (GINs 131, 133, 191). Most of the others are objects that our imaging showed are not early-type galaxies, although there are a few early-type galaxies for which we did not get a spectrum. There are 34 spectra that are unusable ($Q = \mathrm{E}$) either because the spectrum is too poor (13 cases) or because the object was mis-identified (20 cases) or is a known star (one case, GIN 123). Of the 1285 usable spectra (for 706 different galaxies), there are 637 spectra with $Q = \mathrm{A}$, 407 with $Q = \mathrm{B}$, 161 with $Q = \mathrm{C}$ and 80 with $Q = \mathrm{D}$.

The cumulative distributions of the total estimated errors in the individual measurements (combining measurement errors and run correction uncertainties in quadrature) are shown in Fig. 7 for quality classes A, B and C, and for all three classes together. The error distributions can be quantitatively characterized by their 50 and 90 per cent points, which are listed in Table 4. The overall median error in a single redshift measurement is $22\,\mathrm{km\,s^{-1}}$, the median relative errors in single measurements of dispersion and Mg*b* are 10.5 and 8.2 per cent, and the median error in a single measurement of $Mg_2$ is 0.015 mag.

### 4.2 Combining measurements

We use a weighting scheme to combine the individual measurements of each quantity to obtain a best estimate (and its uncertainty) for each galaxy in our sample. The weighting has three components.

(i) *Error weighting.* For multiple measurements $X_i$ having estimated total errors $\Delta_i$ (the measurement errors and run correction uncertainties added in quadrature), we weight the values inversely with their variances, i.e. by $\Delta_i^{-2}$.

(ii) *Quality weighting.* We apply a weighting $W_Q$ which quantifies our degree of belief (over and above the estimated errors) in measurements obtained from spectra with different quality parameters. Following the discussion in Section 2.4, for spectra with $Q = \mathrm{A}$, B, C, D, E we use $W_Q = 1$, 1, 1, 0.5, 0 in computing redshifts, $W_Q = 1$, 1, 0.5, 0, 0 in computing dispersions, and $W_Q = 1$, 1, 0.5, 0, 0 in computing linestrengths.

**Table 4.** The distribution of estimated errors per measurement.

| $Q$ | $\Delta cz$ ($\mathrm{km\,s^{-1}}$) | | $\Delta\sigma/\sigma$ | | $\Delta$Mg*b*/Mg*b* | | $\Delta Mg_2$ (mag) | |
|---|---|---|---|---|---|---|---|---|
| | 50% | 90% | 50% | 90% | 50% | 90% | 50% | 90% |
| All | 22 | 40 | 0.105 | 0.255 | 0.082 | 0.184 | 0.015 | 0.028 |
| A | 20 | 33 | 0.076 | 0.163 | 0.061 | 0.125 | 0.013 | 0.022 |
| B | 24 | 43 | 0.140 | 0.275 | 0.104 | 0.192 | 0.018 | 0.028 |
| C | 25 | 48 | 0.181 | 0.343 | 0.136 | 0.303 | 0.024 | 0.036 |

(iii) *Run weighting.* We also apply a run weighting $W_R = 0$ to exclude run 115, for reasons explained in Section 2.1; all other runs are given $W_R = 1$.

The combined estimate $X$ is thus computed from the individual measurements $X_i$ as the weighted mean

$$X = \sum_i W_i X_i / \sum_i W_i, \tag{10}$$

where $W_i = \Delta_i^{-2} W_{Qi} W_{Ri}$. The uncertainty in this weighted mean is computed as

$$\Delta = (\sum_i W_i)^{-1/2}. \tag{11}$$

This procedure is used to obtain combined estimates of the redshift, dispersion and linestrengths for each galaxy. We estimate the overall quality $Q$ as the highest quality amongst the individual measurements, and obtain a combined estimate of the S/N as

$$\mathrm{S/N} = \left[ \sum_i (\mathrm{S/N})_i^2 W_{Qi} W_{Ri} \right]^{1/2}, \tag{12}$$

using the same weightings as for the dispersions (except when the overall quality is $Q = \mathrm{D}$, when these weightings are omitted).

Table 5 gives the combined estimates of the spectroscopic parameters for each galaxy in the EFAR sample. The table lists galaxy identification number (GIN), galaxy name, cluster assignment number (CAN; see Section 5), and the number of spectra, redshifts, dispersions and Mg*b* and $\mathrm{Mg}_2$ linestrengths obtained for this object; then, for each of redshift, dispersion, Mg*b* and $\mathrm{Mg}_2$, the combined estimate, its estimated total error ($\Delta$) and the weighted rms error from any repeat observations ($\delta$); finally, the combined S/N estimate and the overall quality parameter (with an asterisk if the galaxy possesses emission lines). Note that only objects with useful measurements are included; hence the lowest quality class present in this table is $Q = \mathrm{D}$, and the seven galaxies with only $Q = \mathrm{E}$ spectra (GINs 123, 284, 389, 448, 599, 637 and 679) in Table 3 are omitted.

The cumulative distributions of uncertainties in the combined results are shown in Fig. 8, both for the entire data set and for quality classes A, B and C separately. The error distributions can be quantitatively characterized by their 50 and 90 per cent points, which are listed in Table 6. The overall median error in redshift is $20\,\mathrm{km\,s^{-1}}$, the median relative errors in dispersion and Mg*b* are 9.1 and 7.2 per cent, and the median error in $\mathrm{Mg}_2$ is 0.015 mag. For the whole sample, and for quality classes A and B, the median errors in the combined measurements are smaller than the median errors in the individual measurements, as one expects. However, for dispersion, Mg*b* and $\mathrm{Mg}_2$ the errors are larger for quality class C and at the 90th percentile; this results from assigning a quality weighting of 0.5 to $Q = \mathrm{C}$ when combining the individual measurements of these quantities.

The uncertainties listed in Table 5 represent the best estimates of the total errors in the parameters for each galaxy. However, it must be emphasized that they are *not* independent of each other, as the run correction errors are correlated across all measurements from a run. To simulate the joint distribution of some parameter properly for the whole data set, one must first generate realisations of the run correction errors (drawn from Gaussians with standard deviations given by the uncertainties listed in Table 2) and the individual measurement errors (drawn from Gaussians with standard deviations given by the uncertainties listed Table 3). For each individual measurement, one must add the realization of its measurement error and the realization of the appropriate run correction error (the same for all measurements in a given run) to the measured value of the parameter. The resulting realizations of the individual measurements are finally combined using the recipe described above to yield a realization of the value of the parameter for each galaxy in the data set.

The distributions of redshift, velocity dispersion, Mg*b* and $\mathrm{Mg}_2$ for the galaxies in the EFAR sample are displayed in Fig. 9. The galaxies for which we measured velocity dispersions are only a subset of our sample of programme galaxies (629/743), and represent a refinement of the sample selection criteria. Fig. 10 shows the fraction of programme galaxies with measured dispersions as a function of the galaxy diameter $D_{\mathrm{W}}$ on which the selection function of the programme galaxy sample is defined. There is a steady decline in the fraction of the sample for which usable dispersions were measured, from 100 per cent for the largest galaxies (with $D_{\mathrm{W}} \gtrsim 40$ arcsec) to about 75 per cent for the smallest (with $8 \lesssim D_{\mathrm{W}} \lesssim 15$ arcsec; there are only three programme galaxies with $D_{\mathrm{W}} < 8$ arcsec). This additional selection effect must be allowed for when determining Fundamental Plane distances.

### 4.3 Internal and external comparisons

One of the strengths of our spectroscopic sample is the high fraction of objects with repeat observations: there are 375 galaxies with a single dispersion measurement, 160 with two measurements and 141 with three or more measurements. Fig. 11 shows the cumulative distributions of rms errors in redshift, dispersion, Mg*b* and $\mathrm{Mg}_2$ obtained from these repeat observations. The detailed internal comparisons made possible by these repeat measurements have been used to establish the run corrections (Section 3.5) and to calibrate the estimated errors (Section 3.6). The latter process ensured that the estimated errors were statistically consistent with the rms errors of the repeat measurements.

We also make external comparisons of our measurements with the work of other authors. The EFAR redshifts are compared in Fig. 12 with redshifts given in the literature by the 7 Samurai (Davies et al. 1987), Dressler & Shectman (1988), Beers et al. (1991), Malumuth et al. (1992), Zabludoff et al. (1993), Colless & Dunn (1996) and Lucey et al. (1997). Only 11 of the 256 comparisons give redshift differences greater than $300\,\mathrm{km\,s^{-1}}$: in six cases the EFAR redshift is confirmed either by repeat measurements or other published measurements; in the remaining five cases the identification of the galaxy in question is uncertain in the literature. For the 245 cases in which the redshift difference is less than $300\,\mathrm{km\,s^{-1}}$, there is no significant velocity zero-point error and the rms scatter is $85\,\mathrm{km\,s^{-1}}$. Since our repeat measurements show much smaller errors (90 per cent are less than $36\,\mathrm{km\,s^{-1}}$), most of this scatter must arise in the literature data, some of which were taken at lower resolution or S/N than our data.

Fig. 13 compares the EFAR dispersions with published dispersions from the work of the 7 Samurai (Davies et al. 1987), Guzmán (1993), Jørgensen (1997) and Lucey et al. (1997), and the compilation of earlier measurements by Whitmore, McElroy & Tonry (1985). Note that we do not compare with the more recent compilation by McElroy (1995), since its overlap with our sample is essentially just the sum of above sources. The mean differences, $\Delta = \log \sigma_{\mathrm{EFAR}} - \log \sigma_{\mathrm{lit}}$, and their standard errors are indicated in the figure; none of these scale differences is larger than 6 per cent and in fact all five comparisons are consistent with zero scale error at the $2\sigma$ level or better. The rms scatter in these comparisons is significantly greater than the errors in our dispersion measurements, implying that in general the literature measurements have larger errors and/or that there are unaccounted for uncertainties in the comparison.

**Table 5.** Spectroscopic parameters for the EFAR galaxies.

| (1) GIN | (2) Galaxy Name | (3) CAN | (4) $N$ $s\ z\ \sigma\ b\ 2$ | (5) $cz$ (km s$^{-1}$) | (6) $\Delta cz$ | (7) $\delta cz$ | (8) $\sigma$ (km s$^{-1}$) | (9) $\Delta\sigma$ | (10) $\delta\sigma$ | (11) Mg$b$ | (12) $\Delta$Mg$b$ (Å) | (13) $\delta$Mg$b$ | (14) $Mg_2$ | (15) $\Delta Mg_2$ (mag) | (16) $\delta Mg_2$ | (17) S/N | (18) $Q$ |
|---|---|---|---|---|---|---|---|---|---|---|---|---|---|---|---|---|---|
| 1 | A76 A | 1 | 1 1 1 1 1 | 11296 | 53 | — | 262 | 53 | — | 5.20 | 0.57 | — | 0.353 | 0.024 | — | 21.4 | A |
| 2 | A76 B | 1 | 1 1 1 1 1 | 11317 | 49 | — | 224 | 49 | — | 4.76 | 0.62 | — | 0.326 | 0.024 | — | 18.8 | B |
| 3 | A76 C | 1 | 1 1 1 1 1 | 11973 | 51 | — | 217 | 50 | — | 5.17 | 0.70 | — | 0.392 | 0.025 | — | 17.8 | A |
| 4 | A76 D | 1 | 1 1 1 1 1 | 12184 | 33 | — | 316 | 150 | — | 6.18 | 1.21 | — | 0.326 | 0.041 | — | 10.5 | C |
| 5 | A76 E | 1 | 2 2 2 2 2 | 12189 | 14 | 47 | 184 | 10 | 23 | 6.26 | 0.18 | 0.09 | 0.295 | 0.010 | 0.018 | 46.7 | B |
| 6 | A76 F | 1 | 1 1 1 1 1 | 12371 | 30 | — | 307 | 85 | — | 5.29 | 0.86 | — | 0.331 | 0.028 | — | 17.6 | B |
| 8 | A85 A | 2 | 2 2 1 1 1 | 16604 | 35 | 49 | 290 | 53 | — | 5.14 | 0.61 | — | 0.344 | 0.022 | — | 18.7 | B |
| 9 | A85 B | 2 | 1 1 1 1 0 | 17349 | 35 | — | 436 | 47 | — | 5.74 | 0.25 | — | — | — | — | 37.6 | A |
| 10 | A85 C | 102 | 1 1 0 0 0 | 22837 | 71 | — | — | — | — | — | — | — | — | — | — | 33.9 | D |
| 11 | A85 1 | 2 | 1 1 1 1 1 | 15112 | 22 | — | 195 | 19 | — | 3.82 | 0.42 | — | 0.253 | 0.018 | — | 25.8 | B |
| 12 | A85 2 | 2 | 1 1 1 1 1 | 16264 | 31 | — | 294 | 37 | — | 5.86 | 0.37 | — | 0.337 | 0.019 | — | 28.3 | B |
| 13 | A119 A | 3 | 3 3 3 3 2 | 11459 | 15 | 17 | 297 | 15 | 13 | 5.04 | 0.16 | 0.31 | 0.316 | 0.009 | 0.010 | 56.4 | A |
| 14 | A119 B | 3 | 2 2 2 2 2 | 13330 | 20 | 42 | 278 | 21 | 10 | 4.90 | 0.22 | 0.21 | 0.358 | 0.010 | 0.011 | 36.5 | A |
| 15 | A119 C | 3 | 2 2 2 2 1 | 13500 | 16 | 11 | 253 | 17 | 6 | 5.57 | 0.20 | 0.14 | 0.295 | 0.011 | — | 38.5 | A |
| 16 | A119 D | 3 | 3 3 1 1 1 | 14982 | 16 | 9 | 104 | 18 | — | 3.30 | 0.52 | — | 0.151 | 0.023 | — | 14.7 | C* |
| 17 | A119 E | 3 | 2 2 2 2 1 | 12798 | 14 | 9 | 248 | 14 | 4 | 5.37 | 0.16 | 0.35 | 0.326 | 0.010 | — | 45.1 | A |
| 18 | A119 F | 3 | 2 2 2 2 1 | 13018 | 12 | 14 | 175 | 13 | 33 | 4.88 | 0.28 | 0.11 | 0.245 | 0.013 | — | 32.1 | B |
| 19 | A119 G | 3 | 2 1 1 1 0 | 13457 | 20 | — | 267 | 21 | — | 4.78 | 0.22 | — | — | — | — | 36.7 | A |
| 21 | A119 I | 3 | 1 1 1 1 1 | 13271 | 22 | — | 225 | 20 | — | 4.85 | 0.41 | — | 0.326 | 0.016 | — | 31.0 | A |
| 22 | A119 J | 3 | 1 1 1 1 0 | 13520 | 22 | — | 219 | 25 | — | 4.55 | 0.35 | — | — | — | — | 22.3 | B |
| 23 | A119 1 | 103 | 1 1 1 1 0 | 4127 | 19 | — | 92 | 54 | — | 0.50 | 1.12 | — | — | — | — | 8.1 | C* |
| 24 | A119 2 | 3 | 2 1 1 1 0 | 12346 | 17 | — | 100 | 20 | — | 5.13 | 0.39 | — | — | — | — | 20.4 | B |
| 25 | J3 A | 4 | 1 1 1 1 1 | 14453 | 34 | — | 333 | 114 | — | 6.25 | 0.77 | — | 0.329 | 0.026 | — | 15.2 | B |
| 26 | J3 B | 4 | 1 1 1 1 0 | 13519 | 19 | — | 231 | 16 | — | 4.93 | 0.26 | — | — | — | — | 39.5 | A |
| 27 | J3 C | 4 | 1 1 1 1 1 | 13770 | 23 | — | 163 | 57 | — | 4.33 | 1.26 | — | 0.224 | 0.040 | — | 11.2 | C |
| 28 | J3 D | 4 | 2 2 2 2 0 | 14610 | 15 | 258 | 231 | 13 | 37 | 5.18 | 0.20 | 0.29 | — | — | — | 47.6 | A |
| 31 | J4 A | 5 | 1 1 1 1 1 | 12074 | 26 | — | 185 | 75 | — | 5.35 | 1.11 | — | 0.387 | 0.043 | — | 9.3 | C |
| 32 | J4 B | 5 | 1 1 1 1 1 | 12090 | 33 | — | 302 | 148 | — | 4.11 | 1.56 | — | 0.261 | 0.047 | — | 9.4 | C |
| 33 | J4 C | 105 | 1 1 1 1 1 | 17154 | 36 | — | 358 | 48 | — | 6.20 | 0.32 | — | 0.355 | 0.019 | — | 30.0 | A |
| 36 | A147 A | 6 | 4 4 4 4 4 | 12771 | 11 | 19 | 244 | 9 | 12 | 4.88 | 0.13 | 0.14 | 0.289 | 0.007 | 0.008 | 89.9 | A |
| 37 | A147 B | 6 | 4 4 4 4 4 | 13119 | 11 | 15 | 316 | 10 | 20 | 4.68 | 0.11 | 0.30 | 0.304 | 0.006 | 0.017 | 104.2 | A |
| 38 | A147 C | 6 | 3 3 3 3 3 | 13156 | 13 | 8 | 247 | 12 | 7 | 5.22 | 0.15 | 0.22 | 0.305 | 0.008 | 0.007 | 66.8 | A |
| 39 | A147 D | 6 | 3 3 3 3 3 | 13444 | 12 | 2 | 185 | 9 | 15 | 4.98 | 0.18 | 0.28 | 0.294 | 0.008 | 0.004 | 67.8 | A |
| 40 | A147 E | 6 | 3 3 3 3 3 | 13049 | 10 | 10 | 176 | 8 | 7 | 4.58 | 0.14 | 0.12 | 0.267 | 0.007 | 0.002 | 76.1 | A |
| 41 | A147 F | 6 | 2 2 2 2 2 | 11922 | 12 | 5 | 87 | 10 | 4 | 3.65 | 0.27 | 0.02 | 0.195 | 0.012 | 0.002 | 37.9 | B |
| 42 | A147 1 | 6 | 3 3 3 3 3 | 12832 | 11 | 29 | 148 | 9 | 3 | 4.35 | 0.16 | 0.09 | 0.252 | 0.008 | 0.013 | 65.8 | A |
| 43 | A160 A | 7 | 2 2 2 2 1 | 11401 | 15 | 3 | 181 | 17 | 19 | 3.86 | 0.26 | 0.04 | 0.250 | 0.017 | — | 35.1 | A |
| 44 | A160 B | 107 | 3 3 1 1 1 | 18258 | 24 | 17 | 192 | 21 | — | 6.61 | 0.30 | — | 0.289 | 0.022 | — | 26.3 | B |
| 45 | A160 C | 7 | 1 1 1 1 0 | 12380 | 34 | — | 412 | 58 | — | 4.61 | 0.37 | — | — | — | — | 27.8 | A |
| 46 | A160 D | 107 | 3 3 0 0 0 | 18271 | 41 | 84 | — | — | — | — | — | — | — | — | — | 36.1 | D |
| 47 | A160 E | 7 | 4 4 4 4 2 | 14056 | 13 | 24 | 226 | 16 | 12 | 5.01 | 0.23 | 0.26 | 0.293 | 0.017 | 0.014 | 39.2 | A |
| 48 | A160 F | 7 | 3 3 3 3 2 | 13657 | 14 | 16 | 176 | 18 | 27 | 5.18 | 0.24 | 0.43 | 0.307 | 0.013 | 0.009 | 33.9 | A |
| 49 | A160 G | 7 | 4 4 4 4 2 | 13137 | 13 | 25 | 196 | 20 | 22 | 4.82 | 0.25 | 0.39 | 0.293 | 0.015 | 0.056 | 32.4 | B |
| 50 | A160 H | 7 | 1 1 1 1 0 | 13589 | 21 | — | 195 | 23 | — | 5.18 | 0.30 | — | — | — | — | 21.6 | A |
| 51 | A160 I | 107 | 3 3 0 0 0 | 18643 | 41 | 30 | — | — | — | — | — | — | — | — | — | 43.9 | D |
| 52 | A160 J | 7 | 4 4 4 4 1 | 11254 | 9 | 13 | 145 | 10 | 15 | 2.74 | 0.20 | 0.32 | 0.217 | 0.041 | — | 46.1 | A* |
| 53 | A160 1 | 107 | 2 2 0 0 0 | 18108 | 50 | 103 | — | — | — | — | — | — | — | — | — | 27.3 | D* |
| 54 | A160 2 | 107 | 1 1 0 0 0 | 18201 | 71 | — | — | — | — | — | — | — | — | — | — | 21.7 | D |
| 56 | A168 A | 108 | 1 1 1 1 0 | 5299 | 19 | — | 265 | 16 | — | 4.35 | 0.26 | — | — | — | — | 51.7 | A |
| 57 | A168 B | 108 | 1 1 1 1 0 | 5253 | 23 | — | 310 | 25 | — | 5.29 | 0.30 | — | — | — | — | 43.6 | A |
| 58 | A168 C | 8 | 1 1 1 1 1 | 13313 | 22 | — | 216 | 22 | — | 4.79 | 0.40 | — | 0.273 | 0.016 | — | 27.1 | A |
| 59 | A168 D | 8 | 1 1 1 1 1 | 13545 | 48 | — | 345 | 58 | — | 5.30 | 0.50 | — | 0.396 | 0.021 | — | 21.7 | B |
| 60 | A168 E | 8 | 1 1 1 1 1 | 13402 | 44 | — | 340 | 54 | — | 4.93 | 0.48 | — | 0.333 | 0.020 | — | 23.6 | B |
| 61 | A168 F | 8 | 1 1 1 1 1 | 13582 | 33 | — | 307 | 41 | — | 5.32 | 0.50 | — | 0.345 | 0.017 | — | 26.3 | A |
| 63 | A168 1 | 8 | 1 1 1 1 1 | 13488 | 25 | — | 230 | 26 | — | 3.76 | 0.47 | — | 0.294 | 0.020 | — | 23.5 | B |
| 65 | A189 A | 9 | 1 1 1 1 1 | 5588 | 24 | — | 250 | 24 | — | 4.55 | 0.32 | — | 0.271 | 0.015 | — | 27.2 | A |
| 66 | A189 B | 9 | 1 1 1 1 1 | 4837 | 25 | — | 181 | 15 | — | 5.61 | 0.27 | — | 0.315 | 0.019 | — | 35.6 | A |
| 68 | A189 D | 109 | 1 1 1 1 1 | 9599 | 29 | — | 296 | 31 | — | 5.93 | 0.30 | — | 0.364 | 0.019 | — | 35.7 | A |
| 69 | J30 A | 10 | 2 2 2 2 2 | 15390 | 16 | 3 | 303 | 12 | 26 | 5.77 | 0.14 | 0.07 | 0.328 | 0.008 | 0.001 | 77.7 | A |
| 70 | J30 B | 10 | 2 2 2 2 2 | 14807 | 12 | 8 | 206 | 9 | 2 | 4.95 | 0.15 | 0.22 | 0.293 | 0.008 | 0.011 | 65.2 | A |
| 71 | J30 C | 10 | 2 2 2 2 2 | 14704 | 13 | 9 | 204 | 9 | 20 | 5.17 | 0.18 | 0.09 | 0.303 | 0.009 | 0.007 | 65.6 | A |
| 72 | J30 D | 10 | 2 2 2 2 2 | 16451 | 13 | 19 | 234 | 9 | 4 | 5.50 | 0.14 | 0.06 | 0.313 | 0.008 | 0.001 | 73.4 | A |

**Table 5** – *continued*

| (1) GIN | (2) Galaxy Name | (3) CAN | (4) $N$ $s\ z\ \sigma\ b\ 2$ | (5) $cz$ (km s$^{-1}$) | (6) $\Delta cz$ | (7) $\delta cz$ | (8) $\sigma$ (km s$^{-1}$) | (9) $\Delta\sigma$ | (10) $\delta\sigma$ | (11) Mg$b$ | (12) $\Delta$Mg$b$ (Å) | (13) $\delta$Mg$b$ | (14) $Mg_2$ | (15) $\Delta Mg_2$ (mag) | (16) $\delta Mg_2$ | (17) S/N | (18) $Q$ |
|---|---|---|---|---|---|---|---|---|---|---|---|---|---|---|---|---|---|
| 73 | J30 E | 10 | 2 2 2 2 2 | 15253 | 13 | 3 | 223 | 9 | 0 | 4.81 | 0.18 | 0.03 | 0.284 | 0.008 | 0.000 | 66.4 | A |
| 74 | J30 F | 210 | 2 2 2 2 2 | 20957 | 12 | 6 | 234 | 7 | 9 | 5.43 | 0.14 | 0.12 | 0.317 | 0.007 | 0.001 | 84.4 | A |
| 75 | J30 G | 110 | 2 2 0 0 0 | 12206 | 50 | 4 | — | — | — | — | — | — | — | — | — | 52.4 | D* |
| 76 | J30 1 | 10 | 2 2 2 2 2 | 15752 | 13 | 1 | 202 | 8 | 10 | 4.83 | 0.17 | 0.01 | 0.317 | 0.008 | 0.003 | 71.0 | A |
| 77 | J30 2 | 10 | 2 2 2 2 2 | 16463 | 11 | 6 | 58 | 8 | 8 | 3.16 | 0.30 | 0.11 | 0.211 | 0.011 | 0.010 | 43.0 | B |
| 78 | A193 A | 11 | 1 1 1 1 1 | 14740 | 68 | — | 629 | 132 | — | 2.24 | 0.27 | — | 0.216 | 0.014 | — | 34.4 | A |
| 79 | A193 B | 11 | 1 1 1 1 1 | 14673 | 25 | — | 187 | 16 | — | 5.86 | 0.32 | — | 0.348 | 0.019 | — | 32.3 | B |
| 80 | A193 C | 11 | 1 1 1 1 1 | 14395 | 28 | — | 221 | 26 | — | 5.45 | 0.39 | — | 0.348 | 0.020 | — | 25.6 | B |
| 81 | A193 D | 11 | 1 1 1 1 1 | 15181 | 25 | — | 254 | 29 | — | 4.02 | 0.50 | — | 0.281 | 0.017 | — | 26.5 | B |
| 84 | J32 A | 12 | 3 3 3 3 3 | 12367 | 12 | 6 | 251 | 9 | 11 | 5.18 | 0.15 | 0.33 | 0.339 | 0.008 | 0.009 | 72.3 | A |
| 85 | J32 B | 12 | 3 3 3 3 3 | 11647 | 11 | 7 | 273 | 8 | 6 | 4.99 | 0.13 | 0.27 | 0.309 | 0.007 | 0.012 | 95.6 | A |
| 86 | J32 C | 112 | 3 3 0 0 0 | 20992 | 41 | 62 | — | — | — | — | — | — | — | — | — | 73.9 | D* |
| 87 | J32 D | 12 | 2 2 2 2 2 | 12252 | 13 | 1 | 196 | 8 | 11 | 5.24 | 0.17 | 0.17 | 0.329 | 0.008 | 0.011 | 70.6 | A |
| 88 | J32 E | 12 | 2 2 2 2 2 | 12345 | 13 | 3 | 247 | 8 | 3 | 5.03 | 0.15 | 0.22 | 0.322 | 0.008 | 0.005 | 81.3 | A |
| 89 | J32 F | 12 | 2 2 2 2 2 | 12192 | 11 | 22 | 116 | 8 | 1 | 2.75 | 0.25 | 0.15 | 0.124 | 0.009 | 0.000 | 50.7 | A |
| 90 | J32 G | 12 | 2 2 2 2 2 | 13338 | 11 | 1 | 101 | 7 | 3 | 3.82 | 0.20 | 0.10 | 0.240 | 0.010 | 0.002 | 57.1 | A |
| 92 | J32 1 | 12 | 3 3 2 2 2 | 12694 | 12 | 5 | 109 | 11 | 20 | 3.78 | 0.26 | 0.19 | 0.182 | 0.011 | 0.011 | 36.7 | A |
| 93 | J32 2 | 12 | 2 2 2 2 2 | 12251 | 12 | 6 | 202 | 7 | 4 | 4.84 | 0.17 | 0.47 | 0.291 | 0.008 | 0.001 | 74.7 | A |
| 94 | J32 3 | 12 | 2 2 2 2 2 | 11938 | 12 | 10 | 144 | 8 | 19 | 4.54 | 0.19 | 0.03 | 0.301 | 0.009 | 0.015 | 60.0 | A |
| 95 | J32 4 | 12 | 2 2 2 2 2 | 12398 | 12 | 8 | 127 | 8 | 9 | 3.83 | 0.24 | 0.10 | 0.209 | 0.009 | 0.002 | 51.1 | A |
| 96 | A260 A | 13 | 1 1 1 1 1 | 10651 | 33 | — | 346 | 106 | — | 5.90 | 0.73 | — | 0.415 | 0.024 | — | 17.8 | B |
| 97 | A260 B | 13 | 2 2 1 1 1 | 11391 | 19 | 4 | 182 | 14 | — | 5.64 | 0.31 | — | 0.335 | 0.015 | — | 30.3 | A |
| 98 | A260 C | 13 | 1 1 1 1 1 | 10296 | 30 | — | 295 | 122 | — | 4.09 | 1.23 | — | 0.305 | 0.034 | — | 11.5 | C |
| 99 | A260 D | 13 | 1 1 1 1 1 | 11721 | 17 | — | 139 | 11 | — | 4.36 | 0.29 | — | 0.215 | 0.015 | — | 28.6 | A |
| 100 | A260 E | 13 | 1 1 1 1 1 | 11789 | 31 | — | 283 | 88 | — | 6.51 | 0.77 | — | 0.368 | 0.033 | — | 14.5 | B |
| 101 | A260 F | 13 | 1 1 1 1 1 | 10613 | 23 | — | 154 | 60 | — | 4.50 | 1.41 | — | 0.282 | 0.037 | — | 10.1 | C |
| 102 | A260 G | 13 | 1 1 1 1 1 | 10557 | 20 | — | 257 | 18 | — | 5.22 | 0.25 | — | 0.319 | 0.013 | — | 40.2 | A |
| 103 | A260 H | 13 | 1 1 1 1 1 | 11573 | 19 | — | 223 | 16 | — | 5.14 | 0.25 | — | 0.304 | 0.014 | — | 37.6 | A |
| 105 | A262 A | 14 | 3 3 3 3 2 | 4845 | 16 | 5 | 194 | 23 | 18 | 6.71 | 0.41 | 0.33 | 0.392 | 0.020 | 0.000 | 23.3 | B |
| 106 | A262 B | 14 | 2 2 2 2 1 | 5227 | 18 | 15 | 216 | 17 | 3 | 4.53 | 0.27 | 0.05 | 0.315 | 0.015 | — | 30.4 | B |
| 107 | A262 C | 14 | 2 2 2 2 1 | 5086 | 15 | 10 | 224 | 11 | 1 | 4.36 | 0.21 | 0.19 | 0.317 | 0.012 | — | 50.4 | A |
| 108 | A262 D | 14 | 2 2 2 2 1 | 5036 | 15 | 3 | 229 | 11 | 0 | 4.38 | 0.18 | 0.04 | 0.328 | 0.011 | — | 51.0 | A |
| 109 | A262 E | 14 | 1 1 1 1 1 | 5346 | 18 | — | 178 | 11 | — | 4.12 | 0.26 | — | 0.254 | 0.012 | — | 35.7 | A |
| 110 | A262 F | 14 | 1 1 1 1 1 | 5330 | 20 | — | 221 | 16 | — | 4.40 | 0.28 | — | 0.301 | 0.014 | — | 31.1 | A |
| 111 | A262 G | 14 | 2 2 2 2 1 | 4644 | 17 | 7 | 241 | 14 | 17 | 4.43 | 0.22 | 0.08 | 0.255 | 0.011 | — | 43.3 | A |
| 112 | A262 H | 14 | 1 1 1 1 1 | 4808 | 17 | — | 101 | 10 | — | 3.71 | 0.32 | — | 0.206 | 0.014 | — | 26.4 | B |
| 113 | A262 I | 14 | 1 1 1 1 1 | 5584 | 22 | — | 180 | 19 | — | 4.97 | 0.44 | — | 0.293 | 0.016 | — | 19.4 | B |
| 114 | A262 1 | 14 | 1 1 1 1 0 | 5542 | 18 | — | 102 | 12 | — | 1.27 | 0.34 | — | — | — | — | 34.3 | A |
| 115 | J7 A | 15 | 1 1 1 1 1 | 10801 | 50 | — | 231 | 49 | — | 4.29 | 0.63 | — | 0.289 | 0.025 | — | 19.0 | B |
| 116 | J7 B | 15 | 1 1 1 1 1 | 10009 | 61 | — | 285 | 61 | — | 4.91 | 0.48 | — | 0.307 | 0.023 | — | 21.4 | A |
| 117 | J7 C | 15 | 1 1 1 1 1 | 10683 | 41 | — | 201 | 40 | — | 3.85 | 0.56 | — | 0.286 | 0.024 | — | 19.9 | B |
| 118 | J7 D | 15 | 1 1 1 1 1 | 10538 | 50 | — | 183 | 54 | — | 4.85 | 0.81 | — | 0.315 | 0.028 | — | 14.5 | B |
| 119 | J7 E | 15 | 1 1 1 1 1 | 10765 | 23 | — | 295 | 24 | — | 5.71 | 0.27 | — | 0.333 | 0.014 | — | 36.9 | A |
| 120 | J7 F | 15 | 1 1 1 1 1 | 11553 | 17 | — | 161 | 10 | — | 4.89 | 0.26 | — | 0.300 | 0.014 | — | 37.7 | A |
| 122 | J8 A | 16 | 2 2 2 2 1 | 8528 | 27 | 8 | 294 | 29 | 25 | 4.75 | 0.33 | 0.55 | 0.306 | 0.015 | — | 32.3 | A |
| 124 | J8 C | 16 | 3 3 3 3 3 | 9430 | 23 | 15 | 246 | 26 | 23 | 4.62 | 0.31 | 0.45 | 0.321 | 0.012 | 0.006 | 30.0 | B |
| 125 | J8 D | 16 | 3 3 3 3 3 | 9492 | 15 | 2 | 108 | 17 | 25 | 4.37 | 0.47 | 0.48 | 0.310 | 0.017 | 0.031 | 18.7 | C |
| 126 | J8 E | 16 | 2 2 2 2 2 | 9610 | 25 | 7 | 373 | 27 | 11 | 4.76 | 0.24 | 0.04 | 0.343 | 0.010 | 0.013 | 48.7 | A |
| 127 | J8 F | 16 | 1 1 1 1 1 | 10208 | 20 | — | 198 | 16 | — | 4.89 | 0.33 | — | 0.312 | 0.015 | — | 26.5 | A |
| 128 | J8 G | 16 | 2 2 2 2 1 | 9043 | 14 | 4 | 176 | 12 | 2 | 4.57 | 0.26 | 0.03 | 0.265 | 0.013 | — | 35.9 | A |
| 129 | J8 H | 16 | 1 1 1 1 1 | 9072 | 16 | — | 71 | 9 | — | 3.23 | 0.36 | — | 0.143 | 0.014 | — | 23.3 | B |
| 130 | J8 I | 16 | 1 1 1 1 1 | 9218 | 20 | — | 176 | 15 | — | 4.75 | 0.30 | — | 0.288 | 0.014 | — | 24.8 | B |
| 132 | J8 K | 16 | 1 1 1 1 1 | 9782 | 21 | — | 196 | 18 | — | 4.55 | 0.48 | — | 0.283 | 0.016 | — | 23.3 | B |
| 135 | A376 A | 17 | 1 1 1 1 1 | 14549 | 38 | — | 254 | 51 | — | 6.08 | 0.64 | — | 0.440 | 0.022 | — | 17.2 | B |
| 136 | A376 B | 17 | 1 1 1 1 1 | 13619 | 32 | — | 212 | 39 | — | 4.53 | 0.81 | — | 0.248 | 0.022 | — | 17.0 | B |
| 137 | A376 C | 17 | 1 1 1 1 1 | 14142 | 49 | — | 304 | 73 | — | 4.40 | 0.62 | — | 0.306 | 0.022 | — | 16.7 | B |
| 138 | A376 D | 17 | 1 1 1 1 0 | 14826 | 22 | — | 212 | 20 | — | 5.48 | 0.35 | — | — | — | — | 25.8 | B |
| 139 | A376 E | 17 | 2 2 1 1 1 | 15003 | 21 | 5 | 205 | 22 | — | 4.45 | 0.47 | — | 0.266 | 0.018 | — | 23.9 | B |
| 140 | A376 F | 17 | 2 2 2 2 1 | 13955 | 17 | 10 | 166 | 25 | 23 | 3.33 | 0.49 | 0.49 | 0.267 | 0.034 | — | 18.3 | C |
| 141 | A376 G | 17 | 1 1 1 1 0 | 14823 | 23 | — | 236 | 23 | — | 5.95 | 0.31 | — | — | — | — | 25.7 | B |
| 142 | J9 A | 18 | 3 3 2 2 2 | 7763 | 17 | 18 | 276 | 17 | 41 | 4.99 | 0.22 | 0.24 | 0.341 | 0.009 | 0.001 | 48.9 | A |
| 143 | J9 B | 18 | 3 2 2 2 2 | 8754 | 19 | 3 | 232 | 18 | 17 | 5.30 | 0.27 | 0.62 | 0.328 | 0.012 | 0.011 | 31.0 | A |

**Table 5** – *continued*

| (1) GIN | (2) Galaxy Name | (3) CAN | (4) $N$ $s\ z\ \sigma\ b\ 2$ | (5) $cz$ (km s$^{-1}$) | (6) $\Delta cz$ | (7) $\delta cz$ | (8) $\sigma$ (km s$^{-1}$) | (9) $\Delta\sigma$ | (10) $\delta\sigma$ | (11) Mg$b$ | (12) $\Delta$Mg$b$ (Å) | (13) $\delta$Mg$b$ | (14) $Mg_2$ | (15) $\Delta Mg_2$ (mag) | (16) $\delta Mg_2$ | (17) S/N | (18) $Q$ |
|---|---|---|---|---|---|---|---|---|---|---|---|---|---|---|---|---|---|
| 144 | J9 C | 18 | 2 2 2 2 2 | 8666 | 21 | 13 | 328 | 24 | 18 | 4.92 | 0.22 | 0.08 | 0.341 | 0.009 | 0.018 | 45.1 | A |
| 145 | J9 D | 18 | 1 1 1 1 1 | 8960 | 21 | — | 157 | 18 | — | 3.93 | 0.42 | — | 0.278 | 0.015 | — | 18.6 | B |
| 146 | J9 E | 18 | 1 1 1 1 1 | 8197 | 20 | — | 187 | 16 | — | 4.36 | 0.32 | — | 0.281 | 0.015 | — | 25.3 | A |
| 147 | J9 F | 18 | 1 1 1 1 1 | 7927 | 18 | — | 166 | 11 | — | 4.60 | 0.28 | — | 0.279 | 0.012 | — | 32.5 | A |
| 148 | J9 G | 18 | 1 1 0 0 0 | 8207 | 71 | — | — | — | — | — | — | — | — | — | — | 15.4 | D |
| 149 | J33 A | 19 | 2 1 1 1 1 | 8745 | 24 | — | 266 | 27 | — | 5.62 | 0.34 | — | 0.301 | 0.016 | — | 31.0 | A |
| 150 | J33 B | 19 | 1 1 1 1 1 | 9767 | 20 | — | 162 | 15 | — | 4.48 | 0.34 | — | 0.257 | 0.013 | — | 27.8 | B |
| 151 | A397 A | 20 | 3 3 3 3 3 | 10251 | 13 | 14 | 215 | 10 | 11 | 4.77 | 0.18 | 0.18 | 0.296 | 0.008 | 0.016 | 57.9 | A |
| 152 | A397 B | 20 | 4 4 4 4 4 | 10371 | 12 | 15 | 289 | 11 | 22 | 5.37 | 0.14 | 0.22 | 0.318 | 0.006 | 0.015 | 84.6 | A |
| 153 | A397 C | 20 | 4 4 4 4 4 | 8970 | 11 | 9 | 202 | 9 | 11 | 4.30 | 0.18 | 0.39 | 0.243 | 0.008 | 0.011 | 63.6 | A |
| 154 | A397 D | 20 | 4 4 4 4 4 | 9361 | 12 | 19 | 203 | 10 | 12 | 5.08 | 0.20 | 0.40 | 0.276 | 0.008 | 0.008 | 57.6 | A |
| 155 | A397 E | 20 | 3 2 2 2 2 | 10017 | 12 | 2 | 137 | 9 | 9 | 4.45 | 0.19 | 0.03 | 0.246 | 0.009 | 0.005 | 49.1 | A |
| 156 | A397 F | 20 | 3 3 2 2 2 | 9418 | 15 | 39 | 246 | 13 | 17 | 4.87 | 0.23 | 0.05 | 0.256 | 0.009 | 0.004 | 50.3 | A |
| 157 | A397 G | 20 | 3 3 3 3 3 | 9462 | 12 | 19 | 201 | 10 | 15 | 4.43 | 0.17 | 0.07 | 0.273 | 0.009 | 0.003 | 65.0 | A |
| 158 | A397 H | 120 | 3 3 3 3 2 | 16841 | 15 | 17 | 278 | 14 | 19 | 5.36 | 0.21 | 0.33 | 0.337 | 0.009 | 0.002 | 57.1 | A |
| 159 | A397 I | 20 | 3 3 3 3 3 | 9561 | 11 | 26 | 134 | 9 | 7 | 4.12 | 0.26 | 0.35 | 0.234 | 0.009 | 0.013 | 48.9 | A |
| 160 | A400 A | 21 | 2 2 2 2 1 | 6826 | 18 | 53 | 307 | 17 | 17 | 4.83 | 0.18 | 0.10 | 0.342 | 0.013 | — | 56.0 | A |
| 162 | A400 C | 21 | 2 2 2 2 1 | 7559 | 16 | 15 | 222 | 15 | 13 | 4.06 | 0.23 | 0.32 | 0.290 | 0.014 | — | 39.2 | A |
| 163 | A400 D | 21 | 3 3 3 3 1 | 6758 | 12 | 7 | 185 | 10 | 7 | 4.45 | 0.18 | 0.20 | 0.283 | 0.014 | — | 44.3 | A |
| 164 | A400 E | 21 | 3 3 3 3 1 | 6748 | 14 | 10 | 279 | 15 | 13 | 4.93 | 0.18 | 0.21 | 0.350 | 0.013 | — | 55.3 | A |
| 165 | A400 F | 21 | 3 3 3 3 1 | 7385 | 11 | 9 | 128 | 9 | 7 | 3.72 | 0.27 | 0.35 | 0.215 | 0.015 | — | 35.2 | A |
| 166 | A400 G | 21 | 3 3 3 3 1 | 7225 | 11 | 10 | 153 | 9 | 5 | 4.74 | 0.22 | 0.24 | 0.285 | 0.014 | — | 40.8 | A |
| 167 | A400 H | 21 | 2 2 2 2 1 | 8205 | 12 | 6 | 103 | 14 | 23 | 3.41 | 0.40 | 0.05 | 0.133 | 0.027 | — | 20.7 | C* |
| 168 | A400 I | 21 | 2 2 2 2 0 | 6665 | 13 | 24 | 133 | 26 | 25 | 2.78 | 0.56 | 0.05 | — | — | — | 16.4 | C* |
| 169 | A400 J | 21 | 3 3 3 3 1 | 6287 | 11 | 22 | 207 | 11 | 7 | 4.71 | 0.17 | 0.16 | 0.306 | 0.012 | — | 51.8 | A |
| 170 | A400 K | 21 | 1 1 1 1 0 | 8569 | 20 | — | 157 | 28 | — | 2.49 | 0.53 | — | — | — | — | 17.3 | B* |
| 171 | A400 L | 21 | 2 2 0 0 0 | 6788 | 50 | 28 | — | — | — | — | — | — | — | — | — | 38.1 | D |
| 172 | A400 1 | 21 | 1 1 1 1 0 | 6617 | 21 | — | 135 | 38 | — | 4.49 | 0.61 | — | — | — | — | 13.3 | B |
| 173 | A400 2 | 21 | 1 1 0 0 0 | 8501 | 71 | — | — | — | — | — | — | — | — | — | — | 10.7 | D |
| 174 | J28 A | 22 | 2 2 2 2 2 | 8717 | 17 | 10 | 233 | 14 | 29 | 4.75 | 0.24 | 0.30 | 0.276 | 0.010 | 0.006 | 41.0 | A |
| 175 | J28 B | 22 | 1 1 1 1 1 | 8661 | 19 | — | 210 | 14 | — | 4.09 | 0.32 | — | 0.265 | 0.012 | — | 34.6 | A |
| 176 | J28 C | 22 | 1 1 1 1 1 | 8621 | 20 | — | 207 | 16 | — | 4.81 | 0.33 | — | 0.285 | 0.012 | — | 27.1 | B |
| 177 | A419 A | 23 | 4 4 4 4 4 | 20331 | 13 | 7 | 323 | 12 | 14 | 5.55 | 0.15 | 0.17 | 0.344 | 0.006 | 0.010 | 87.3 | A |
| 178 | A419 B | 23 | 4 4 3 3 3 | 21197 | 10 | 9 | 110 | 8 | 16 | 3.56 | 0.22 | 0.16 | 0.229 | 0.009 | 0.012 | 50.3 | B |
| 179 | A419 C | 23 | 3 3 3 3 3 | 21099 | 12 | 20 | 277 | 10 | 8 | 6.33 | 0.16 | 0.42 | 0.310 | 0.007 | 0.008 | 75.7 | A |
| 180 | A419 D | 23 | 3 3 3 3 3 | 20909 | 10 | 3 | 222 | 7 | 6 | 5.13 | 0.15 | 0.24 | 0.302 | 0.007 | 0.003 | 79.7 | A |
| 182 | A419 F | 23 | 3 3 3 3 3 | 19510 | 11 | 19 | 250 | 9 | 15 | 5.39 | 0.16 | 0.27 | 0.319 | 0.007 | 0.007 | 75.4 | A |
| 183 | A419 G | 123 | 3 3 3 3 3 | 11818 | 10 | 5 | 184 | 6 | 0 | 4.76 | 0.14 | 0.16 | 0.300 | 0.007 | 0.003 | 90.4 | A |
| 184 | A419 H | 23 | 4 4 4 4 4 | 20122 | 11 | 17 | 249 | 7 | 17 | 5.19 | 0.13 | 0.52 | 0.329 | 0.006 | 0.015 | 96.6 | A |
| 185 | A419 I | 23 | 4 4 4 4 4 | 20382 | 10 | 7 | 232 | 8 | 17 | 4.89 | 0.15 | 0.28 | 0.300 | 0.007 | 0.011 | 80.4 | A |
| 186 | A419 J | 123 | 3 3 3 3 3 | 11887 | 10 | 27 | 214 | 7 | 18 | 5.54 | 0.14 | 0.22 | 0.338 | 0.007 | 0.005 | 82.6 | A |
| 187 | A419 1 | 23 | 3 3 3 3 3 | 19943 | 10 | 19 | 143 | 7 | 6 | 4.90 | 0.21 | 0.37 | 0.292 | 0.008 | 0.005 | 58.5 | A |
| 188 | A419 2 | 23 | 3 3 3 3 3 | 20108 | 10 | 18 | 142 | 8 | 11 | 4.59 | 0.21 | 0.75 | 0.277 | 0.009 | 0.017 | 52.8 | B |
| 189 | A496 A | 24 | 5 5 5 5 5 | 9835 | 11 | 21 | 248 | 10 | 16 | 5.67 | 0.15 | 0.28 | 0.323 | 0.007 | 0.019 | 71.7 | A |
| 190 | A496 B | 24 | 3 3 3 3 3 | 10393 | 11 | 7 | 222 | 9 | 12 | 5.40 | 0.14 | 0.23 | 0.305 | 0.007 | 0.007 | 71.9 | A |
| 192 | A496 D | 24 | 3 3 3 3 3 | 9677 | 11 | 5 | 204 | 9 | 5 | 5.31 | 0.15 | 0.09 | 0.307 | 0.007 | 0.005 | 74.8 | A |
| 193 | A496 1 | 24 | 3 3 3 3 3 | 9405 | 12 | 10 | 204 | 9 | 14 | 4.90 | 0.15 | 0.18 | 0.290 | 0.008 | 0.004 | 71.3 | A |
| 194 | A496 2 | 24 | 4 4 4 4 4 | 9715 | 10 | 19 | 232 | 9 | 33 | 4.93 | 0.12 | 0.11 | 0.273 | 0.006 | 0.018 | 82.4 | A |
| 195 | A496 3 | 24 | 4 4 4 4 4 | 8883 | 9 | 32 | 187 | 6 | 10 | 4.64 | 0.11 | 0.14 | 0.283 | 0.006 | 0.005 | 98.1 | A |
| 196 | J34 A | 25 | 2 2 2 2 1 | 10790 | 22 | 13 | 273 | 30 | 20 | 7.10 | 0.31 | 1.36 | 0.310 | 0.023 | — | 24.0 | B |
| 197 | J34 B | 25 | 2 2 2 2 1 | 12237 | 15 | 6 | 223 | 15 | 7 | 4.89 | 0.25 | 0.69 | 0.304 | 0.016 | — | 36.5 | A |
| 198 | J34 C | 25 | 1 1 1 1 1 | 10380 | 27 | — | 240 | 39 | — | 4.45 | 0.53 | — | 0.293 | 0.022 | — | 14.3 | C |
| 199 | J34 D | 25 | 2 2 2 2 1 | 10329 | 14 | 16 | 210 | 12 | 21 | 4.81 | 0.22 | 0.27 | 0.272 | 0.014 | — | 39.3 | A |
| 200 | J34 E | 25 | 2 2 2 2 1 | 11610 | 12 | 1 | 153 | 13 | 40 | 4.97 | 0.26 | 0.13 | 0.291 | 0.014 | — | 31.8 | B |
| 201 | J34 F | 25 | 1 1 1 1 1 | 11743 | 19 | — | 232 | 15 | — | 4.42 | 0.23 | — | 0.311 | 0.012 | — | 37.5 | A |
| 202 | J34 1 | 25 | 2 2 1 1 0 | 10882 | 22 | 26 | 251 | 28 | — | 5.74 | 0.28 | — | — | — | — | 24.1 | A |
| 203 | J34 2 | 25 | 2 2 1 1 0 | 10436 | 19 | 6 | 193 | 21 | — | 3.80 | 0.38 | — | — | — | — | 24.2 | A |
| 204 | J34 3 | 25 | 1 1 1 1 0 | 10777 | 17 | — | 71 | 37 | — | 4.23 | 0.76 | — | — | — | — | 10.5 | C* |
| 205 | J34 4 | 25 | 1 1 1 1 1 | 10808 | 35 | — | 238 | 42 | — | 6.24 | 0.50 | — | 0.322 | 0.028 | — | 23.2 | B |
| 206 | J10 A | 26 | 4 4 4 4 4 | 8918 | 17 | 32 | 293 | 17 | 25 | 5.10 | 0.20 | 0.13 | 0.313 | 0.009 | 0.017 | 46.7 | A |
| 207 | J10 B | 26 | 3 2 0 0 0 | 8087 | 50 | 30 | — | — | — | — | — | — | — | — | — | 13.2 | D |
| 208 | J10 C | 26 | 5 5 5 5 5 | 9026 | 17 | 7 | 124 | 22 | 10 | 4.88 | 0.66 | 1.13 | 0.241 | 0.016 | 0.043 | 27.4 | A |

**Table 5** – *continued*

| (1) GIN | (2) Galaxy Name | (3) CAN | (4) $N$ $s\ z\ \sigma\ b\ 2$ | (5) $cz$ (km s$^{-1}$) | (6) $\Delta cz$ | (7) $\delta cz$ | (8) $\sigma$ (km s$^{-1}$) | (9) $\Delta\sigma$ | (10) $\delta\sigma$ | (11) Mg$b$ | (12) $\Delta$Mg$b$ (Å) | (13) $\delta$Mg$b$ | (14) Mg$_2$ | (15) $\Delta$Mg$_2$ (mag) | (16) $\delta$Mg$_2$ | (17) S/N | (18) $Q$ |
|---|---|---|---|---|---|---|---|---|---|---|---|---|---|---|---|---|---|
| 209 | P597-1 A | 27 | 2 2 2 2 0 | 4496 | 21 | 24 | 233 | 40 | 20 | 6.17 | 0.61 | 0.16 | — | — | — | 25.3 | A |
| 210 | P597-1 B | 27 | 3 3 3 3 0 | 4712 | 16 | 33 | 167 | 25 | 13 | 5.12 | 0.51 | 0.15 | — | — | — | 30.0 | B |
| 211 | P597-1 C | 27 | 2 2 2 2 0 | 4165 | 25 | 9 | 200 | 39 | 18 | 5.26 | 0.77 | 0.41 | — | — | — | 23.3 | B |
| 212 | P597-1 D | 27 | 2 2 2 2 0 | 4165 | 26 | 9 | 207 | 39 | 18 | 5.40 | 0.72 | 0.41 | — | — | — | 23.4 | A |
| 213 | P597-1 E | 27 | 2 2 1 1 0 | 5167 | 39 | 33 | 175 | 94 | — | 5.59 | 1.88 | — | — | — | — | 7.4 | C |
| 215 | J35 A | 28 | 2 2 1 1 1 | 9673 | 48 | 271 | 337 | 99 | — | 6.04 | 1.15 | — | 0.367 | 0.041 | — | 10.5 | C |
| 216 | J35 B | 28 | 1 1 1 1 1 | 9461 | 54 | — | 324 | 83 | — | 4.44 | 0.70 | — | 0.370 | 0.026 | — | 16.2 | B |
| 217 | J35 C | 28 | 1 1 1 1 1 | 9530 | 37 | — | 226 | 46 | — | 4.60 | 0.60 | — | 0.351 | 0.023 | — | 16.2 | B |
| 218 | J35 D | 28 | 1 1 1 1 1 | 10061 | 24 | — | 62 | 30 | — | 1.02 | 1.25 | — | 0.204 | 0.044 | — | 8.8 | C |
| 219 | J35 E | 128 | 1 1 1 1 0 | 16920 | 28 | — | 379 | 34 | — | 5.21 | 0.27 | — | — | — | — | 40.5 | A |
| 220 | J35 1 | 28 | 1 1 1 1 1 | 11423 | 18 | — | 153 | 12 | — | 4.50 | 0.29 | — | 0.262 | 0.013 | — | 34.3 | A |
| 221 | J34/35 A | 29 | 1 1 1 1 1 | 9502 | 22 | — | 198 | 26 | — | 3.19 | 0.64 | — | 0.249 | 0.021 | — | 20.0 | B |
| 222 | J34/35 B | 29 | 1 1 1 1 1 | 10733 | 32 | — | 220 | 39 | — | 4.10 | 0.59 | — | 0.277 | 0.021 | — | 17.4 | A |
| 223 | J34/35 C | 29 | 1 1 1 1 1 | 8994 | 18 | — | 124 | 16 | — | 3.94 | 0.60 | — | 0.175 | 0.024 | — | 15.1 | C |
| 224 | J34/35 D | 29 | 1 1 1 1 1 | 8774 | 17 | — | 75 | 13 | — | 2.90 | 0.44 | — | 0.182 | 0.024 | — | 17.6 | C |
| 226 | J34/35 2 | 129 | 1 1 1 1 1 | 16483 | 26 | — | 210 | 20 | — | 5.87 | 0.33 | — | 0.312 | 0.020 | — | 30.5 | B |
| 227 | J34/35 3 | 29 | 1 1 1 1 1 | 9455 | 24 | — | 69 | 6 | — | 4.79 | 0.27 | — | 0.266 | 0.019 | — | 29.7 | B |
| 229 | P777-1 B | 130 | 2 2 2 2 2 | 16760 | 15 | 7 | 211 | 14 | 4 | 5.75 | 0.23 | 0.61 | 0.357 | 0.011 | 0.002 | 31.3 | B |
| 230 | P777-1 C | 30 | 2 2 2 2 2 | 12711 | 19 | 16 | 243 | 20 | 4 | 5.27 | 0.30 | 0.28 | 0.344 | 0.012 | 0.003 | 31.5 | A |
| 232 | P777-2 A | 31 | 2 2 2 2 1 | 7356 | 14 | 22 | 199 | 9 | 8 | 4.72 | 0.15 | 0.25 | 0.300 | 0.009 | — | 51.1 | A |
| 233 | P777-2 B | 131 | 2 2 2 2 2 | 9139 | 12 | 3 | 156 | 8 | 4 | 4.31 | 0.15 | 0.42 | 0.246 | 0.008 | 0.014 | 52.3 | A |
| 235 | P777-2 D | 131 | 1 1 1 1 1 | 9713 | 16 | — | 140 | 7 | — | 4.72 | 0.17 | — | 0.276 | 0.010 | — | 43.0 | A |
| 236 | P777-2 E | 31 | 1 1 1 1 1 | 7309 | 17 | — | 214 | 12 | — | 4.65 | 0.17 | — | 0.300 | 0.011 | — | 39.6 | A |
| 237 | P777-2 F | 31 | 2 2 2 2 2 | 7198 | 11 | 5 | 58 | 11 | 11 | 2.38 | 0.40 | 0.16 | 0.184 | 0.016 | 0.010 | 18.1 | C |
| 238 | P777-2 1 | 131 | 1 1 1 1 1 | 9301 | 24 | — | 182 | 22 | — | 5.85 | 0.37 | — | 0.299 | 0.015 | — | 21.2 | B |
| 239 | P777-3 A | 32 | 3 3 3 3 3 | 16258 | 12 | 43 | 285 | 11 | 7 | 5.28 | 0.12 | 0.30 | 0.325 | 0.006 | 0.008 | 82.7 | A |
| 240 | P777-3 B | 32 | 3 3 3 3 3 | 16583 | 10 | 8 | 255 | 8 | 8 | 4.81 | 0.10 | 0.04 | 0.281 | 0.006 | 0.012 | 100.4 | A |
| 241 | P777-3 C | 232 | 4 4 4 4 4 | 8926 | 9 | 20 | 220 | 6 | 5 | 5.30 | 0.10 | 0.20 | 0.313 | 0.005 | 0.010 | 113.6 | A |
| 242 | P777-3 D | 332 | 3 3 3 3 3 | 4758 | 9 | 10 | 127 | 5 | 3 | 4.10 | 0.08 | 0.10 | 0.249 | 0.005 | 0.002 | 133.3 | A |
| 243 | P777-3 E | 132 | 3 3 3 3 3 | 13461 | 10 | 8 | 218 | 8 | 2 | 5.26 | 0.12 | 0.12 | 0.318 | 0.007 | 0.007 | 83.1 | A |
| 244 | P777-3 F | 32 | 3 3 3 3 3 | 16674 | 11 | 11 | 283 | 10 | 12 | 5.54 | 0.10 | 0.15 | 0.336 | 0.006 | 0.014 | 94.5 | A |
| 245 | P777-3 G | 32 | 4 4 4 4 4 | 16382 | 11 | 14 | 306 | 9 | 12 | 5.33 | 0.11 | 0.13 | 0.342 | 0.006 | 0.019 | 105.4 | A |
| 246 | P777-3 H | 132 | 3 3 3 3 3 | 13270 | 10 | 10 | 262 | 8 | 6 | 4.97 | 0.10 | 0.11 | 0.301 | 0.006 | 0.003 | 110.0 | A |
| 247 | P777-3 1 | 32 | 3 3 3 3 3 | 16179 | 13 | 14 | 264 | 12 | 14 | 4.83 | 0.17 | 0.29 | 0.299 | 0.008 | 0.014 | 69.7 | A |
| 248 | P777-3 2 | 132 | 2 2 2 2 2 | 13765 | 12 | 15 | 93 | 13 | 38 | 3.58 | 0.45 | 0.00 | 0.161 | 0.017 | 0.009 | 28.8 | C |
| 249 | A533-1 A | 33 | 2 2 2 2 2 | 12423 | 28 | 85 | 315 | 35 | 3 | 4.67 | 0.31 | 0.18 | 0.348 | 0.012 | 0.000 | 34.1 | A |
| 250 | A533-1 B | 33 | 1 1 1 1 1 | 11963 | 26 | — | 182 | 49 | — | 5.04 | 0.40 | — | 0.322 | 0.015 | — | 22.6 | B |
| 251 | A533-1 C | 33 | 2 2 2 2 2 | 12599 | 27 | 28 | 274 | 39 | 9 | 4.67 | 0.42 | 0.46 | 0.354 | 0.018 | 0.001 | 31.0 | A |
| 252 | A533-1 D | 33 | 2 2 2 2 2 | 10346 | 17 | 29 | 214 | 22 | 11 | 4.16 | 0.35 | 0.25 | 0.333 | 0.015 | 0.036 | 29.4 | A |
| 253 | A533-1 E | 33 | 1 1 1 1 1 | 11076 | 23 | — | 163 | 27 | — | 4.81 | 0.66 | — | 0.257 | 0.024 | — | 16.4 | B |
| 254 | A533-1 F | 34 | 1 1 1 1 1 | 14262 | 36 | — | 261 | 44 | — | 4.31 | 0.43 | — | 0.319 | 0.027 | — | 26.3 | B |
| 255 | A533-1 G | 34 | 1 1 1 1 1 | 14061 | 34 | — | 237 | 38 | — | 4.67 | 0.54 | — | 0.326 | 0.028 | — | 25.7 | B |
| 257 | A533 A | 34 | 2 2 2 2 1 | 14512 | 21 | 31 | 274 | 25 | 12 | 5.09 | 0.29 | 0.29 | 0.350 | 0.028 | — | 31.6 | A |
| 258 | A533 B | 34 | 1 1 1 1 1 | 14287 | 74 | — | 381 | 122 | — | 4.03 | 0.77 | — | 0.307 | 0.023 | — | 14.8 | B |
| 259 | A533 C | 34 | 2 2 2 1 1 | 15838 | 24 | 5 | 303 | 33 | 29 | 4.61 | 1.62 | — | 0.371 | 0.041 | — | 28.2 | A |
| 260 | A533 D | 34 | 2 2 2 2 1 | 14922 | 27 | 27 | 326 | 37 | 35 | 5.85 | 0.35 | 0.54 | 0.305 | 0.025 | — | 29.3 | A |
| 261 | A533 E | 34 | 2 2 1 1 0 | 14849 | 22 | 14 | 251 | 28 | — | 4.75 | 0.36 | — | — | — | — | 23.9 | A |
| 262 | A533 F | 34 | 1 1 0 0 0 | 13256 | 71 | — | — | — | — | — | — | — | — | — | — | 12.1 | D |
| 263 | A533 G | 33 | 2 1 1 1 0 | 12362 | 18 | — | 208 | 16 | — | 4.97 | 0.23 | — | — | — | — | 33.5 | A |
| 264 | A533 H | 33 | 1 1 0 0 0 | 10802 | 71 | — | — | — | — | — | — | — | — | — | — | 19.3 | D* |
| 266 | A548-1 A | 35 | 1 1 1 1 1 | 11874 | 19 | — | 207 | 17 | — | 5.96 | 0.31 | — | 0.384 | 0.012 | — | 25.8 | B |
| 267 | A548-1 B | 35 | 1 1 1 1 1 | 12000 | 22 | — | 295 | 24 | — | 5.85 | 0.22 | — | 0.345 | 0.011 | — | 34.0 | A |
| 268 | A548-1 C | 35 | 3 3 3 3 3 | 12806 | 10 | 9 | 148 | 9 | 34 | 4.29 | 0.23 | 0.42 | 0.241 | 0.009 | 0.045 | 45.6 | A |
| 269 | A548-1 D | 35 | 3 3 3 3 3 | 13096 | 12 | 11 | 270 | 10 | 2 | 5.19 | 0.16 | 0.26 | 0.313 | 0.007 | 0.006 | 72.0 | A |
| 270 | A548-1 E | 36 | 3 3 3 3 3 | 13615 | 14 | 7 | 323 | 14 | 33 | 5.22 | 0.15 | 0.16 | 0.331 | 0.006 | 0.009 | 73.4 | A |
| 271 | A548-1 F | 35 | 3 3 3 3 3 | 12775 | 9 | 13 | 115 | 8 | 28 | 4.34 | 0.22 | 0.32 | 0.233 | 0.009 | 0.012 | 46.3 | A |
| 272 | A548-1 G | 35 | 3 3 3 3 3 | 11287 | 11 | 21 | 225 | 9 | 8 | 4.45 | 0.14 | 0.19 | 0.269 | 0.007 | 0.016 | 72.2 | A |
| 273 | A548-1 H | 35 | 1 1 1 1 1 | 11845 | 18 | — | 244 | 14 | — | 4.82 | 0.16 | — | 0.281 | 0.010 | — | 39.9 | A |
| 274 | A548-1 I | 36 | 1 1 1 1 1 | 12769 | 19 | — | 246 | 17 | — | 5.26 | 0.22 | — | 0.300 | 0.010 | — | 36.2 | A |
| 275 | A548-1 J | 36 | 1 1 1 1 1 | 12653 | 19 | — | 243 | 18 | — | 5.41 | 0.25 | — | 0.319 | 0.012 | — | 33.4 | A |
| 276 | A548-1 K | 35 | 3 1 1 1 1 | 12651 | 19 | — | 178 | 16 | — | 4.18 | 0.40 | — | 0.268 | 0.015 | — | 27.4 | B |
| 277 | A548-1 L | 35 | 1 1 1 1 1 | 11386 | 17 | — | 238 | 13 | — | 4.28 | 0.20 | — | 0.237 | 0.010 | — | 43.3 | A |

**Table 5** – *continued*

| (1) GIN | (2) Galaxy Name | (3) CAN | (4) $N$ $s\,z\,\sigma\,b\,2$ | (5) $cz$ (km s$^{-1}$) | (6) $\Delta cz$ | (7) $\delta cz$ | (8) $\sigma$ (km s$^{-1}$) | (9) $\Delta\sigma$ | (10) $\delta\sigma$ | (11) Mg$b$ | (12) $\Delta$Mg$b$ (Å) | (13) $\delta$Mg$b$ | (14) $Mg_2$ | (15) $\Delta Mg_2$ (mag) | (16) $\delta Mg_2$ | (17) S/N | (18) $Q$ |
|---|---|---|---|---|---|---|---|---|---|---|---|---|---|---|---|---|---|
| 278 | A548-1 M | 35 | 1 1 1 1 1 | 11558 | 17 | — | 208 | 13 | — | 4.73 | 0.22 | — | 0.258 | 0.010 | — | 35.2 | A |
| 279 | A548-1 N | 35 | 3 3 3 3 3 | 11541 | 12 | 25 | 250 | 10 | 11 | 5.53 | 0.16 | 0.21 | 0.301 | 0.006 | 0.013 | 68.5 | A |
| 280 | A548-1 O | 35 | 3 3 3 3 3 | 10730 | 10 | 7 | 177 | 8 | 12 | 4.32 | 0.14 | 0.34 | 0.247 | 0.006 | 0.014 | 70.9 | A |
| 281 | A548-1 P | 36 | 1 1 1 1 1 | 12709 | 21 | — | 250 | 22 | — | 4.67 | 0.28 | — | 0.280 | 0.012 | — | 28.3 | B |
| 282 | A548-1 Q | 36 | 4 4 4 4 3 | 13755 | 11 | 50 | 223 | 10 | 27 | 5.28 | 0.18 | 0.44 | 0.330 | 0.008 | 0.005 | 57.9 | A |
| 283 | A548-1 R | 35 | 4 2 2 2 2 | 12645 | 20 | 20 | 230 | 24 | 10 | 4.06 | 0.35 | 0.09 | 0.285 | 0.014 | 0.009 | 26.0 | B |
| 285 | A548-2 A | 35 | 5 5 5 5 3 | 11861 | 11 | 107 | 269 | 11 | 12 | 5.09 | 0.12 | 0.24 | 0.303 | 0.007 | 0.016 | 66.0 | A |
| 286 | A548-2 B | 35 | 3 3 3 3 2 | 11548 | 14 | 26 | 284 | 14 | 17 | 5.05 | 0.15 | 0.27 | 0.274 | 0.008 | 0.028 | 53.2 | A |
| 287 | A548-2 C | 35 | 3 3 0 0 0 | 11040 | 41 | 34 | — | — | — | — | — | — | — | — | — | 30.5 | D* |
| 288 | A548-2 D | 35 | 2 2 2 2 1 | 11831 | 15 | 11 | 272 | 14 | 10 | 5.16 | 0.16 | 0.06 | 0.295 | 0.010 | — | 50.8 | A |
| 289 | A548-2 E | 35 | 1 1 1 1 0 | 11141 | 18 | — | 80 | 51 | — | 4.11 | 0.96 | — | — | — | — | 7.9 | C |
| 290 | A548-2 F | 35 | 4 4 3 3 1 | 11345 | 12 | 32 | 215 | 12 | 17 | 4.25 | 0.19 | 0.15 | 0.287 | 0.013 | — | 47.4 | A |
| 291 | A548-2 G | 35 | 3 3 3 3 1 | 11919 | 10 | 11 | 173 | 8 | 7 | 4.32 | 0.14 | 0.31 | 0.240 | 0.010 | — | 52.5 | A |
| 292 | A548-2 H | 35 | 4 4 4 4 1 | 12765 | 11 | 22 | 220 | 11 | 12 | 4.90 | 0.17 | 0.13 | 0.250 | 0.014 | — | 49.0 | A |
| 293 | A548-2 I | 136 | 2 2 2 2 1 | 8998 | 14 | 27 | 226 | 11 | 4 | 4.75 | 0.15 | 0.04 | 0.296 | 0.010 | — | 45.7 | A |
| 294 | A548-2 J | 136 | 2 2 2 2 1 | 8529 | 11 | 20 | 62 | 12 | 9 | 3.56 | 0.32 | 0.19 | 0.202 | 0.019 | — | 24.9 | B |
| 295 | A548-2 K | 35 | 4 4 4 4 2 | 12662 | 11 | 17 | 197 | 10 | 12 | 5.61 | 0.19 | 0.59 | 0.304 | 0.010 | 0.008 | 48.6 | A |
| 296 | A548-2 L | 35 | 3 1 0 0 0 | 12569 | 71 | — | — | — | — | — | — | — | — | — | — | 12.3 | D |
| 297 | A548-2 M | 35 | 3 1 0 0 0 | 10600 | 71 | — | — | — | — | — | — | — | — | — | — | 7.9 | D* |
| 298 | A548-2 N | 36 | 2 2 2 2 1 | 11667 | 20 | 9 | 311 | 24 | 20 | 4.83 | 0.25 | 0.24 | 0.290 | 0.015 | — | 38.4 | A |
| 299 | A548-2 O | 35 | 3 3 3 3 1 | 11310 | 14 | 8 | 204 | 16 | 23 | 4.66 | 0.27 | 0.43 | 0.303 | 0.028 | — | 36.5 | A |
| 300 | A548-2 1 | 35 | 3 3 3 3 0 | 11161 | 10 | 16 | 69 | 15 | 2 | 3.53 | 0.31 | 0.25 | — | — | — | 26.2 | B |
| 301 | A548-2 2 | 35 | 3 3 3 3 0 | 11581 | 16 | 37 | 277 | 19 | 19 | 4.57 | 0.21 | 0.07 | — | — | — | 39.7 | A |
| 302 | J11 A | 37 | 7 7 7 7 3 | 8853 | 9 | 22 | 217 | 8 | 11 | 4.87 | 0.16 | 0.14 | 0.297 | 0.010 | 0.007 | 75.2 | A |
| 303 | J11 B | 37 | 5 4 4 4 3 | 8825 | 11 | 20 | 249 | 10 | 11 | 4.93 | 0.18 | 0.13 | 0.305 | 0.009 | 0.003 | 81.6 | A |
| 304 | J11 C | 37 | 2 2 2 2 2 | 8915 | 19 | 60 | 219 | 20 | 3 | 3.98 | 0.43 | 0.15 | 0.261 | 0.015 | 0.001 | 40.7 | A |
| 305 | J11 D | 37 | 1 1 1 1 1 | 8705 | 21 | — | 143 | 19 | — | 4.10 | 0.49 | — | 0.239 | 0.021 | — | 30.5 | A |
| 306 | J11 E | 137 | 2 1 1 1 1 | 11399 | 20 | — | 126 | 12 | — | 2.62 | 0.67 | — | 0.161 | 0.025 | — | 23.3 | B |
| 307 | J11 F | 37 | 3 3 3 3 1 | 8763 | 13 | 17 | 136 | 12 | 17 | 3.93 | 0.45 | 0.28 | 0.237 | 0.024 | — | 28.5 | B |
| 308 | J11 1 | 37 | 1 1 1 1 1 | 9265 | 33 | — | 210 | 37 | — | 3.79 | 0.58 | — | 0.230 | 0.029 | — | 21.0 | B |
| 310 | J12 A | 38 | 1 1 1 1 1 | 12115 | 41 | — | 268 | 45 | — | 4.00 | 0.74 | — | 0.270 | 0.025 | — | 19.8 | B |
| 311 | J12 B | 338 | 1 1 1 1 1 | 10873 | 36 | — | 298 | 37 | — | 4.66 | 0.51 | — | 0.331 | 0.019 | — | 28.6 | A |
| 312 | J12 C | 38 | 1 1 1 1 1 | 13206 | 34 | — | 202 | 39 | — | 5.01 | 0.77 | — | 0.322 | 0.028 | — | 17.3 | B |
| 313 | J12 D | 238 | 1 1 1 1 1 | 17845 | 28 | — | 232 | 40 | — | 5.82 | 0.66 | — | 0.312 | 0.024 | — | 19.0 | B |
| 314 | J12 E | 38 | 2 2 2 2 2 | 13288 | 15 | 11 | 213 | 11 | 23 | 4.93 | 0.28 | 0.17 | 0.312 | 0.011 | 0.008 | 51.4 | A |
| 315 | J12 F | 38 | 2 2 2 2 2 | 12542 | 18 | 23 | 258 | 17 | 12 | 5.75 | 0.29 | 0.14 | 0.335 | 0.011 | 0.002 | 43.6 | A |
| 316 | J12 1 | 138 | 2 2 2 2 1 | 15408 | 17 | 37 | 218 | 14 | 20 | 4.53 | 0.31 | 0.15 | 0.320 | 0.016 | — | 44.3 | A |
| 317 | J12 2 | 38 | 1 1 1 1 1 | 34905 | 65 | — | 284 | 124 | — | 4.49 | 1.08 | — | 0.331 | 0.048 | — | 10.7 | C |
| 318 | J13 A | 39 | 1 1 1 1 1 | 9333 | 32 | — | 264 | 31 | — | 4.39 | 0.56 | — | 0.286 | 0.022 | — | 20.0 | A |
| 319 | J13 B | 39 | 1 1 1 1 1 | 9323 | 24 | — | 183 | 23 | — | 4.28 | 0.54 | — | 0.238 | 0.020 | — | 27.9 | B |
| 320 | J13 C | 39 | 1 1 1 1 1 | 8724 | 27 | — | 130 | 45 | — | 2.35 | 1.04 | — | 0.107 | 0.038 | — | 11.7 | C |
| 321 | J13 D | 39 | 1 1 1 1 1 | 8728 | 32 | — | 217 | 34 | — | 3.93 | 0.64 | — | 0.269 | 0.022 | — | 21.3 | A |
| 322 | J13 E | 239 | 1 1 1 1 1 | 17438 | 56 | — | 368 | 64 | — | 5.91 | 0.69 | — | 0.305 | 0.024 | — | 21.2 | B |
| 323 | J13 F | 39 | 1 1 1 1 1 | 8625 | 25 | — | 172 | 26 | — | 3.75 | 0.69 | — | 0.253 | 0.022 | — | 24.0 | B |
| 324 | J13 G | 39 | 1 1 1 1 1 | 9060 | 37 | — | 303 | 39 | — | 4.96 | 0.50 | — | 0.313 | 0.022 | — | 28.3 | A |
| 325 | J13 H | 39 | 1 1 1 1 1 | 8764 | 21 | — | 248 | 30 | — | 4.83 | 0.56 | — | 0.282 | 0.023 | — | 24.6 | A |
| 326 | J13 I | 39 | 1 1 1 1 1 | 8857 | 20 | — | 179 | 29 | — | 4.20 | 0.95 | — | 0.287 | 0.025 | — | 19.7 | A |
| 328 | J13 K | 39 | 1 1 1 1 0 | 8927 | 24 | — | 199 | 26 | — | 4.25 | 0.57 | — | — | — | — | 24.1 | A |
| 329 | J13 L | 339 | 1 1 1 1 0 | 15651 | 31 | — | 225 | 40 | — | 5.40 | 0.63 | — | — | — | — | 13.6 | C |
| 330 | J13 M | 39 | 2 2 2 2 2 | 8808 | 16 | 20 | 145 | 18 | 21 | 4.56 | 0.38 | 0.08 | 0.239 | 0.013 | 0.011 | 28.3 | B |
| 331 | J13 N | 139 | 1 1 0 0 0 | 18872 | 72 | — | — | — | — | — | — | — | — | — | — | 17.3 | D |
| 332 | J13 O | 39 | 1 1 0 0 0 | 8762 | 75 | — | — | — | — | — | — | — | — | — | — | 11.8 | D |
| 333 | J13 P | 39 | 1 1 1 1 1 | 8671 | 17 | — | 180 | 10 | — | 4.22 | 0.27 | — | 0.269 | 0.013 | — | 44.6 | A |
| 334 | J13 1 | 139 | 1 1 1 1 0 | 18851 | 47 | — | 331 | 65 | — | 5.57 | 0.67 | — | — | — | — | 15.0 | C |
| 335 | J13 2 | 139 | 1 1 1 1 0 | 19410 | 25 | — | 178 | 29 | — | 6.21 | 0.64 | — | — | — | — | 13.4 | C |
| 336 | J36 A | 40 | 2 2 2 2 2 | 11230 | 23 | 11 | 289 | 25 | 38 | 5.85 | 0.50 | 0.71 | 0.360 | 0.016 | 0.001 | 29.4 | A |
| 337 | J36 B | 40 | 2 2 2 2 2 | 11624 | 19 | 14 | 231 | 21 | 33 | 6.14 | 0.50 | 0.47 | 0.318 | 0.019 | 0.008 | 23.7 | B |
| 338 | J36 C | 140 | 2 2 2 2 0 | 9966 | 27 | 10 | 194 | 23 | 5 | 5.41 | 0.60 | 0.35 | — | — | — | 18.5 | B |
| 339 | J36 D | 40 | 3 3 3 3 3 | 11982 | 16 | 26 | 250 | 14 | 14 | 5.48 | 0.36 | 0.35 | 0.313 | 0.014 | 0.010 | 35.5 | A |
| 340 | J36 1 | 340 | 2 2 1 1 1 | 28974 | 32 | 10 | 159 | 54 | — | 4.42 | 0.99 | — | 0.316 | 0.044 | — | 11.2 | C |
| 341 | J36 2 | 240 | 1 1 1 1 0 | 17291 | 27 | — | 253 | 23 | — | 5.31 | 0.35 | — | — | — | — | 28.6 | A |
| 342 | J36 3 | 140 | 1 1 1 1 1 | 9647 | 21 | — | 187 | 14 | — | 5.16 | 0.35 | — | 0.295 | 0.015 | — | 29.6 | B |

**Table 5** – *continued*

| (1) GIN | (2) Galaxy Name | (3) CAN | (4) $N$ $s\ z\ \sigma\ b\ 2$ | (5) $cz$ (km s$^{-1}$) | (6) $\Delta cz$ | (7) $\delta cz$ | (8) $\sigma$ (km s$^{-1}$) | (9) $\Delta\sigma$ | (10) $\delta\sigma$ | (11) Mg$b$ | (12) $\Delta$Mg$b$ (Å) | (13) $\delta$Mg$b$ | (14) $Mg_2$ | (15) $\Delta Mg_2$ (mag) | (16) $\delta Mg_2$ | (17) S/N | (18) $Q$ |
|---|---|---|---|---|---|---|---|---|---|---|---|---|---|---|---|---|---|
| 343 | J14 A | 41 | 1 1 1 1 1 | 8722 | 30 | — | 255 | 30 | — | 4.45 | 0.52 | — | 0.303 | 0.018 | — | 29.4 | A |
| 344 | J14 B | 41 | 1 1 1 1 1 | 8955 | 28 | — | 205 | 28 | — | 4.30 | 0.62 | — | 0.277 | 0.023 | — | 25.5 | A |
| 345 | J14 C | 41 | 1 1 1 1 1 | 8632 | 31 | — | 158 | 61 | — | 4.16 | 1.78 | — | 0.193 | 0.048 | — | 7.6 | C |
| 346 | J14 D | 41 | 1 1 1 1 1 | 9247 | 34 | — | 213 | 78 | — | 4.00 | 1.12 | — | 0.208 | 0.042 | — | 9.4 | C |
| 347 | J14 1 | 241 | 1 1 1 1 0 | 20534 | 81 | — | 529 | 142 | — | 5.49 | 0.58 | — | — | — | — | 14.6 | C |
| 348 | J14 2 | 41 | 2 2 2 2 2 | 9307 | 16 | 11 | 157 | 14 | 19 | 4.22 | 0.43 | 0.37 | 0.250 | 0.016 | 0.023 | 23.6 | C |
| 349 | J14 3 | 141 | 1 1 1 1 1 | 13280 | 25 | — | 196 | 30 | — | 5.85 | 0.60 | — | 0.299 | 0.024 | — | 14.5 | C* |
| 350 | J14 4 | 141 | 1 1 1 1 0 | 14090 | 19 | — | 164 | 11 | — | 2.83 | 0.31 | — | — | — | — | 32.0 | B |
| 351 | J14 5 | 241 | 1 1 1 1 1 | 20345 | 41 | — | 151 | 61 | — | 4.16 | 1.22 | — | 0.249 | 0.050 | — | 9.4 | C |
| 352 | J14-1 A | 42 | 1 1 1 1 1 | 8721 | 29 | — | 247 | 29 | — | 4.53 | 0.46 | — | 0.307 | 0.020 | — | 29.4 | A |
| 353 | J14-1 B | 42 | 1 1 1 1 1 | 8954 | 28 | — | 205 | 28 | — | 4.29 | 0.61 | — | 0.276 | 0.021 | — | 25.5 | A |
| 354 | J14-1 C | 42 | 1 1 1 1 1 | 8306 | 28 | — | 179 | 30 | — | 3.96 | 0.69 | — | 0.258 | 0.023 | — | 21.3 | A |
| 355 | J14-1 D | 42 | 1 1 1 1 1 | 8842 | 21 | — | 122 | 21 | — | 3.99 | 0.59 | — | 0.238 | 0.021 | — | 26.2 | A |
| 356 | J14-1 E | 42 | 2 2 2 2 0 | 9138 | 19 | 6 | 182 | 15 | 2 | 4.38 | 0.53 | 0.03 | — | — | — | 23.2 | B |
| 357 | J14-1 F | 42 | 2 2 2 2 1 | 8734 | 14 | 9 | 188 | 8 | 20 | 4.31 | 0.25 | 0.13 | 0.263 | 0.013 | — | 59.4 | A |
| 358 | J14-1 1 | 142 | 1 1 1 1 1 | 16133 | 32 | — | 282 | 38 | — | 6.35 | 0.29 | — | 0.311 | 0.016 | — | 30.9 | B |
| 359 | J14-1 2 | 142 | 1 1 1 1 0 | 15649 | 37 | — | 272 | 34 | — | 4.28 | 0.50 | — | — | — | — | 20.9 | B |
| 360 | J14-1 3 | 142 | 1 1 0 0 0 | 16096 | 72 | — | — | — | — | — | — | — | — | — | — | 13.6 | D |
| 361 | J14-1 4 | 142 | 1 1 0 0 0 | 15574 | 73 | — | — | — | — | — | — | — | — | — | — | 25.7 | D* |
| 362 | A1983 A | 43 | 1 1 1 1 1 | 13601 | 47 | — | 298 | 56 | — | 5.36 | 0.67 | — | 0.350 | 0.030 | — | 18.3 | A |
| 363 | A1983 B | 43 | 2 2 2 2 2 | 13205 | 19 | 18 | 289 | 17 | 7 | 5.42 | 0.26 | 0.04 | 0.327 | 0.011 | 0.009 | 55.2 | A |
| 364 | A1983 C | 43 | 1 1 1 1 1 | 14069 | 36 | — | 178 | 48 | — | 6.21 | 1.01 | — | 0.364 | 0.040 | — | 9.9 | B |
| 365 | A1983 D | 43 | 1 1 1 1 1 | 13749 | 43 | — | 254 | 53 | — | 5.55 | 0.77 | — | 0.332 | 0.030 | — | 15.1 | B |
| 366 | A1983 E | 43 | 1 1 1 1 1 | 13426 | 37 | — | 275 | 51 | — | 5.04 | 0.61 | — | 0.278 | 0.024 | — | 18.0 | B |
| 367 | A1983 F | 43 | 1 1 1 1 1 | 13819 | 18 | — | 179 | 13 | — | 4.13 | 0.28 | — | 0.278 | 0.015 | — | 35.2 | B |
| 368 | A1983 G | 43 | 1 1 1 1 1 | 13718 | 18 | — | 221 | 13 | — | 4.79 | 0.28 | — | 0.290 | 0.013 | — | 42.9 | A |
| 369 | A1983 1 | 43 | 2 2 2 2 1 | 13631 | 22 | 8 | 210 | 19 | 20 | 4.80 | 0.37 | 0.14 | 0.314 | 0.036 | — | 27.5 | B |
| 370 | A1983 2 | 43 | 1 1 1 1 0 | 13786 | 18 | — | 127 | 12 | — | 2.96 | 0.55 | — | — | — | — | 22.7 | C* |
| 371 | A1983 3 | 143 | 1 1 1 1 1 | 21438 | 23 | — | 218 | 20 | — | 4.05 | 0.46 | — | 0.357 | 0.018 | — | 33.8 | B |
| 372 | A1991 A | 44 | 1 1 1 1 1 | 17752 | 46 | — | 365 | 67 | — | 6.99 | 0.81 | — | 0.312 | 0.029 | — | 14.5 | B |
| 373 | A1991 B | 44 | 1 1 1 1 1 | 16954 | 35 | — | 260 | 61 | — | 7.28 | 1.50 | — | 0.297 | 0.043 | — | 9.1 | C |
| 374 | A1991 C | 44 | 1 1 1 1 1 | 16696 | 30 | — | 229 | 56 | — | 4.65 | 1.65 | — | 0.227 | 0.048 | — | 9.5 | C |
| 375 | A1991 D | 144 | 1 1 1 1 1 | 13213 | 44 | — | 369 | 65 | — | 5.45 | 0.85 | — | 0.303 | 0.028 | — | 15.4 | B |
| 376 | A1991 E | 144 | 1 1 1 1 1 | 13167 | 51 | — | 446 | 84 | — | 5.75 | 0.93 | — | 0.329 | 0.027 | — | 16.9 | B |
| 377 | A1991 F | 244 | 1 1 1 1 0 | 21199 | 64 | — | 383 | 100 | — | 7.68 | 0.63 | — | — | — | — | 13.0 | C |
| 378 | A1991 1 | 44 | 1 1 1 1 1 | 17578 | 20 | — | 83 | 17 | — | 4.01 | 0.64 | — | 0.277 | 0.025 | — | 22.3 | C |
| 379 | A1991 2 | 44 | 2 2 2 2 0 | 16636 | 28 | 20 | 266 | 38 | 12 | 5.25 | 0.51 | 0.55 | — | — | — | 18.9 | C |
| 380 | A1991 3 | 44 | 2 2 2 2 0 | 16214 | 23 | 28 | 257 | 20 | 17 | 5.87 | 0.27 | 0.30 | — | — | — | 33.5 | B |
| 381 | A1991 4 | 44 | 1 1 0 0 0 | 16504 | 73 | — | — | — | — | — | — | — | — | — | — | 25.4 | D |
| 382 | A1991 5 | 44 | 1 1 1 1 0 | 17261 | 23 | — | 189 | 19 | — | 5.91 | 0.38 | — | — | — | — | 22.8 | B |
| 383 | J16 A | 45 | 1 1 1 1 1 | 10948 | 44 | — | 304 | 49 | — | 5.27 | 0.73 | — | 0.337 | 0.021 | — | 22.3 | A |
| 384 | J16 B | 245 | 1 1 1 1 1 | 14024 | 40 | — | 288 | 44 | — | 4.80 | 0.67 | — | 0.321 | 0.021 | — | 23.1 | A |
| 385 | J16 C | 345 | 1 1 1 1 1 | 7789 | 37 | — | 216 | 44 | — | 4.24 | 0.94 | — | 0.219 | 0.033 | — | 14.9 | B |
| 386 | J16 D | 145 | 1 1 1 1 1 | 15684 | 51 | — | 309 | 65 | — | 4.77 | 0.82 | — | 0.338 | 0.023 | — | 16.9 | B |
| 387 | J16 E | 45 | 2 2 2 2 2 | 10810 | 15 | 14 | 255 | 11 | 11 | 4.89 | 0.22 | 0.12 | 0.305 | 0.011 | 0.009 | 62.4 | A |
| 388 | J16 F | 45 | 2 2 2 2 1 | 11405 | 14 | 53 | 241 | 12 | 7 | 4.65 | 0.21 | 0.21 | 0.301 | 0.014 | — | 77.1 | A |
| 390 | J16 1 | 145 | 1 1 1 1 1 | 15972 | 23 | — | 161 | 14 | — | 3.85 | 0.38 | — | 0.277 | 0.016 | — | 30.0 | B |
| 392 | J16 3 | 45 | 2 1 0 0 0 | 11533 | 72 | — | — | — | — | — | — | — | — | — | — | 13.6 | D |
| 393 | J16 4 | 145 | 1 1 1 1 0 | 15616 | 24 | — | 252 | 19 | — | 4.64 | 0.36 | — | — | — | — | 33.9 | A |
| 394 | J16 5 | 45 | 1 1 1 1 1 | 10930 | 20 | — | 187 | 13 | — | 5.58 | 0.32 | — | 0.326 | 0.016 | — | 33.2 | A |
| 395 | J16-W A | 46 | 1 1 1 1 0 | 10800 | 22 | — | 258 | 35 | — | 5.57 | 0.34 | — | — | — | — | 76.0 | A |
| 396 | J16-W B | 46 | 1 1 1 1 1 | 11325 | 24 | — | 127 | 27 | — | 4.33 | 0.71 | — | 0.282 | 0.027 | — | 16.5 | B |
| 397 | J16-W C | 46 | 1 1 1 1 0 | 10404 | 22 | — | 218 | 33 | — | 4.39 | 0.36 | — | — | — | — | 58.4 | B |
| 398 | J16-W D | 46 | 1 1 1 1 1 | 11137 | 27 | — | 325 | 24 | — | 5.40 | 0.42 | — | 0.356 | 0.021 | — | 29.5 | A |
| 399 | J16-W E | 46 | 1 1 1 1 1 | 10788 | 35 | — | 209 | 44 | — | 5.28 | 0.80 | — | 0.273 | 0.028 | — | 15.9 | B |
| 400 | J16-W F | 46 | 1 1 1 1 0 | 10717 | 21 | — | 142 | 70 | — | 3.51 | 0.36 | — | — | — | — | 67.9 | A |
| 401 | J16-W G | 46 | 1 1 1 1 1 | 11325 | 23 | — | 203 | 16 | — | 4.83 | 0.61 | — | 0.306 | 0.023 | — | 21.9 | A |
| 402 | J16-W H | 46 | 1 1 1 1 0 | 12462 | 23 | — | 234 | 36 | — | 5.23 | 0.38 | — | — | — | — | 48.7 | B |
| 403 | J16-W I | 146 | 1 1 1 1 1 | 23945 | 25 | — | 215 | 23 | — | 2.80 | 0.39 | — | 0.233 | 0.016 | — | 29.3 | B |
| 404 | J16-W 1 | 46 | 1 1 1 1 1 | 11269 | 21 | — | 93 | 9 | — | 2.27 | 0.38 | — | 0.156 | 0.016 | — | 30.0 | B |
| 406 | A2063-S A | 50 | 2 2 2 2 1 | 11785 | 19 | 42 | 221 | 48 | 42 | 5.07 | 0.55 | 0.11 | 0.286 | 0.038 | — | 26.4 | A |
| 408 | A2063-S C | 47 | 1 1 1 1 0 | 13876 | 27 | — | 246 | 23 | — | 6.12 | 0.38 | — | — | — | — | 26.8 | B |

**Table 5** – *continued*

| (1) GIN | (2) Galaxy Name | (3) CAN | (4) *N* *s z σ b* 2 | (5) *cz* (km s$^{-1}$) | (6) Δ*cz* | (7) δ*cz* | (8) *σ* (km s$^{-1}$) | (9) Δ*σ* | (10) δ*σ* | (11) Mg*b* | (12) ΔMg*b* (Å) | (13) δMg*b* | (14) $Mg_2$ | (15) $\Delta Mg_2$ (mag) | (16) $\delta Mg_2$ | (17) S/N | (18) *Q* |
|---|---|---|---|---|---|---|---|---|---|---|---|---|---|---|---|---|---|
| 409 | A2040 A | 48 | 1 1 1 1 0 | 13709 | 24 | — | 187 | 28 | — | 6.14 | 0.60 | — | — | — | — | 15.1 | C |
| 410 | A2040 B | 48 | 1 1 1 1 0 | 13722 | 24 | — | 223 | 20 | — | 5.11 | 0.36 | — | — | — | — | 27.9 | A |
| 411 | A2040 C | 48 | 2 2 2 2 2 | 13213 | 15 | 28 | 196 | 12 | 4 | 5.20 | 0.28 | 0.01 | 0.300 | 0.012 | 0.010 | 37.1 | B |
| 412 | A2040 D | 48 | 1 1 1 1 1 | 31895 | 23 | — | 239 | 22 | — | 5.34 | 0.34 | — | 0.311 | 0.017 | — | 25.5 | B |
| 413 | A2040 E | 48 | 1 1 1 1 1 | 12927 | 63 | — | 336 | 125 | — | 4.97 | 1.11 | — | 0.283 | 0.039 | — | 8.1 | B |
| 414 | A2040 F | 48 | 1 1 1 1 1 | 13449 | 42 | — | 353 | 61 | — | 4.41 | 0.53 | — | 0.314 | 0.027 | — | 29.8 | A |
| 415 | A2040 G | 48 | 1 1 0 0 0 | 13520 | 75 | — | — | — | — | — | — | — | — | — | — | 16.6 | D |
| 416 | A2040 H | 148 | 1 1 0 0 0 | 23099 | 73 | — | — | — | — | — | — | — | — | — | — | 6.6 | D |
| 418 | A2040 2 | 48 | 1 1 1 1 1 | 13723 | 48 | — | 272 | 82 | — | 4.58 | 0.99 | — | 0.312 | 0.037 | — | 9.6 | A |
| 419 | A2052 A | 49 | 2 2 2 2 2 | 10308 | 30 | 9 | 300 | 45 | 19 | 6.04 | 0.71 | 0.32 | 0.323 | 0.023 | 0.020 | 18.2 | B |
| 420 | A2052 B | 49 | 2 2 2 2 2 | 9359 | 17 | 0 | 168 | 21 | 25 | 5.81 | 0.42 | 0.13 | 0.299 | 0.014 | 0.003 | 24.2 | B |
| 421 | A2052 C | 49 | 1 1 1 1 1 | 9983 | 21 | — | 218 | 15 | — | 5.63 | 0.30 | — | 0.302 | 0.014 | — | 36.5 | A |
| 422 | A2052 D | 49 | 1 1 1 1 1 | 9085 | 20 | — | 134 | 18 | — | 4.90 | 0.58 | — | 0.255 | 0.023 | — | 16.5 | C |
| 423 | A2052 E | 49 | 1 1 1 1 1 | 9571 | 22 | — | 160 | 20 | — | 4.67 | 0.61 | — | 0.255 | 0.024 | — | 16.3 | C |
| 424 | A2052 F | 49 | 1 1 1 1 1 | 10328 | 19 | — | 119 | 15 | — | 4.39 | 0.49 | — | 0.183 | 0.024 | — | 18.3 | C |
| 425 | A2052 G | 49 | 1 1 1 1 0 | 10974 | 22 | — | 230 | 15 | — | 4.54 | 0.41 | — | — | — | — | 51.0 | A |
| 426 | A2063 A | 50 | 1 1 1 1 1 | 10223 | 35 | — | 240 | 52 | — | 5.97 | 0.69 | — | 0.344 | 0.023 | — | 17.3 | B |
| 427 | A2063 B | 50 | 2 2 2 2 2 | 10354 | 16 | 90 | 175 | 11 | 5 | 4.73 | 0.29 | 0.13 | 0.268 | 0.012 | 0.001 | 36.3 | A |
| 428 | A2063 C | 50 | 1 1 1 1 1 | 10351 | 21 | — | 198 | 14 | — | 4.36 | 0.33 | — | 0.307 | 0.014 | — | 31.8 | A |
| 429 | A2063 D | 50 | 1 1 1 1 1 | 10375 | 20 | — | 147 | 12 | — | 5.11 | 0.39 | — | 0.304 | 0.015 | — | 25.5 | B |
| 430 | A2063 E | 50 | 1 1 1 1 1 | 9835 | 23 | — | 204 | 18 | — | 5.44 | 0.38 | — | 0.286 | 0.017 | — | 26.3 | B |
| 431 | A2063 F | 50 | 1 1 1 1 1 | 10732 | 19 | — | 137 | 10 | — | 4.82 | 0.38 | — | 0.277 | 0.016 | — | 26.2 | B |
| 432 | A2063 G | 50 | 1 1 1 1 1 | 9868 | 22 | — | 186 | 16 | — | 6.16 | 0.39 | — | 0.367 | 0.017 | — | 26.8 | B |
| 433 | A2063 H | 50 | 1 1 1 1 0 | 10318 | 21 | — | 217 | 14 | — | 4.73 | 0.42 | — | — | — | — | 53.6 | A |
| 436 | A2107 A | 51 | 2 2 2 2 2 | 12525 | 25 | 39 | 324 | 31 | 46 | 4.41 | 0.46 | 0.60 | 0.347 | 0.014 | 0.029 | 25.7 | B |
| 437 | A2107 B | 51 | 1 1 1 1 1 | 12579 | 21 | — | 258 | 33 | — | 4.61 | 0.70 | — | 0.256 | 0.021 | — | 19.9 | B |
| 438 | A2107 C | 51 | 1 1 1 1 1 | 12165 | 26 | — | 172 | 29 | — | 4.16 | 0.70 | — | 0.218 | 0.023 | — | 17.8 | B |
| 439 | A2107 D | 51 | 1 1 1 1 1 | 12955 | 23 | — | 265 | 22 | — | 4.90 | 0.31 | — | 0.316 | 0.015 | — | 40.6 | A |
| 440 | A2107 E | 51 | 1 1 1 1 1 | 12388 | 22 | — | 136 | 13 | — | 4.51 | 0.36 | — | 0.225 | 0.016 | — | 26.5 | B |
| 441 | A2107 1 | 51 | 2 1 1 1 1 | 12949 | 20 | — | 75 | 11 | — | 4.65 | 0.44 | — | 0.292 | 0.018 | — | 30.5 | B |
| 443 | J17 A | 52 | 2 2 2 2 2 | 10102 | 26 | 11 | 264 | 27 | 6 | 5.23 | 0.44 | 0.20 | 0.329 | 0.017 | 0.000 | 33.8 | A |
| 444 | J17 B | 52 | 2 2 2 2 2 | 9980 | 22 | 59 | 175 | 28 | 10 | 3.98 | 0.70 | 0.22 | 0.261 | 0.020 | 0.004 | 21.3 | B |
| 445 | J17 C | 52 | 1 1 1 1 1 | 8956 | 32 | — | 195 | 36 | — | 3.71 | 0.80 | — | 0.239 | 0.025 | — | 17.9 | A |
| 446 | J17 D | 52 | 1 1 1 1 1 | 9925 | 43 | — | 308 | 47 | — | 5.13 | 0.66 | — | 0.330 | 0.022 | — | 23.9 | A |
| 447 | J17 E | 52 | 1 1 1 1 1 | 9955 | 36 | — | 224 | 57 | — | 6.22 | 0.83 | — | 0.251 | 0.029 | — | 13.6 | B |
| 449 | J17 G | 52 | 1 1 1 1 1 | 10978 | 27 | — | 147 | 49 | — | 4.19 | 1.43 | — | 0.219 | 0.037 | — | 9.4 | C |
| 453 | A2147 A | 53 | 1 1 1 1 1 | 10588 | 38 | — | 264 | 59 | — | 4.82 | 0.72 | — | 0.289 | 0.022 | — | 15.4 | B |
| 454 | A2147 B | 53 | 1 1 1 1 1 | 10700 | 35 | — | 246 | 51 | — | 5.97 | 0.80 | — | 0.352 | 0.029 | — | 15.9 | B |
| 455 | A2147 C | 53 | 1 1 1 1 1 | 11654 | 39 | — | 221 | 69 | — | 5.83 | 1.13 | — | 0.348 | 0.039 | — | 10.5 | B |
| 456 | A2147 D | 53 | 1 1 1 1 1 | 11877 | 57 | — | 337 | 109 | — | 5.32 | 1.08 | — | 0.330 | 0.033 | — | 11.4 | B |
| 457 | A2147 E | 53 | 1 1 1 1 0 | 11032 | 22 | — | 253 | 16 | — | 4.42 | 0.41 | — | — | — | — | 59.1 | A |
| 459 | A2147 G | 53 | 1 1 1 1 1 | 11056 | 30 | — | 222 | 40 | — | 5.11 | 0.71 | — | 0.248 | 0.022 | — | 18.2 | A |
| 460 | A2147 H | 53 | 1 1 1 1 1 | 10602 | 48 | — | 259 | 100 | — | 4.57 | 1.13 | — | 0.334 | 0.036 | — | 10.3 | C |
| 461 | A2147 I | 53 | 1 1 1 1 1 | 10418 | 25 | — | 249 | 21 | — | 5.35 | 0.35 | — | 0.307 | 0.014 | — | 30.3 | B |
| 462 | A2147 J | 53 | 1 1 1 1 1 | 11538 | 21 | — | 155 | 14 | — | 4.94 | 0.40 | — | 0.302 | 0.015 | — | 22.1 | B |
| 466 | A2147 4 | 53 | 1 1 1 1 0 | 10673 | 21 | — | 155 | 12 | — | 4.39 | 0.43 | — | — | — | — | 40.9 | B |
| 467 | A2147 5 | 53 | 1 1 1 1 0 | 9498 | 21 | — | 216 | 14 | — | 3.91 | 0.42 | — | — | — | — | 51.4 | A |
| 468 | P386-1 A | 54 | 1 1 1 1 1 | 4410 | 21 | — | 249 | 27 | — | 4.46 | 0.52 | — | 0.309 | 0.019 | — | 30.3 | A |
| 469 | P386-1 B | 154 | 1 1 1 1 1 | 13830 | 22 | — | 191 | 34 | — | 4.56 | 0.94 | — | 0.310 | 0.028 | — | 16.0 | B |
| 471 | P386-1 1 | 254 | 1 1 1 1 1 | 26612 | 74 | — | 382 | 160 | — | 4.54 | 1.45 | — | 0.308 | 0.049 | — | 6.6 | B |
| 472 | P386-2 A | 55 | 2 2 2 2 1 | 9607 | 15 | 29 | 259 | 11 | 2 | 4.90 | 0.21 | 0.10 | 0.296 | 0.013 | — | 68.6 | A |
| 473 | P386-2 B | 55 | 2 2 1 1 1 | 9715 | 17 | 21 | 170 | 10 | — | 4.51 | 0.28 | — | 0.287 | 0.013 | — | 44.1 | A |
| 474 | P386-2 C | 55 | 2 2 2 2 1 | 9589 | 17 | 11 | 210 | 11 | 1 | 4.90 | 0.24 | 0.09 | 0.287 | 0.013 | — | 49.0 | A |
| 476 | P386-2 1 | 155 | 1 1 1 1 1 | 20285 | 32 | — | 134 | 48 | — | 4.59 | 1.86 | — | 0.229 | 0.056 | — | 4.9 | B |
| 478 | A2148 A | 56 | 1 1 1 1 1 | 26874 | 34 | — | 284 | 40 | — | 4.88 | 0.35 | — | 0.283 | 0.017 | — | 30.2 | A |
| 479 | A2148 B | 56 | 1 1 1 1 1 | 25701 | 29 | — | 255 | 30 | — | 4.83 | 0.33 | — | 0.274 | 0.016 | — | 30.6 | A |
| 480 | A2148 C | 256 | 1 1 1 1 1 | 12730 | 23 | — | 123 | 27 | — | 3.83 | 0.60 | — | 0.096 | 0.029 | — | 12.9 | C* |
| 481 | A2148 D | 156 | 1 1 1 1 1 | 7955 | 21 | — | 65 | 12 | — | 1.45 | 0.58 | — | 0.018 | 0.023 | — | 21.3 | C* |
| 482 | A2148 E | 356 | 1 1 0 0 0 | 21558 | 73 | — | — | — | — | — | — | — | — | — | — | 18.7 | D |
| 485 | A2148 2 | 56 | 1 1 1 1 1 | 26265 | 55 | — | 278 | 96 | — | 4.54 | 1.37 | — | 0.288 | 0.045 | — | 6.3 | B |
| 487 | J18 A | 57 | 1 1 1 1 1 | 9630 | 54 | — | 384 | 60 | — | 5.65 | 0.63 | — | 0.371 | 0.019 | — | 24.9 | A |
| 488 | J18 B | 57 | 1 1 1 1 1 | 9018 | 24 | — | 128 | 27 | — | 3.97 | 0.66 | — | 0.234 | 0.022 | — | 20.2 | A |

**Table 5** – *continued*

| (1) GIN | (2) Galaxy Name | (3) CAN | (4) $N$ $s\ z\ \sigma\ b\ 2$ | (5) $cz$ (km s$^{-1}$) | (6) $\Delta cz$ | (7) $\delta cz$ | (8) $\sigma$ (km s$^{-1}$) | (9) $\Delta\sigma$ | (10) $\delta\sigma$ | (11) Mg$b$ | (12) $\Delta$Mg$b$ (Å) | (13) $\delta$Mg$b$ | (14) $Mg_2$ | (15) $\Delta Mg_2$ (mag) | (16) $\delta Mg_2$ | (17) S/N | (18) $Q$ |
|---|---|---|---|---|---|---|---|---|---|---|---|---|---|---|---|---|---|
| 489 | J18 C | 57 | 1 1 1 1 1 | 9517 | 60 | — | 358 | 80 | — | 5.43 | 0.80 | — | 0.299 | 0.028 | — | 16.8 | A |
| 490 | J18 D | 57 | 2 2 2 2 1 | 9729 | 17 | 66 | 106 | 10 | 14 | 3.82 | 0.43 | 0.07 | 0.253 | 0.046 | — | 41.2 | A |
| 491 | J18 E | 57 | 1 1 1 1 1 | 9507 | 23 | — | 179 | 15 | — | 4.12 | 0.33 | — | 0.274 | 0.016 | — | 30.6 | A |
| 492 | J18 F | 57 | 1 1 1 1 1 | 9725 | 21 | — | 114 | 13 | — | 4.68 | 0.32 | — | 0.275 | 0.018 | — | 23.6 | B |
| 493 | J18 1 | 157 | 1 1 1 1 1 | 16075 | 47 | — | 221 | 74 | — | 5.09 | 1.86 | — | 0.254 | 0.055 | — | 4.8 | B |
| 495 | A2151 A | 58 | 1 1 1 1 1 | 10526 | 68 | — | 409 | 128 | — | 5.91 | 0.91 | — | 0.349 | 0.028 | — | 14.8 | B |
| 496 | A2151 B | 58 | 1 1 1 1 1 | 10705 | 22 | — | 209 | 24 | — | 5.06 | 0.43 | — | 0.310 | 0.023 | — | 24.9 | A |
| 497 | A2151 C | 58 | 1 1 1 1 1 | 9917 | 46 | — | 224 | 73 | — | 4.80 | 1.63 | — | 0.272 | 0.055 | — | 5.7 | B |
| 498 | A2151 D | 58 | 1 1 1 1 1 | 9360 | 22 | — | 213 | 16 | — | 4.74 | 0.30 | — | 0.327 | 0.015 | — | 38.8 | A |
| 499 | A2151 E | 58 | 1 1 1 1 1 | 9936 | 21 | — | 162 | 10 | — | 3.49 | 0.31 | — | 0.250 | 0.015 | — | 40.4 | A |
| 500 | A2151 F | 58 | 1 1 1 1 1 | 10355 | 37 | — | 192 | 53 | — | 3.48 | 1.19 | — | 0.221 | 0.037 | — | 8.9 | A |
| 501 | A2151 G | 58 | 1 1 1 1 1 | 12076 | 33 | — | 366 | 51 | — | 5.12 | 0.33 | — | 0.325 | 0.016 | — | 36.3 | A |
| 502 | A2151 H | 58 | 1 1 1 1 1 | 11689 | 23 | — | 225 | 18 | — | 4.11 | 0.33 | — | 0.280 | 0.015 | — | 38.2 | A |
| 503 | A2151 I | 58 | 1 1 1 1 1 | 12020 | 21 | — | 108 | 10 | — | 4.22 | 0.36 | — | 0.203 | 0.016 | — | 27.7 | B |
| 504 | A2151 J | 58 | 1 1 1 1 1 | 11324 | 25 | — | 270 | 27 | — | 4.53 | 0.31 | — | 0.272 | 0.015 | — | 37.1 | A |
| 505 | A2151 K | 58 | 2 2 2 2 2 | 10595 | 16 | 9 | 195 | 11 | 19 | 4.72 | 0.24 | 0.50 | 0.298 | 0.011 | 0.011 | 45.0 | A |
| 506 | A2151 L | 58 | 1 1 1 1 1 | 11373 | 21 | — | 110 | 11 | — | 3.36 | 0.34 | — | 0.188 | 0.017 | — | 27.0 | B |
| 507 | A2151 M | 58 | 1 1 1 1 1 | 11044 | 27 | — | 323 | 29 | — | 5.03 | 0.26 | — | 0.304 | 0.015 | — | 46.7 | A |
| 508 | A2151 N | 58 | 1 1 1 1 1 | 11404 | 23 | — | 251 | 20 | — | 4.67 | 0.30 | — | 0.304 | 0.016 | — | 41.3 | A |
| 509 | A2151 O | 58 | 1 1 1 1 1 | 11631 | 24 | — | 213 | 19 | — | 4.97 | 0.31 | — | 0.282 | 0.016 | — | 33.9 | B |
| 510 | A2151 1 | 58 | 1 1 1 1 1 | 11136 | 58 | — | 285 | 149 | — | 2.11 | 2.74 | — | 0.128 | 0.079 | — | 3.7 | C |
| 511 | A2152 A | 59 | 2 2 2 2 2 | 12066 | 20 | 13 | 280 | 19 | 0 | 5.96 | 0.33 | 0.44 | 0.359 | 0.013 | 0.003 | 32.3 | A |
| 512 | A2152 B | 59 | 1 1 1 1 1 | 13246 | 26 | — | 237 | 19 | — | 5.32 | 0.65 | — | 0.359 | 0.025 | — | 21.3 | A |
| 513 | A2152 C | 59 | 2 2 2 2 2 | 12311 | 17 | 7 | 240 | 15 | 13 | 4.56 | 0.33 | 0.30 | 0.313 | 0.012 | 0.016 | 50.1 | A |
| 514 | A2152 D | 53 | 2 2 2 2 2 | 10896 | 16 | 18 | 162 | 13 | 13 | 4.95 | 0.40 | 0.35 | 0.274 | 0.014 | 0.001 | 28.4 | B |
| 515 | A2152 E | 59 | 1 1 1 1 1 | 11893 | 24 | — | 134 | 33 | — | 5.58 | 0.46 | — | 0.275 | 0.017 | — | 17.1 | B |
| 517 | A2152 G | 53 | 2 2 1 1 0 | 10142 | 19 | 9 | 153 | 11 | — | 4.37 | 0.43 | — | — | — | — | 46.4 | B |
| 518 | A2152 H | 59 | 1 1 1 1 1 | 13283 | 30 | — | 280 | 26 | — | 5.19 | 0.61 | — | 0.321 | 0.024 | — | 20.6 | A |
| 519 | A2152 I | 59 | 1 1 1 1 1 | 13624 | 40 | — | 313 | 34 | — | 6.03 | 0.74 | — | 0.383 | 0.022 | — | 19.1 | A |
| 524 | A2152 N | 59 | 2 2 2 2 2 | 12930 | 19 | 21 | 150 | 13 | 16 | 3.98 | 0.46 | 0.02 | 0.267 | 0.016 | 0.003 | 32.4 | B |
| 525 | A2152 1 | 59 | 1 1 1 1 1 | 13559 | 26 | — | 263 | 26 | — | 4.18 | 0.46 | — | 0.294 | 0.016 | — | 33.6 | A |
| 527 | A2152 3 | 53 | 1 1 1 1 0 | 10412 | 20 | — | 112 | 12 | — | 3.59 | 0.45 | — | — | — | — | 33.7 | B |
| 528 | P445-1 A | 60 | 1 1 1 1 1 | 13618 | 25 | — | 252 | 25 | — | 5.02 | 0.28 | — | 0.313 | 0.016 | — | 35.5 | A |
| 529 | P445-1 B | 60 | 1 1 1 1 1 | 14323 | 24 | — | 181 | 19 | — | 4.19 | 0.31 | — | 0.233 | 0.018 | — | 26.2 | A |
| 530 | P445-1 C | 60 | 1 1 1 1 1 | 13880 | 30 | — | 283 | 35 | — | 4.78 | 0.30 | — | 0.304 | 0.017 | — | 33.3 | A |
| 531 | P445-1 D | 60 | 1 1 1 1 1 | 14329 | 23 | — | 161 | 15 | — | 3.53 | 0.38 | — | 0.217 | 0.016 | — | 27.5 | A |
| 532 | P445-1 E | 260 | 1 1 1 1 1 | 18545 | 30 | — | 247 | 33 | — | 4.23 | 0.38 | — | 0.365 | 0.017 | — | 27.5 | B |
| 533 | P445-1 F | 60 | 1 1 1 1 1 | 13817 | 24 | — | 211 | 18 | — | 5.16 | 0.31 | — | 0.315 | 0.016 | — | 34.6 | A |
| 534 | P445-1 G | 160 | 1 1 1 1 1 | 9823 | 22 | — | 162 | 13 | — | 4.10 | 0.36 | — | 0.297 | 0.016 | — | 31.9 | B |
| 535 | P445-1 1 | 160 | 1 1 1 1 1 | 11125 | 30 | — | 132 | 44 | — | 2.44 | 1.62 | — | 0.232 | 0.047 | — | 6.6 | B |
| 536 | P445-2 A | 53 | 1 1 1 1 1 | 11106 | 25 | — | 343 | 35 | — | 5.24 | 0.31 | — | 0.334 | 0.016 | — | 40.0 | A |
| 537 | P445-2 B | 53 | 1 1 1 1 1 | 10388 | 24 | — | 225 | 20 | — | 5.18 | 0.34 | — | 0.320 | 0.016 | — | 36.2 | A |
| 538 | P445-2 C | 61 | 1 1 1 1 1 | 4742 | 21 | — | 185 | 10 | — | 4.39 | 0.27 | — | 0.251 | 0.014 | — | 48.6 | A |
| 539 | P445-2 D | 61 | 1 1 1 1 1 | 4742 | 21 | — | 137 | 7 | — | 4.13 | 0.26 | — | 0.227 | 0.014 | — | 50.4 | A |
| 540 | A2162-N A | 62 | 1 1 1 1 1 | 14847 | 22 | — | 172 | 16 | — | 6.16 | 0.65 | — | 0.345 | 0.024 | — | 19.8 | A |
| 541 | A2162-N B | 62 | 1 1 1 1 0 | 14395 | 28 | — | 222 | 25 | — | 5.00 | 0.43 | — | — | — | — | 21.2 | B |
| 542 | A2162-N C | 62 | 2 2 2 2 1 | 15172 | 20 | 14 | 201 | 18 | 19 | 5.71 | 0.43 | 0.36 | 0.306 | 0.040 | — | 26.4 | B |
| 543 | A2162-N D | 62 | 1 1 1 1 1 | 15367 | 31 | — | 234 | 24 | — | 5.01 | 0.76 | — | 0.326 | 0.025 | — | 18.6 | B |
| 545 | A2162-N 1 | 62 | 1 1 1 1 1 | 14811 | 53 | — | 301 | 100 | — | 4.89 | 1.12 | — | 0.298 | 0.036 | — | 9.4 | A |
| 546 | A2162-S A | 63 | 2 2 2 2 2 | 9602 | 28 | 16 | 288 | 31 | 31 | 5.53 | 0.41 | 0.24 | 0.360 | 0.015 | 0.006 | 34.6 | A |
| 547 | A2162-S B | 163 | 1 1 1 1 1 | 14994 | 85 | — | 487 | 142 | — | 4.45 | 1.11 | — | 0.354 | 0.032 | — | 15.3 | B |
| 548 | A2162-S C | 163 | 2 2 2 2 2 | 14905 | 18 | 5 | 256 | 13 | 2 | 5.17 | 0.24 | 0.05 | 0.297 | 0.013 | 0.005 | 49.2 | A |
| 549 | A2162-S D | 163 | 1 1 1 1 0 | 16237 | 18 | — | 71 | 14 | — | 4.95 | 0.72 | — | — | — | — | 14.3 | C* |
| 550 | A2162-S E | 163 | 2 2 2 2 1 | 16086 | 14 | 7 | 183 | 10 | 11 | 4.48 | 0.24 | 0.04 | 0.286 | 0.014 | — | 43.0 | B |
| 552 | A2162-S G | 63 | 1 1 1 1 1 | 9613 | 84 | — | 448 | 196 | — | 4.77 | 1.30 | — | 0.281 | 0.045 | — | 7.4 | A |
| 554 | A2162-S I | 163 | 1 1 1 1 1 | 15593 | 40 | — | 223 | 61 | — | 4.27 | 1.14 | — | 0.273 | 0.036 | — | 9.6 | A |
| 555 | A2162-S 1 | 63 | 1 1 1 1 1 | 9883 | 32 | — | 147 | 45 | — | 3.45 | 1.13 | — | 0.190 | 0.039 | — | 7.5 | B |
| 556 | A2162-S 2 | 263 | 1 1 0 0 0 | 27486 | 73 | — | — | — | — | — | — | — | — | — | — | 3.4 | D |
| 557 | J20 A | 64 | 1 1 1 1 0 | 9429 | 31 | — | 266 | 43 | — | 5.14 | 0.59 | — | — | — | — | 21.3 | A |
| 558 | J20 B | 64 | 2 2 2 2 0 | 8921 | 16 | 17 | 204 | 21 | 12 | 4.56 | 0.33 | 0.26 | — | — | — | 70.2 | A |
| 559 | J20 C | 64 | 1 1 1 1 0 | 9431 | 23 | — | 283 | 37 | — | 5.53 | 0.33 | — | — | — | — | 77.4 | A |
| 560 | J20 D | 64 | 1 1 1 1 0 | 8695 | 22 | — | 192 | 39 | — | 5.11 | 0.33 | — | — | — | — | 67.1 | B |

**Table 5** – *continued*

| (1) GIN | (2) Galaxy Name | (3) CAN | (4) $N$ $s\ z\ \sigma\ b\ 2$ | (5) $cz$ (km s$^{-1}$) | (6) $\Delta cz$ | (7) $\delta cz$ | (8) $\sigma$ (km s$^{-1}$) | (9) $\Delta\sigma$ | (10) $\delta\sigma$ | (11) Mg$b$ | (12) $\Delta$Mg$b$ (Å) | (13) $\delta$Mg$b$ | (14) $Mg_2$ | (15) $\Delta Mg_2$ (mag) | (16) $\delta Mg_2$ | (17) S/N | (18) $Q$ |
|---|---|---|---|---|---|---|---|---|---|---|---|---|---|---|---|---|---|
| 561 | J20 E | 64 | 1 1 1 1 0 | 8836 | 21 | — | 206 | 13 | — | 5.31 | 0.40 | — | — | — | — | 49.7 | A |
| 562 | A2197 A | 65 | 4 3 3 3 3 | 8784 | 15 | 12 | 257 | 18 | 5 | 4.87 | 0.32 | 0.05 | 0.313 | 0.011 | 0.002 | 49.7 | A |
| 563 | A2197 B | 65 | 2 2 2 2 2 | 9523 | 21 | 0 | 210 | 21 | 22 | 5.27 | 0.47 | 0.28 | 0.331 | 0.015 | 0.000 | 33.9 | A |
| 564 | A2197 C | 65 | 3 3 3 3 2 | 8820 | 16 | 7 | 276 | 18 | 8 | 4.48 | 0.28 | 0.04 | 0.284 | 0.013 | 0.000 | 59.5 | A |
| 565 | A2197 D | 65 | 1 1 1 1 1 | 8970 | 19 | — | 110 | 17 | — | 3.11 | 0.64 | — | 0.119 | 0.025 | — | 14.5 | C* |
| 566 | A2197 E | 65 | 4 3 3 3 3 | 8922 | 13 | 60 | 261 | 13 | 13 | 5.46 | 0.24 | 0.36 | 0.310 | 0.010 | 0.010 | 52.2 | A |
| 568 | A2197 G | 65 | 1 1 1 1 1 | 8248 | 24 | — | 156 | 29 | — | 4.69 | 0.78 | — | 0.264 | 0.029 | — | 12.2 | C |
| 571 | A2197 J | 65 | 3 3 3 3 3 | 9092 | 13 | 15 | 154 | 8 | 13 | 3.81 | 0.25 | 0.09 | 0.247 | 0.011 | 0.008 | 38.2 | A |
| 572 | A2197 K | 65 | 1 1 1 1 1 | 9553 | 33 | — | 168 | 47 | — | 3.82 | 1.24 | — | 0.243 | 0.036 | — | 8.7 | B |
| 573 | A2197 L | 65 | 1 1 1 1 1 | 9673 | 20 | — | 192 | 12 | — | 4.54 | 0.30 | — | 0.278 | 0.014 | — | 37.7 | A |
| 574 | A2197 M | 65 | 1 1 1 1 1 | 9524 | 34 | — | 177 | 47 | — | 3.72 | 0.98 | — | 0.244 | 0.035 | — | 9.7 | B |
| 578 | A2197 3 | 65 | 1 1 1 1 1 | 10344 | 34 | — | 168 | 47 | — | 4.37 | 1.11 | — | 0.266 | 0.037 | — | 8.6 | A |
| 579 | A2199 A | 66 | 1 1 1 1 1 | 9303 | 30 | — | 281 | 39 | — | 5.67 | 0.83 | — | 0.365 | 0.029 | — | 17.3 | B |
| 580 | A2199 B | 66 | 1 1 1 1 1 | 8800 | 21 | — | 158 | 30 | — | 4.98 | 0.74 | — | 0.301 | 0.028 | — | 16.3 | B |
| 581 | A2199 C | 66 | 1 1 1 1 1 | 7834 | 21 | — | 160 | 11 | — | 4.59 | 0.29 | — | 0.272 | 0.015 | — | 35.9 | A |
| 582 | A2199 D | 66 | 1 1 1 1 1 | 8716 | 21 | — | 194 | 12 | — | 4.80 | 0.27 | — | 0.309 | 0.015 | — | 41.6 | A |
| 583 | A2199 E | 66 | 1 1 1 1 1 | 9517 | 21 | — | 117 | 8 | — | 3.48 | 0.29 | — | 0.188 | 0.015 | — | 39.9 | B* |
| 584 | A2199 F | 66 | 2 2 2 2 2 | 8652 | 14 | 4 | 192 | 9 | 0 | 4.39 | 0.22 | 0.09 | 0.288 | 0.010 | 0.034 | 55.8 | A |
| 585 | A2199 G | 66 | 1 1 1 1 1 | 10701 | 21 | — | 109 | 8 | — | 2.92 | 0.32 | — | 0.183 | 0.017 | — | 32.6 | B* |
| 586 | A2199 H | 66 | 1 1 1 1 1 | 8856 | 23 | — | 189 | 15 | — | 4.78 | 0.32 | — | 0.331 | 0.016 | — | 34.0 | A |
| 588 | A2199 J | 66 | 1 1 1 1 1 | 9092 | 24 | — | 171 | 16 | — | 4.57 | 0.32 | — | 0.298 | 0.016 | — | 27.4 | A |
| 589 | A2199 K | 66 | 1 1 1 1 1 | 9127 | 21 | — | 168 | 12 | — | 5.09 | 0.31 | — | 0.292 | 0.016 | — | 36.1 | A |
| 590 | A2199 L | 66 | 1 1 1 1 1 | 8897 | 21 | — | 166 | 12 | — | 4.47 | 0.32 | — | 0.308 | 0.015 | — | 36.4 | A |
| 591 | A2199 M | 66 | 1 1 1 1 1 | 10108 | 21 | — | 181 | 12 | — | 3.89 | 0.33 | — | 0.247 | 0.016 | — | 38.5 | A |
| 592 | A2199 N | 66 | 1 1 1 1 1 | 9918 | 21 | — | 144 | 11 | — | 2.70 | 0.36 | — | 0.178 | 0.016 | — | 33.4 | B* |
| 593 | A2199 O | 66 | 1 1 1 1 1 | 9006 | 22 | — | 192 | 14 | — | 5.11 | 0.31 | — | 0.355 | 0.015 | — | 37.2 | A |
| 595 | A2199 1 | 66 | 2 2 2 2 1 | 8814 | 19 | 1 | 193 | 14 | 0 | 4.10 | 0.43 | 0.24 | 0.229 | 0.049 | — | 39.6 | A |
| 596 | A2199 2 | 166 | 1 1 1 1 1 | 17795 | 46 | — | 256 | 77 | — | 4.18 | 1.31 | — | 0.288 | 0.035 | — | 9.0 | B |
| 598 | J21 A | 167 | 2 2 2 2 0 | 6085 | 16 | 5 | 200 | 21 | 8 | 4.61 | 0.30 | 0.53 | — | — | — | 49.0 | A |
| 600 | J21 C | 67 | 1 1 1 1 1 | 13119 | 33 | — | 287 | 47 | — | 5.12 | 0.51 | — | 0.314 | 0.020 | — | 22.9 | A |
| 601 | J21 D | 67 | 1 1 1 1 0 | 13778 | 22 | — | 198 | 17 | — | 6.14 | 0.37 | — | — | — | — | 26.7 | A |
| 602 | J21 E | 67 | 2 2 2 2 1 | 14348 | 21 | 20 | 327 | 22 | 22 | 5.13 | 0.23 | 0.04 | 0.333 | 0.023 | — | 52.8 | A |
| 604 | J21 G | 67 | 1 1 1 1 1 | 14201 | 21 | — | 178 | 96 | — | 3.38 | 0.57 | — | 0.179 | 0.040 | — | 30.3 | C |
| 606 | J21 I | 67 | 1 1 1 1 1 | 13259 | 24 | — | 222 | 20 | — | 5.65 | 0.39 | — | 0.294 | 0.015 | — | 27.3 | B |
| 607 | J21 1 | 67 | 1 1 1 1 0 | 13750 | 23 | — | 197 | 18 | — | 5.70 | 0.41 | — | — | — | — | 25.9 | B |
| 608 | J21 2 | 67 | 1 1 1 1 0 | 14675 | 23 | — | 172 | 17 | — | 4.61 | 0.46 | — | — | — | — | 20.8 | B |
| 609 | A2247 A | 68 | 1 1 1 1 0 | 11111 | 22 | — | 209 | 33 | — | 2.81 | 0.38 | — | — | — | — | 63.6 | A |
| 610 | A2247 B | 68 | 1 1 1 1 0 | 11844 | 22 | — | 229 | 34 | — | 4.40 | 0.37 | — | — | — | — | 57.0 | A |
| 611 | A2247 C | 68 | 1 1 1 1 0 | 11796 | 22 | — | 226 | 37 | — | 5.67 | 0.35 | — | — | — | — | 49.8 | A |
| 612 | A2247 D | 68 | 1 1 1 1 0 | 11251 | 22 | — | 214 | 36 | — | 4.05 | 0.38 | — | — | — | — | 44.4 | A |
| 613 | A2247 E | 68 | 1 1 1 1 0 | 11366 | 22 | — | 223 | 36 | — | 4.52 | 0.40 | — | — | — | — | 47.3 | A |
| 614 | A2247 F | 68 | 1 1 1 1 1 | 11679 | 24 | — | 270 | 20 | — | 5.00 | 0.28 | — | 0.312 | 0.014 | — | 37.0 | A |
| 615 | A2247 1 | 68 | 1 1 1 1 1 | 11696 | 32 | — | 136 | 69 | — | 2.97 | 2.98 | — | 0.239 | 0.077 | — | 3.4 | C |
| 616 | A2247 2 | 68 | 1 1 1 1 1 | 11371 | 17 | — | 97 | 25 | — | 4.39 | 0.45 | — | 0.246 | 0.017 | — | 24.9 | B |
| 617 | P332-1 A | 70 | 2 2 2 2 1 | 10675 | 14 | 15 | 204 | 11 | 0 | 4.79 | 0.21 | 0.10 | 0.281 | 0.013 | — | 89.1 | A |
| 618 | P332-1 B | 70 | 1 1 1 1 0 | 10785 | 23 | — | 260 | 38 | — | 2.22 | 0.41 | — | — | — | — | 51.5 | B |
| 619 | P332-1 C | 70 | 2 2 2 2 1 | 10066 | 14 | 34 | 164 | 17 | 5 | 3.95 | 0.27 | 0.06 | 0.221 | 0.019 | — | 62.1 | A |
| 620 | P332-1 D | 69 | 1 1 1 1 1 | 16941 | 24 | — | 204 | 33 | — | 1.19 | 0.79 | — | 0.079 | 0.029 | — | 14.4 | C |
| 621 | P332-1 E | 69 | 1 1 1 1 1 | 17747 | 24 | — | 234 | 25 | — | 4.21 | 0.41 | — | 0.265 | 0.017 | — | 25.8 | B |
| 622 | P332-1 F | 70 | 1 1 1 1 1 | 10522 | 22 | — | 177 | 20 | — | 3.82 | 0.54 | — | 0.247 | 0.022 | — | 21.6 | B |
| 623 | P332-1 G | 70 | 1 1 1 1 1 | 10042 | 47 | — | 284 | 84 | — | 4.84 | 0.89 | — | 0.288 | 0.037 | — | 11.0 | A |
| 626 | J22 A | 70 | 3 3 3 3 3 | 10448 | 24 | 37 | 330 | 32 | 17 | 5.38 | 0.28 | 0.14 | 0.339 | 0.011 | 0.019 | 40.9 | A |
| 627 | J22 B | 70 | 2 2 2 2 2 | 10358 | 30 | 20 | 296 | 33 | 29 | 5.41 | 0.34 | 0.68 | 0.309 | 0.013 | 0.021 | 34.5 | A |
| 628 | J22 C | 70 | 2 2 2 2 2 | 9729 | 21 | 1 | 222 | 23 | 15 | 5.37 | 0.30 | 0.60 | 0.315 | 0.013 | 0.019 | 37.2 | A |
| 629 | J22 D | 70 | 1 1 1 1 1 | 9723 | 34 | — | 243 | 38 | — | 5.95 | 0.33 | — | 0.296 | 0.016 | — | 26.3 | B |
| 630 | J22 E | 70 | 2 2 2 2 2 | 10542 | 20 | 10 | 233 | 24 | 9 | 4.40 | 0.34 | 0.18 | 0.281 | 0.012 | 0.003 | 34.8 | A |
| 631 | J22 F | 70 | 1 1 1 1 1 | 10952 | 28 | — | 141 | 32 | — | 3.79 | 0.76 | — | 0.220 | 0.025 | — | 15.0 | B |
| 632 | J22 G | 70 | 2 2 2 2 2 | 9949 | 21 | 20 | 273 | 20 | 18 | 5.58 | 0.30 | 0.27 | 0.318 | 0.011 | 0.009 | 36.6 | A |
| 633 | J22 H | 70 | 2 2 2 2 2 | 10376 | 14 | 34 | 172 | 9 | 10 | 4.49 | 0.24 | 0.26 | 0.253 | 0.011 | 0.009 | 49.3 | A |
| 634 | J23 A | 71 | 2 2 2 2 1 | 8220 | 26 | 3 | 347 | 40 | 64 | 5.44 | 0.44 | 0.18 | 0.377 | 0.019 | — | 30.1 | A |
| 635 | J23 B | 71 | 2 2 2 2 2 | 8867 | 19 | 18 | 245 | 25 | 3 | 4.01 | 0.49 | 0.05 | 0.292 | 0.015 | 0.003 | 26.1 | B |
| 636 | J23 C | 71 | 2 2 2 2 2 | 8496 | 20 | 69 | 185 | 29 | 29 | 4.63 | 0.63 | 0.08 | 0.258 | 0.021 | 0.003 | 18.7 | B |

**Table 5** – *continued*

| (1) GIN | (2) Galaxy Name | (3) CAN | (4) $N$ $s\ z\ \sigma\ b\ 2$ | (5) $cz$ (km s$^{-1}$) | (6) $\Delta cz$ | (7) $\delta cz$ | (8) $\sigma$ (km s$^{-1}$) | (9) $\Delta\sigma$ | (10) $\delta\sigma$ | (11) Mg$b$ | (12) $\Delta$Mg$b$ (Å) | (13) $\delta$Mg$b$ | (14) $Mg_2$ | (15) $\Delta Mg_2$ (mag) | (16) $\delta Mg_2$ | (17) S/N | (18) $Q$ |
|---|---|---|---|---|---|---|---|---|---|---|---|---|---|---|---|---|---|
| 638 | J23 E | 71 | 2 2 2 2 1 | 8275 | 20 | 15 | 147 | 24 | 4 | 3.42 | 0.64 | 0.31 | 0.206 | 0.040 | — | 18.7 | B |
| 639 | J24 A | 72 | 2 2 2 2 2 | 9858 | 27 | 46 | 253 | 37 | 30 | 5.58 | 0.60 | 0.91 | 0.324 | 0.018 | 0.004 | 19.7 | B |
| 640 | J24 B | 72 | 2 2 2 2 2 | 10228 | 16 | 11 | 103 | 22 | 20 | 3.69 | 0.63 | 0.25 | 0.248 | 0.021 | 0.002 | 17.8 | B |
| 641 | J24 C | 72 | 3 3 2 2 2 | 10346 | 22 | 45 | 208 | 40 | 3 | 4.72 | 0.70 | 0.36 | 0.290 | 0.025 | 0.007 | 14.6 | A |
| 642 | J24 D | 72 | 1 1 0 0 0 | 10695 | 72 | — | — | — | — | — | — | — | — | — | — | 10.6 | D |
| 643 | J24 E | 72 | 1 1 1 1 1 | 10427 | 25 | — | 195 | 37 | — | 4.09 | 1.02 | — | 0.243 | 0.030 | — | 13.9 | B |
| 645 | J25 A | 73 | 2 2 2 2 1 | 8233 | 23 | 12 | 204 | 27 | 12 | 5.14 | 0.54 | 0.73 | 0.381 | 0.027 | — | 25.0 | A |
| 646 | J25 B | 73 | 2 2 2 2 2 | 8354 | 21 | 11 | 206 | 24 | 4 | 5.35 | 0.42 | 0.21 | 0.329 | 0.017 | 0.000 | 27.8 | A |
| 647 | J25 C | 73 | 3 3 2 2 2 | 7775 | 18 | 46 | 140 | 24 | 33 | 4.30 | 0.76 | 0.00 | 0.306 | 0.025 | 0.019 | 16.4 | A |
| 648 | J26 A | 74 | 3 2 2 2 2 | 15045 | 20 | 43 | 269 | 30 | 20 | 6.31 | 0.44 | 1.06 | 0.366 | 0.015 | 0.006 | 26.8 | B |
| 649 | J26 B | 174 | 1 1 1 1 1 | 18187 | 37 | — | 284 | 65 | — | 6.40 | 1.38 | — | 0.286 | 0.043 | — | 9.8 | C |
| 650 | J26 C | 74 | 2 2 2 2 2 | 15292 | 20 | 15 | 281 | 41 | 2 | 4.30 | 0.43 | 0.11 | 0.315 | 0.019 | 0.001 | 35.5 | B |
| 651 | J26 1 | 74 | 1 1 0 0 0 | 15341 | 71 | — | — | — | — | — | — | — | — | — | — | 15.5 | D |
| 652 | J26 2 | 74 | 1 1 1 1 1 | 14188 | 19 | — | 134 | 35 | — | 5.11 | 0.72 | — | 0.269 | 0.027 | — | 14.8 | C |
| 653 | J27 A | 75 | 3 2 2 2 2 | 10646 | 30 | 13 | 289 | 46 | 31 | 5.25 | 0.55 | 0.23 | 0.340 | 0.020 | 0.001 | 22.7 | A |
| 654 | J27 B | 75 | 3 2 2 2 1 | 9325 | 29 | 0 | 235 | 40 | 5 | 5.68 | 0.64 | 0.62 | 0.328 | 0.032 | — | 20.2 | B |
| 655 | J27 C | 75 | 2 1 1 1 1 | 9784 | 32 | — | 221 | 43 | — | 4.72 | 0.60 | — | 0.248 | 0.024 | — | 17.6 | B |
| 656 | J27 D | 75 | 2 1 1 1 1 | 9424 | 20 | — | 95 | 21 | — | 4.05 | 0.81 | — | 0.279 | 0.028 | — | 16.5 | B |
| 657 | J27 E | 75 | 3 2 2 2 2 | 9740 | 15 | 17 | 192 | 22 | 32 | 4.91 | 0.48 | 0.16 | 0.278 | 0.016 | 0.016 | 27.2 | B |
| 658 | J38 A | 76 | 3 3 3 3 3 | 15519 | 31 | 45 | 385 | 42 | 7 | 4.48 | 0.28 | 0.06 | 0.335 | 0.012 | 0.026 | 34.6 | A |
| 659 | J38 B | 76 | 3 3 3 3 3 | 14818 | 16 | 16 | 190 | 21 | 23 | 4.09 | 0.44 | 1.46 | 0.248 | 0.015 | 0.014 | 25.2 | B |
| 660 | J38 C | 76 | 5 5 2 2 2 | 16207 | 19 | 19 | 125 | 21 | 25 | 4.29 | 0.56 | 0.20 | 0.206 | 0.022 | 0.008 | 17.6 | C |
| 661 | J38 1 | 76 | 1 1 1 1 1 | 14918 | 26 | — | 108 | 43 | — | 0.56 | 1.14 | — | 0.088 | 0.041 | — | 9.7 | C |
| 662 | P522-1 A | 77 | 7 6 6 6 4 | 7318 | 10 | 18 | 288 | 6 | 11 | 5.22 | 0.09 | 0.33 | 0.331 | 0.005 | 0.004 | 147.2 | A |
| 663 | P522-1 B | 77 | 6 5 5 5 3 | 7847 | 10 | 11 | 249 | 7 | 14 | 5.35 | 0.10 | 0.18 | 0.328 | 0.006 | 0.014 | 119.3 | A |
| 664 | P522-1 C | 77 | 4 4 4 4 2 | 7697 | 10 | 5 | 101 | 6 | 7 | 4.11 | 0.16 | 0.26 | 0.246 | 0.008 | 0.001 | 74.1 | A |
| 665 | P522-1 D | 77 | 5 5 5 5 3 | 7933 | 8 | 7 | 184 | 6 | 16 | 4.43 | 0.11 | 0.35 | 0.266 | 0.006 | 0.002 | 107.6 | A |
| 666 | P522-1 E | 77 | 5 5 5 5 3 | 7315 | 10 | 9 | 166 | 8 | 12 | 4.54 | 0.18 | 0.27 | 0.274 | 0.009 | 0.006 | 61.9 | A |
| 667 | P522-1 F | 77 | 4 4 4 4 3 | 8340 | 10 | 39 | 134 | 6 | 10 | 4.38 | 0.16 | 0.19 | 0.255 | 0.008 | 0.004 | 74.0 | A |
| 668 | P522-1 G | 77 | 4 4 3 3 2 | 7118 | 11 | 22 | 191 | 6 | 8 | 4.45 | 0.12 | 0.15 | 0.267 | 0.007 | 0.007 | 111.9 | A |
| 669 | P522-1 1 | 77 | 3 3 3 3 2 | 7572 | 11 | 2 | 186 | 6 | 8 | 4.60 | 0.13 | 0.21 | 0.292 | 0.007 | 0.000 | 88.5 | A |
| 670 | P522-1 2 | 177 | 2 2 2 2 2 | 23926 | 13 | 12 | 216 | 11 | 5 | 3.97 | 0.23 | 0.12 | 0.266 | 0.009 | 0.004 | 51.8 | A |
| 672 | P522-1 4 | 77 | 3 3 3 3 3 | 7607 | 10 | 8 | 85 | 6 | 17 | 3.83 | 0.19 | 0.10 | 0.200 | 0.009 | 0.010 | 56.4 | A |
| 673 | P522-1 5 | 277 | 2 2 2 2 2 | 27282 | 13 | 31 | 119 | 12 | 42 | 5.17 | 0.33 | 0.25 | 0.234 | 0.012 | 0.001 | 35.8 | B |
| 674 | A2572 A | 78 | 2 2 2 2 2 | 11793 | 20 | 12 | 305 | 21 | 9 | 5.11 | 0.21 | 0.68 | 0.300 | 0.009 | 0.015 | 45.0 | A |
| 675 | A2572 B | 78 | 3 3 3 3 3 | 11384 | 15 | 16 | 263 | 17 | 20 | 5.10 | 0.24 | 0.07 | 0.320 | 0.009 | 0.013 | 45.9 | A |
| 676 | A2572 C | 78 | 2 2 2 2 2 | 11263 | 23 | 34 | 296 | 24 | 15 | 5.38 | 0.32 | 0.26 | 0.328 | 0.012 | 0.003 | 31.9 | A |
| 677 | A2572 D | 78 | 2 2 2 2 2 | 11260 | 16 | 12 | 182 | 12 | 16 | 5.63 | 0.23 | 0.65 | 0.315 | 0.011 | 0.016 | 37.6 | B |
| 678 | A2572 E | 78 | 2 2 0 0 0 | 11297 | 50 | 54 | — | — | — | — | — | — | — | — | — | 20.5 | D* |
| 680 | A2572 2 | 78 | 2 2 2 2 2 | 12027 | 14 | 7 | 149 | 16 | 8 | 3.22 | 0.45 | 0.96 | 0.290 | 0.017 | 0.042 | 23.7 | B |
| 681 | A2589 A | 79 | 6 5 5 5 5 | 12327 | 10 | 7 | 254 | 9 | 7 | 5.45 | 0.13 | 0.16 | 0.345 | 0.006 | 0.014 | 85.7 | A |
| 682 | A2589 B | 79 | 5 5 5 5 5 | 12773 | 11 | 35 | 261 | 10 | 16 | 4.80 | 0.14 | 0.25 | 0.301 | 0.006 | 0.007 | 81.1 | A |
| 683 | A2589 C | 79 | 3 3 3 3 3 | 14145 | 10 | 12 | 165 | 8 | 31 | 4.42 | 0.17 | 0.13 | 0.272 | 0.007 | 0.004 | 65.4 | A |
| 684 | A2589 D | 79 | 3 3 3 3 3 | 13549 | 11 | 15 | 225 | 9 | 11 | 5.08 | 0.18 | 0.30 | 0.306 | 0.007 | 0.012 | 63.7 | A |
| 685 | A2589 E | 79 | 3 3 3 3 3 | 10403 | 9 | 24 | 70 | 8 | 12 | 2.53 | 0.27 | 0.34 | 0.103 | 0.010 | 0.002 | 40.8 | B |
| 686 | A2589 F | 79 | 3 3 3 3 3 | 12124 | 12 | 2 | 254 | 10 | 11 | 5.17 | 0.13 | 0.07 | 0.284 | 0.006 | 0.007 | 77.0 | A |
| 687 | A2589 G | 79 | 3 3 3 3 3 | 12535 | 12 | 30 | 183 | 10 | 20 | 5.33 | 0.21 | 0.20 | 0.277 | 0.009 | 0.014 | 45.0 | A |
| 688 | A2589 H | 79 | 3 3 3 3 3 | 13420 | 13 | 12 | 244 | 11 | 21 | 4.63 | 0.18 | 0.31 | 0.269 | 0.008 | 0.003 | 56.2 | A |
| 689 | A2589 1 | 79 | 3 3 3 3 3 | 13329 | 11 | 26 | 121 | 9 | 3 | 4.75 | 0.24 | 0.13 | 0.248 | 0.010 | 0.003 | 45.9 | B |
| 690 | A2589 2 | 79 | 3 3 2 2 2 | 12312 | 13 | 32 | 113 | 17 | 38 | 4.85 | 0.53 | 0.57 | 0.233 | 0.018 | 0.006 | 21.4 | C |
| 691 | A2593-N A | 80 | 2 2 2 2 2 | 12489 | 17 | 3 | 246 | 13 | 4 | 5.62 | 0.15 | 0.10 | 0.345 | 0.009 | 0.015 | 49.9 | A |
| 692 | A2593-N B | 80 | 6 6 6 6 4 | 11601 | 8 | 18 | 208 | 8 | 18 | 4.83 | 0.14 | 0.29 | 0.321 | 0.007 | 0.029 | 74.1 | A |
| 693 | A2593-N C | 80 | 3 3 3 3 3 | 13381 | 10 | 4 | 204 | 8 | 18 | 4.61 | 0.14 | 0.24 | 0.293 | 0.007 | 0.012 | 74.0 | A |
| 694 | A2593-N D | 80 | 4 4 4 4 4 | 12637 | 9 | 13 | 231 | 6 | 15 | 4.83 | 0.11 | 0.23 | 0.308 | 0.005 | 0.014 | 91.8 | A |
| 695 | A2593-N E | 80 | 4 4 4 4 4 | 11591 | 11 | 8 | 311 | 10 | 9 | 5.18 | 0.10 | 0.13 | 0.330 | 0.006 | 0.014 | 103.3 | A |
| 696 | A2593-N F | 80 | 4 4 4 4 4 | 12424 | 9 | 6 | 165 | 6 | 10 | 4.99 | 0.11 | 0.07 | 0.294 | 0.006 | 0.003 | 82.4 | A |
| 697 | A2593-N G | 80 | 5 5 4 4 3 | 11747 | 9 | 22 | 142 | 7 | 15 | 4.46 | 0.18 | 0.27 | 0.240 | 0.008 | 0.023 | 55.6 | A |
| 698 | A2593-N H | 80 | 4 4 4 4 4 | 12645 | 10 | 12 | 239 | 7 | 9 | 5.37 | 0.11 | 0.23 | 0.325 | 0.006 | 0.024 | 88.1 | A |
| 699 | A2593-N I | 80 | 5 5 5 5 3 | 12263 | 10 | 14 | 256 | 8 | 10 | 5.06 | 0.13 | 0.23 | 0.318 | 0.006 | 0.012 | 84.2 | A |
| 700 | A2593-N J | 80 | 7 7 7 7 5 | 12617 | 8 | 12 | 235 | 6 | 18 | 5.46 | 0.11 | 0.39 | 0.319 | 0.005 | 0.019 | 101.7 | A |
| 701 | A2593-N K | 80 | 7 7 7 7 5 | 12634 | 8 | 17 | 238 | 6 | 6 | 5.03 | 0.10 | 0.22 | 0.337 | 0.005 | 0.009 | 109.8 | A |
| 702 | A2593-N L | 80 | 5 5 5 5 3 | 11823 | 8 | 16 | 202 | 6 | 11 | 5.03 | 0.13 | 0.28 | 0.309 | 0.006 | 0.014 | 84.0 | A |

**Table 5** – *continued*

| (1) GIN | (2) Galaxy Name | (3) CAN | (4) $N$ $s\ z\ \sigma\ b\ 2$ | (5) $cz$ (km s$^{-1}$) | (6) $\Delta cz$ | (7) $\delta cz$ | (8) $\sigma$ (km s$^{-1}$) | (9) $\Delta\sigma$ | (10) $\delta\sigma$ | (11) Mg$b$ | (12) $\Delta$Mg$b$ (Å) | (13) $\delta$Mg$b$ | (14) $Mg_2$ | (15) $\Delta Mg_2$ (mag) | (16) $\delta Mg_2$ | (17) S/N | (18) $Q$ |
|---|---|---|---|---|---|---|---|---|---|---|---|---|---|---|---|---|---|
| 703 | A2593-N M | 80 | 5 5 5 5 3 | 13189 | 8 | 24 | 182 | 7 | 12 | 4.62 | 0.14 | 0.27 | 0.288 | 0.007 | 0.018 | 74.3 | A |
| 704 | A2593-N 1 | 80 | 3 3 3 3 3 | 11704 | 11 | 19 | 240 | 8 | 11 | 4.73 | 0.15 | 0.24 | 0.290 | 0.007 | 0.011 | 76.4 | A |
| 705 | A2593-N 2 | 80 | 3 3 3 3 3 | 13110 | 10 | 18 | 170 | 7 | 10 | 4.52 | 0.17 | 0.26 | 0.298 | 0.008 | 0.014 | 63.5 | A |
| 706 | A2593-N 3 | 180 | 7 7 6 4 4 | 27822 | 8 | 28 | 229 | 7 | 29 | 4.90 | 0.15 | 0.21 | 0.325 | 0.007 | 0.009 | 84.0 | A |
| 707 | A2593-N 4 | 80 | 5 5 3 3 3 | 11781 | 10 | 20 | 125 | 6 | 10 | 4.29 | 0.19 | 0.35 | 0.256 | 0.008 | 0.013 | 57.4 | A |
| 708 | A2593-N 5 | 80 | 5 5 2 2 2 | 11096 | 11 | 28 | 57 | 9 | 3 | 3.65 | 0.36 | 0.24 | 0.175 | 0.012 | 0.002 | 36.3 | B |
| 709 | A2593-S A | 80 | 5 5 5 5 3 | 12713 | 11 | 19 | 330 | 11 | 39 | 5.23 | 0.10 | 0.23 | 0.326 | 0.006 | 0.008 | 100.9 | A |
| 710 | A2593-S B | 80 | 5 5 5 5 3 | 12150 | 8 | 15 | 178 | 7 | 8 | 4.86 | 0.12 | 0.20 | 0.279 | 0.007 | 0.031 | 78.4 | A |
| 711 | A2593-S C | 80 | 3 3 3 3 3 | 13066 | 12 | 41 | 293 | 12 | 8 | 5.18 | 0.14 | 0.11 | 0.317 | 0.007 | 0.010 | 77.6 | A |
| 712 | A2593-S D | 80 | 5 5 5 5 3 | 11046 | 9 | 21 | 214 | 8 | 6 | 4.75 | 0.12 | 0.18 | 0.280 | 0.006 | 0.020 | 85.0 | A |
| 713 | A2593-S E | 80 | 7 5 3 3 3 | 12554 | 10 | 9 | 143 | 7 | 7 | 4.19 | 0.19 | 0.60 | 0.225 | 0.009 | 0.024 | 57.4 | A |
| 714 | A2593-S F | 80 | 3 3 3 3 3 | 12805 | 10 | 10 | 124 | 8 | 16 | 4.59 | 0.16 | 0.18 | 0.253 | 0.008 | 0.011 | 56.8 | A |
| 715 | A2593-S G | 80 | 3 3 3 3 3 | 12880 | 10 | 7 | 107 | 9 | 8 | 3.68 | 0.25 | 0.29 | 0.201 | 0.010 | 0.011 | 42.6 | B |
| 716 | A2634 A | 82 | 3 3 3 3 2 | 9060 | 14 | 11 | 312 | 11 | 10 | 5.40 | 0.08 | 0.06 | 0.329 | 0.006 | 0.011 | 105.6 | A |
| 717 | A2634 B | 82 | 3 3 3 3 3 | 9274 | 12 | 10 | 236 | 8 | 9 | 4.98 | 0.08 | 0.11 | 0.295 | 0.006 | 0.003 | 90.1 | A |
| 718 | A2634 C | 82 | 3 3 3 3 3 | 9502 | 12 | 23 | 190 | 7 | 20 | 3.65 | 0.12 | 1.03 | 0.297 | 0.007 | 0.022 | 69.4 | A |
| 719 | A2634 D | 82 | 3 2 2 2 2 | 10774 | 15 | 1 | 231 | 12 | 15 | 4.84 | 0.16 | 0.02 | 0.297 | 0.009 | 0.005 | 45.4 | A |
| 720 | A2634 E | 82 | 3 3 3 3 3 | 9272 | 14 | 11 | 269 | 13 | 7 | 4.85 | 0.16 | 0.11 | 0.316 | 0.007 | 0.006 | 54.7 | A |
| 721 | A2634 F | 82 | 2 2 2 2 2 | 10211 | 13 | 16 | 135 | 10 | 4 | 4.75 | 0.16 | 0.03 | 0.288 | 0.009 | 0.014 | 41.3 | A |
| 722 | A2634 G | 82 | 4 4 4 4 4 | 9398 | 15 | 16 | 333 | 17 | 7 | 5.06 | 0.13 | 0.31 | 0.327 | 0.007 | 0.018 | 62.8 | A |
| 723 | A2634 H | 82 | 3 3 3 3 3 | 11694 | 15 | 21 | 271 | 19 | 24 | 4.60 | 0.18 | 0.24 | 0.266 | 0.008 | 0.006 | 48.5 | A |
| 724 | A2634 I | 82 | 3 3 3 3 3 | 9958 | 13 | 25 | 211 | 12 | 8 | 4.84 | 0.18 | 0.10 | 0.297 | 0.009 | 0.013 | 43.2 | A |
| 725 | A2634 J | 82 | 2 2 2 2 2 | 8701 | 17 | 25 | 219 | 16 | 15 | 5.30 | 0.21 | 0.55 | 0.309 | 0.011 | 0.016 | 35.3 | A |
| 726 | A2634 K | 82 | 3 3 3 3 3 | 10011 | 13 | 55 | 214 | 12 | 8 | 5.28 | 0.15 | 0.22 | 0.333 | 0.008 | 0.008 | 46.5 | A |
| 728 | A2634 2 | 82 | 1 1 1 1 1 | 9406 | 31 | — | 296 | 35 | — | 5.76 | 0.41 | — | 0.295 | 0.018 | — | 24.1 | B |
| 729 | A2657 A | 83 | 2 2 2 2 1 | 12063 | 14 | 15 | 179 | 18 | 19 | 4.84 | 0.30 | 0.24 | 0.312 | 0.020 | — | 24.7 | A |
| 730 | A2657 B | 83 | 2 2 2 2 2 | 12354 | 18 | 9 | 281 | 20 | 14 | 4.86 | 0.20 | 0.08 | 0.271 | 0.010 | 0.032 | 41.9 | B |
| 731 | A2657 C | 83 | 3 3 3 3 2 | 12298 | 12 | 5 | 196 | 13 | 9 | 4.25 | 0.20 | 0.14 | 0.254 | 0.011 | 0.006 | 37.8 | A |
| 732 | A2657 D | 83 | 1 1 1 1 1 | 12542 | 19 | — | 221 | 19 | — | 4.14 | 0.29 | — | 0.263 | 0.012 | — | 27.0 | B |
| 733 | A2657 E | 83 | 2 2 2 2 1 | 10725 | 15 | 17 | 215 | 14 | 9 | 5.12 | 0.20 | 0.29 | 0.295 | 0.012 | — | 35.8 | A |
| 734 | A2657 F | 83 | 2 2 2 2 1 | 11876 | 15 | 9 | 239 | 15 | 24 | 5.72 | 0.20 | 0.08 | 0.351 | 0.011 | — | 41.8 | A |
| 735 | A2657 G | 83 | 2 2 2 2 1 | 13594 | 12 | 17 | 150 | 11 | 7 | 4.18 | 0.22 | 0.13 | 0.224 | 0.014 | — | 33.5 | A |
| 736 | A2657 H | 83 | 2 2 2 2 1 | 12249 | 14 | 0 | 219 | 13 | 3 | 5.05 | 0.19 | 0.23 | 0.321 | 0.012 | — | 40.7 | A |
| 737 | A2657 1 | 83 | 1 1 1 1 0 | 11719 | 20 | — | 152 | 25 | — | 4.73 | 0.46 | — | — | — | — | 18.4 | B |
| 738 | A2666 A | 84 | 2 2 2 2 1 | 8153 | 17 | 3 | 257 | 19 | 15 | 5.24 | 0.28 | 0.19 | 0.311 | 0.013 | — | 35.5 | A |
| 739 | A2666 B | 84 | 2 2 2 2 1 | 7649 | 14 | 64 | 84 | 20 | 1 | 3.43 | 0.66 | 0.30 | 0.185 | 0.030 | — | 12.8 | C |
| 740 | A2666 C | 84 | 2 2 1 1 1 | 8511 | 17 | 8 | 93 | 11 | — | 4.53 | 0.39 | — | 0.259 | 0.015 | — | 22.8 | B |
| 741 | A2666 D | 84 | 1 1 0 0 0 | 9018 | 71 | — | — | — | — | — | — | — | — | — | — | 19.4 | D |
| 742 | A2666 E | 84 | 1 1 1 1 1 | 8391 | 19 | — | 181 | 14 | — | 4.31 | 0.35 | — | 0.277 | 0.014 | — | 27.4 | B |
| 750 | COMA 70 | 90 | 1 1 1 1 1 | 6368 | 21 | — | 139 | 13 | — | 5.02 | 0.44 | — | 0.295 | 0.018 | — | 21.3 | B |
| 751 | COMA 69 | 90 | 1 1 1 1 1 | 7065 | 29 | — | 206 | 25 | — | 5.37 | 0.43 | — | 0.333 | 0.018 | — | 18.9 | B |
| 752 | COMA 240 | 90 | 1 1 1 1 1 | 6761 | 24 | — | 286 | 24 | — | 5.29 | 0.28 | — | 0.287 | 0.015 | — | 44.1 | A |
| 753 | COMA 239 | 90 | 1 1 1 1 1 | 6266 | 22 | — | 196 | 14 | — | 4.76 | 0.29 | — | 0.257 | 0.015 | — | 37.4 | A |
| 754 | COMA 194 | 90 | 1 1 1 1 0 | 7963 | 36 | — | 276 | 45 | — | 4.54 | 0.44 | — | — | — | — | 28.5 | A |
| 755 | COMA 159 | 90 | 2 2 2 2 2 | 6811 | 15 | 1 | 179 | 9 | 18 | 4.47 | 0.25 | 0.11 | 0.261 | 0.011 | 0.009 | 48.7 | A |
| 756 | COMA 133 | 90 | 2 2 2 2 2 | 4829 | 15 | 8 | 208 | 11 | 12 | 4.82 | 0.24 | 0.41 | 0.262 | 0.011 | 0.000 | 47.5 | A |
| 758 | COMA 31 | 90 | 1 1 1 1 0 | 7376 | 33 | — | 204 | 36 | — | 4.30 | 0.55 | — | — | — | — | 20.0 | A |
| 759 | COMA 49 | 90 | 1 1 1 1 1 | 7853 | 24 | — | 293 | 18 | — | 5.52 | 0.24 | — | 0.308 | 0.014 | — | 57.9 | A |
| 761 | COMA 103 | 90 | 1 1 1 1 1 | 4752 | 16 | — | 205 | 17 | — | 3.94 | 0.26 | — | 0.274 | 0.011 | — | 46.1 | A |
| 762 | COMA 106 | 90 | 1 1 1 1 1 | 5132 | 21 | — | 151 | 14 | — | 4.85 | 0.40 | — | 0.252 | 0.015 | — | 21.9 | B |
| 763 | COMA 107 | 90 | 1 1 1 1 1 | 6499 | 21 | — | 133 | 20 | — | 4.89 | 0.74 | — | 0.229 | 0.025 | — | 13.9 | C |
| 764 | COMA 118 | 90 | 1 1 1 1 1 | 7497 | 21 | — | 170 | 11 | — | 4.83 | 0.26 | — | 0.257 | 0.015 | — | 41.4 | A |
| 765 | COMA 129 | 90 | 3 3 3 3 2 | 7199 | 21 | 13 | 250 | 20 | 21 | 4.64 | 0.24 | 0.20 | 0.285 | 0.011 | 0.011 | 40.6 | B |
| 766 | COMA 134 | 90 | 1 1 1 1 1 | 7021 | 21 | — | 141 | 13 | — | 5.23 | 0.41 | — | 0.260 | 0.016 | — | 21.7 | B |
| 767 | COMA 135 | 90 | 2 2 2 2 2 | 8312 | 14 | 15 | 117 | 15 | 2 | 4.38 | 0.54 | 0.29 | 0.215 | 0.019 | 0.025 | 17.7 | C |
| 768 | COMA 136 | 90 | 1 1 1 1 1 | 5706 | 24 | — | 181 | 18 | — | 4.86 | 0.51 | — | 0.253 | 0.018 | — | 20.5 | B |
| 769 | COMA 148 | 90 | 3 3 3 3 3 | 6451 | 20 | 31 | 356 | 20 | 11 | 5.45 | 0.18 | 0.14 | 0.333 | 0.008 | 0.009 | 62.0 | A |
| 770 | COMA 160 | 90 | 1 1 1 1 0 | 7673 | 20 | — | 148 | 10 | — | 3.88 | 0.43 | — | — | — | — | 50.3 | A |
| 771 | COMA 172 | 90 | 1 1 1 1 1 | 5734 | 34 | — | 171 | 48 | — | 3.96 | 1.29 | — | 0.212 | 0.039 | — | 8.4 | A |
| 772 | COMA 217 | 90 | 1 1 1 1 1 | 6713 | 30 | — | 200 | 41 | — | 4.23 | 0.84 | — | 0.271 | 0.031 | — | 14.5 | A |
| 773 | N3379 | 95 | 2 2 2 2 0 | 908 | 12 | 10 | 185 | 7 | 4 | 4.76 | 0.21 | 0.11 | — | — | — | 78.1 | A |
| 774 | N 936 | 95 | 3 3 3 3 3 | 1425 | 9 | 17 | 150 | 6 | 2 | 4.67 | 0.11 | 0.03 | 0.330 | 0.006 | 0.019 | 102.7 | A |

**Table 5** – *continued*

| (1) GIN | (2) Galaxy Name | (3) CAN | (4) $N$ $s\ z\ \sigma\ b\ 2$ | (5) $cz$ (km s$^{-1}$) | (6) $\Delta cz$ | (7) $\delta cz$ | (8) $\sigma$ (km s$^{-1}$) | (9) $\Delta\sigma$ | (10) $\delta\sigma$ | (11) Mg$b$ | (12) $\Delta$Mg$b$ (Å) | (13) $\delta$Mg$b$ | (14) $Mg_2$ | (15) $\Delta Mg_2$ (mag) | (16) $\delta Mg_2$ | (17) S/N | (18) $Q$ |
|---|---|---|---|---|---|---|---|---|---|---|---|---|---|---|---|---|---|
| 775 | N3115 | 95 | 1 1 1 1 0 | 732 | 20 | — | 239 | 14 | — | 4.44 | 0.34 | — | — | — | — | 50.8 | A |
| 776 | N3377 | 95 | 1 1 1 1 1 | 643 | 18 | — | 116 | 15 | — | 3.72 | 0.40 | — | 0.289 | 0.017 | — | 52.5 | A |
| 777 | N4365 | 95 | 1 1 1 1 0 | 1252 | 19 | — | 236 | 16 | — | 4.95 | 0.38 | — | — | — | — | 43.9 | A |
| 778 | N4374 | 91 | 1 1 1 1 0 | 1028 | 18 | — | 236 | 13 | — | 4.45 | 0.35 | — | — | — | — | 53.9 | A |
| 779 | N4382 | 91 | 1 1 1 1 0 | 719 | 18 | — | 134 | 11 | — | 2.88 | 0.26 | — | — | — | — | 59.1 | A |
| 780 | N4406 | 91 | 1 1 1 1 0 | −209 | 20 | — | 246 | 17 | — | 5.45 | 0.34 | — | — | — | — | 43.4 | A |
| 781 | N4472 | 91 | 1 1 1 1 0 | 984 | 18 | — | 260 | 11 | — | 4.69 | 0.34 | — | — | — | — | 57.7 | A |
| 782 | N4473 | 91 | 2 2 2 2 1 | 2250 | 13 | 5 | 164 | 6 | 10 | 5.03 | 0.19 | 0.06 | 0.311 | 0.013 | — | 103.5 | A |
| 783 | N4486B | 91 | 1 1 1 1 0 | 1494 | 21 | — | 158 | 17 | — | 3.40 | 0.44 | — | — | — | — | 29.2 | A |
| 784 | N4494 | 95 | 1 1 1 1 0 | 1351 | 17 | — | 145 | 10 | — | 4.20 | 0.37 | — | — | — | — | 44.3 | A |
| 785 | COMA 130 | 90 | 1 1 1 1 1 | 7247 | 29 | — | 236 | 26 | — | 4.70 | 0.49 | — | 0.258 | 0.016 | — | 23.0 | B |
| 786 | COMA 153 | 90 | 2 1 1 1 0 | 6693 | 21 | — | 149 | 12 | — | 3.92 | 0.44 | — | — | — | — | 38.6 | B |
| 787 | COMA 124 | 90 | 1 1 1 1 1 | 6705 | 22 | — | 204 | 16 | — | 4.58 | 0.36 | — | 0.260 | 0.016 | — | 29.0 | B |
| 788 | COMA 125 | 90 | 1 1 1 1 1 | 6926 | 23 | — | 186 | 18 | — | 4.16 | 0.43 | — | 0.207 | 0.015 | — | 23.7 | B |
| 789 | COMA 143 | 90 | 1 1 1 1 1 | 5000 | 38 | — | 219 | 57 | — | 4.68 | 0.95 | — | 0.294 | 0.033 | — | 10.9 | A |
| 790 | COMA 168 | 90 | 1 1 1 1 1 | 7044 | 41 | — | 244 | 66 | — | 4.51 | 1.07 | — | 0.269 | 0.033 | — | 10.7 | A |
| 791 | COMA 151 | 90 | 4 4 4 4 4 | 6379 | 10 | 16 | 152 | 7 | 7 | 4.85 | 0.21 | 0.66 | 0.256 | 0.009 | 0.033 | 47.0 | A |
| 792 | COMA 150 | 90 | 2 2 2 2 2 | 7258 | 14 | 12 | 112 | 12 | 0 | 5.30 | 0.37 | 0.37 | 0.268 | 0.015 | 0.027 | 22.6 | B |
| 794 | N 584 | 95 | 2 2 2 2 1 | 1854 | 11 | 8 | 179 | 6 | 3 | 4.28 | 0.11 | 0.25 | 0.337 | 0.008 | — | 113.2 | A |
| 795 | N 596 | 95 | 2 2 2 2 1 | 1876 | 11 | 8 | 146 | 6 | 9 | 3.96 | 0.13 | 0.04 | 0.293 | 0.009 | — | 96.0 | A |
| 796 | N4697 | 95 | 1 1 1 1 0 | 1237 | 19 | — | 164 | 7 | — | 3.96 | 0.40 | — | — | — | — | 90.8 | A |
| 797 | N5846 | 95 | 1 1 1 1 1 | 1724 | 32 | — | 221 | 47 | — | 4.43 | 0.86 | — | 0.307 | 0.030 | — | 14.4 | A |
| 799 | N7626 | 95 | 4 4 4 4 3 | 3403 | 10 | 35 | 244 | 8 | 8 | 5.07 | 0.13 | 0.29 | 0.338 | 0.007 | 0.018 | 80.9 | A |
| 800 | N4486 | 91 | 1 1 1 1 0 | 1290 | 22 | — | 321 | 14 | — | 5.04 | 0.39 | — | — | — | — | 97.9 | A |

The columns of this table give: (1) galaxy identification number (GIN); (2) galaxy name; (3) the cluster assignment number (CAN); (4) the number of spectra $N_s$, redshifts $N_z$, dispersions $N_\sigma$, Mg$b$ linestrengths $N_b$ and $Mg_2$ linestrengths $N_2$ obtained for this object; then the combined estimate, its estimated total error ($\Delta$) and the weighted rms error from any repeat observations ($\delta$) for each of (5)–(7) redshift, (8)–(10) dispersion, (11)–(13) Mg$b$ linestrength and (14)–(16) $Mg_2$ linestrength; (17) the combined S/N estimate; and (18) the overall quality parameter (with an asterisk if the galaxy possesses emission lines). Only objects with useful measurements are included; hence the lowest quality class present in this table is $Q$ = D, and the seven galaxies with only $Q$ = E spectra (GINs 123, 284, 389, 448, 599, 637 and 679) are omitted. The data in this table are available from NASA's Astrophysical Data Center (ADC, http://adc.gsfc.nasa.gov, J/MNRAS/305/259) and from the Centre de Données astronomiques de Strasbourg (CDS, http://cdsweb.u-strasbg.fr, J/MNRAS/305/259).

We determine the zero-point calibration of our linestrength measurements with respect to the Lick system (see Section 3.2) by comparing our Mg$b'$ and $Mg_2$ linestrengths with measurements for the same galaxies given by Trager et al. (1998). We find that slightly different calibrations are needed for objects with different redshifts, the result of slight variations in the non-linear continuum shape as the spectra are redshifted with respect to the instrumental response and the sky background (see Section 3.2). Good agreement with Trager et al. is obtained if we use different zero-points for galaxies with redshifts above and below $cz = 3000\,\mathrm{km\,s^{-1}}$ (although there are no objects in the comparison at $cz > 10\,000\,\mathrm{km\,s^{-1}}$). Excluding a few outliers, we find weighted mean differences between the EFAR and Trager et al. linestrengths of $\langle\Delta\mathrm{Mg}b'\rangle = -0.022$ mag and $\langle\Delta\mathrm{Mg_2}\rangle = -0.083$ mag for $cz < 3000\,\mathrm{km\,s^{-1}}$, and $\langle\Delta\mathrm{Mg}b'\rangle = -0.008$ mag and $\langle\Delta\mathrm{Mg_2}\rangle = -0.028$ mag for $cz \geq 3000\,\mathrm{km\,s^{-1}}$. Subtracting these zero-point corrections gives the final, fully corrected linestrength measurements as listed in Tables 3 and 5. Figs 14 and 15 show the residual differences between the EFAR and Trager et al. linestrength measurements after applying these zero-point corrections. The rms scatter is 0.019 mag in Mg$b'$ for the 41 objects in common, and 0.023 mag in $Mg_2$ for the 24 objects in common. There is no statistically significant trend with linestrength, velocity dispersion or redshift remaining in the residuals after these zero-point corrections are applied.

Fig. 16 compares our calibrated $Mg_2$ linestrengths with those obtained in A2199, A2634 and Coma by Lucey et al. (1997). The overall agreement for the 36 objects in common is very good, with a statistically non-significant zero-point offset and an rms scatter of 0.029 mag, similar to that found in the comparison with Trager et al.

The relation between the measured Mg$b'$ and $Mg_2$ linestrengths for all the galaxies in the EFAR sample is shown in Fig. 17. We fit this relation using a maximum likelihood technique which accounts for both measurement errors and selection effects (Saglia et al., in preparation; Paper VI). We find

$$\mathrm{Mg_2} = 1.94\mathrm{Mg}b' - 0.05, \qquad (13)$$

with a perpendicular rms residual of 0.019 mag (corresponding to an rms of 0.041 mag in $Mg_2$, or 0.021 mag in Mg$b'$). The relation is the same if we fit ellipticals, E/S0s, cDs or spirals separately. This relation is similar to those derived by Burstein et al. (1984) and Jørgensen (1997). We can therefore use Mg$b'$ as a predictor of $Mg_2$ (albeit with larger uncertainties) for those cases in which $Mg_2$ cannot be measured directly.

Also shown in Fig. 17 is the predicted relation between Mg$b'$ and $Mg_2$ as a function of age and metallicity given by Worthey (1994). His models correctly predict the slope of the relation, but are offset by −0.025 mag in Mg$b'$(or by +0.05 mag in $Mg_2$), indicating a difference in the zero-point calibration of the model for one or both indices.

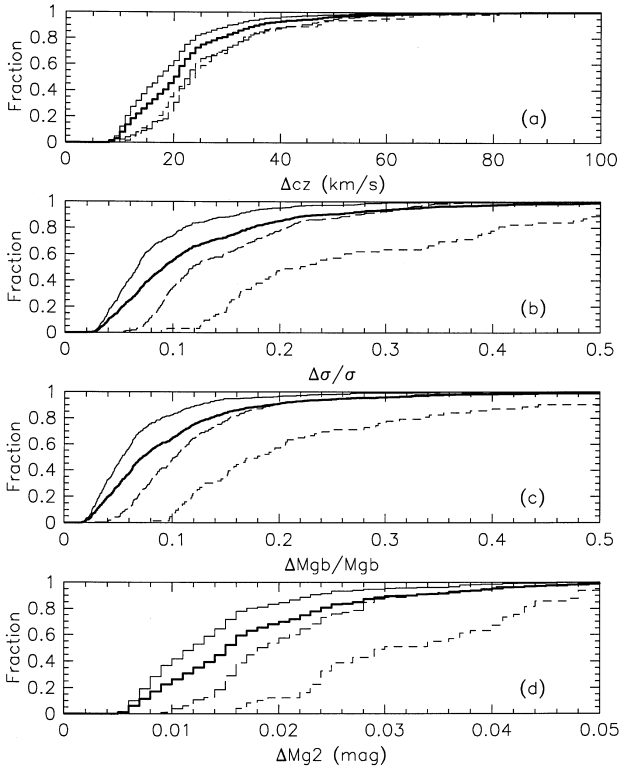


**Figure 8.** The cumulative distributions of the total estimated errors in the combined measurements of redshift, velocity dispersion, Mg*b* and $Mg_2$ for each galaxy. The distributions for quality classes A, B and C are shown as full, long-dashed and short-dashed lines respectively; the overall distribution is shown as the thick full line. (a) The distribution of combined errors in *cz*; (b) combined relative errors in $\sigma$; (c) combined relative errors in Mg*b*; (d) combined errors in $Mg_2$.

## 5 CLUSTER ASSIGNMENTS

The correct assignment of galaxies to clusters (or groups) is crucial to obtaining reliable redshifts and distances for the EFAR cluster sample. We also need to increase the precision of the cluster redshifts in order to minimize uncertainties in the peculiar velocities of the clusters. To achieve these goals we merged the EFAR redshifts with redshifts for all galaxies in ZCAT (Huchra et al. 1992, version of 1997 May 29) that lie within $3\,h^{-1}$ Mpc (2 Abell radii) of each nominal EFAR cluster centre (see table 1 of Paper I). We then examined the redshift distributions of the combined sample in order to distinguish groups, clusters and field galaxies along the line of sight to a nominal EFAR 'cluster'. We also considered the distribution of galaxies on the sky before assigning the EFAR galaxies to specific groupings.

The results of this process are shown in Fig. 18, which shows the redshift distributions of galaxies within $3\,h^{-1}$ Mpc around each of the nominal EFAR clusters (labelled by their cluster ID number, CID; see Paper I) and the adopted groupings in redshift space. Note that CID = 81 (A2593-S) does not appear since it was merged with CID = 80 (A2593-N) – see below. Each EFAR galaxy was assigned to one of these groupings and given a cluster assignment number

**Table 6.** The distribution of errors per galaxy.

| *Q* | $\Delta cz$ (km s$^{-1}$) | | $\Delta\sigma/\sigma$ | | $\Delta$Mg*b*/Mg*b* | | $\Delta Mg_2$ (mag) | |
|---|---|---|---|---|---|---|---|---|
| | 50% | 90% | 50% | 90% | 50% | 90% | 50% | 90% |
| All | 20 | 36 | 0.091 | 0.240 | 0.072 | 0.188 | 0.015 | 0.032 |
| A | 17 | 30 | 0.067 | 0.161 | 0.053 | 0.120 | 0.012 | 0.023 |
| B | 23 | 44 | 0.118 | 0.270 | 0.103 | 0.194 | 0.018 | 0.033 |
| C | 24 | 47 | 0.220 | 0.507 | 0.180 | 0.425 | 0.030 | 0.048 |

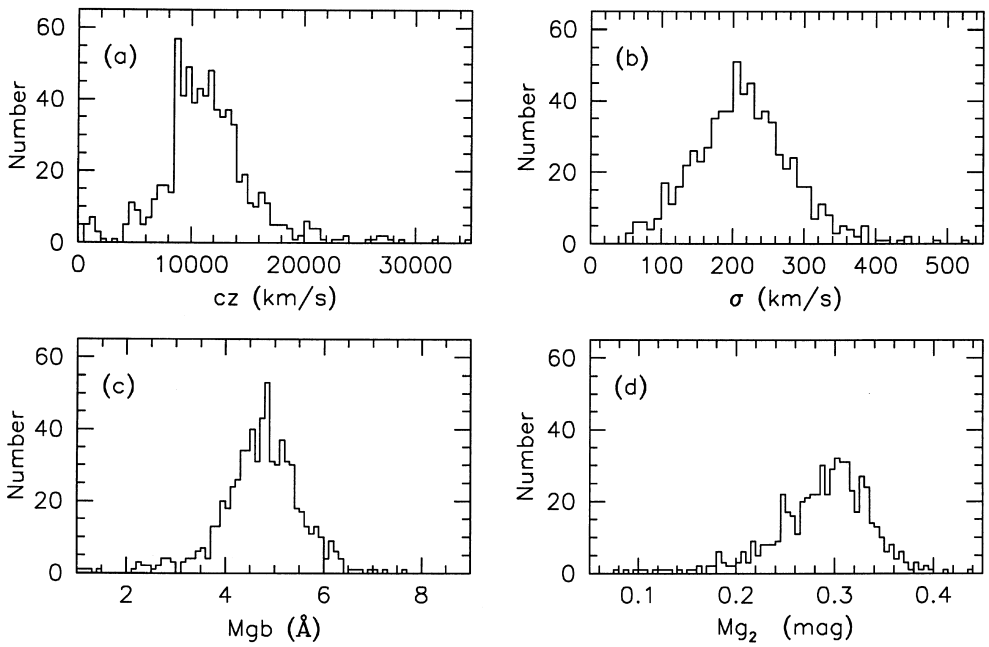


**Figure 9.** The distributions of (a) redshift, (b) velocity dispersion, (c) Mg*b* linestrength and (d) $Mg_2$ linestrength for the galaxies in the EFAR sample.

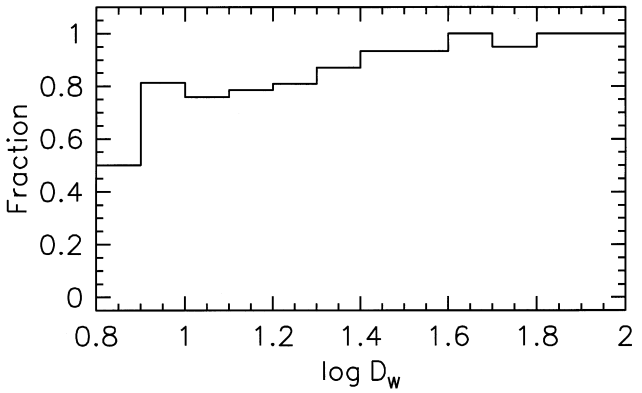


**Figure 10.** The fraction of programme objects for which we measured a velocity dispersion as a function of the logarithm of the selection diameter $D_W$ (in arcsec).

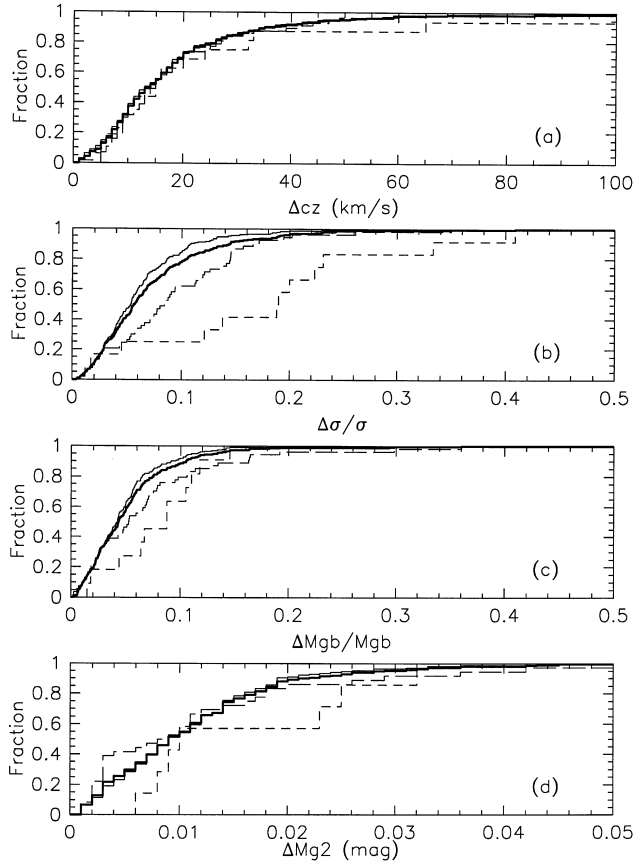


**Figure 11.** The cumulative distributions of the rms errors from repeat measurements of redshift, velocity dispersion, Mg*b* and $Mg_2$. The distributions for spectral types A, B and C are shown as full, long-dashed and short-dashed lines respectively; the overall distribution is shown as the thick full line. (a) The distribution of rms errors in $cz$ in $km\,s^{-1}$; (b) relative rms errors in $\sigma$; (c) relative rms errors in Mg*b*; (d) rms errors in $Mg_2$.

(CAN), listed in Table 5. The main grouping along the line of sight has a CAN which is simply the original two-digit CID; other groupings have CANs with a distinguishing third leading digit. The groupings (which we will hereafter call clusters regardless of their size) are labelled by their CANs in Fig. 18, which also shows the boundaries of each cluster in redshift space. The last two digits of each galaxy's CAN is its CID, apart from 41 galaxies which were

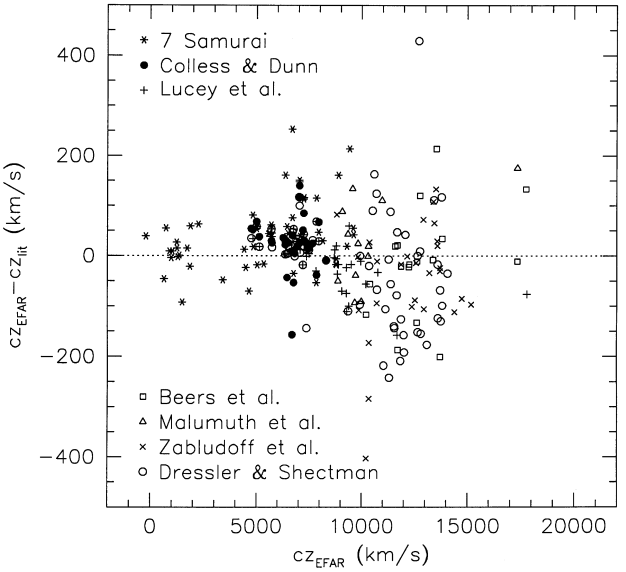


**Figure 12.** Differences between EFAR redshifts and those from various sources in the literature.

reassigned to other neighbouring clusters: two galaxies in CID = 33 were reassigned to CAN = 34 (GINs 254 and 255); two galaxies in CID = 34 were reassigned to CAN = 33 (GINs 263 and 264); five galaxies in CID = 35 were reassigned to CAN = 36 (GINs 270, 274, 275, 281 and 282); 14 galaxies in CID = 36 were reassigned to CAN = 35 (GINS 285–292, 295–297 and 299–301); one galaxy in CID = 47 was reassigned to CAN = 50 (GIN 406); three galaxies in CID = 59 and two in CID = 61 were reassigned to CAN = 53 (GINs 514, 517, 527, 536 and 537); five galaxies with CID = 69 were reassigned to CAN = 70 (GINs 617, 618, 619, 622 and 623); and all seven galaxies with CID = 81 were reassigned to CAN = 80 (GINs 709–715).

Table 7 lists, for each CAN, the number of EFAR galaxies, the number of EFAR+ZCAT galaxies, and the mean redshift, its standard error (taken to the error in the redshift for clusters with only one member) and the velocity dispersion. These quantities are computed both from the EFAR sample and from the EFAR+ZCAT sample. In many of the clusters the EFAR sample is greatly supplemented by the ZCAT galaxies, leading to much improved estimates of the mean cluster redshift: using EFAR galaxies only, the median uncertainty in the mean cluster redshift (for clusters with more than one member) is $177\,km\,s^{-1}$; with EFAR+ZCAT galaxies, the median uncertainty is reduced to $133\,km\,s^{-1}$.

## 6 CONCLUSIONS

We have described the observations, reductions and analysis of 1319 spectra of 714 early-type galaxies studied as part of the EFAR project. We have obtained redshifts for 706 galaxies, velocity dispersions and Mg*b* linestrengths for 676 galaxies, and $Mg_2$ linestrengths for 582 galaxies. Although obtained in 33 observing runs spanning seven years and 10 different telescopes, we have applied uniform procedures to derive the spectroscopic parameters and brought all the measurements of each parameter on to a standard system, which we ensure is internally consistent through comparisons of the large numbers of repeat measurements, and externally consistent through comparisons with published data. We have performed detailed simulations to estimate measurement errors, and calibrated these error estimates using the repeat observations.

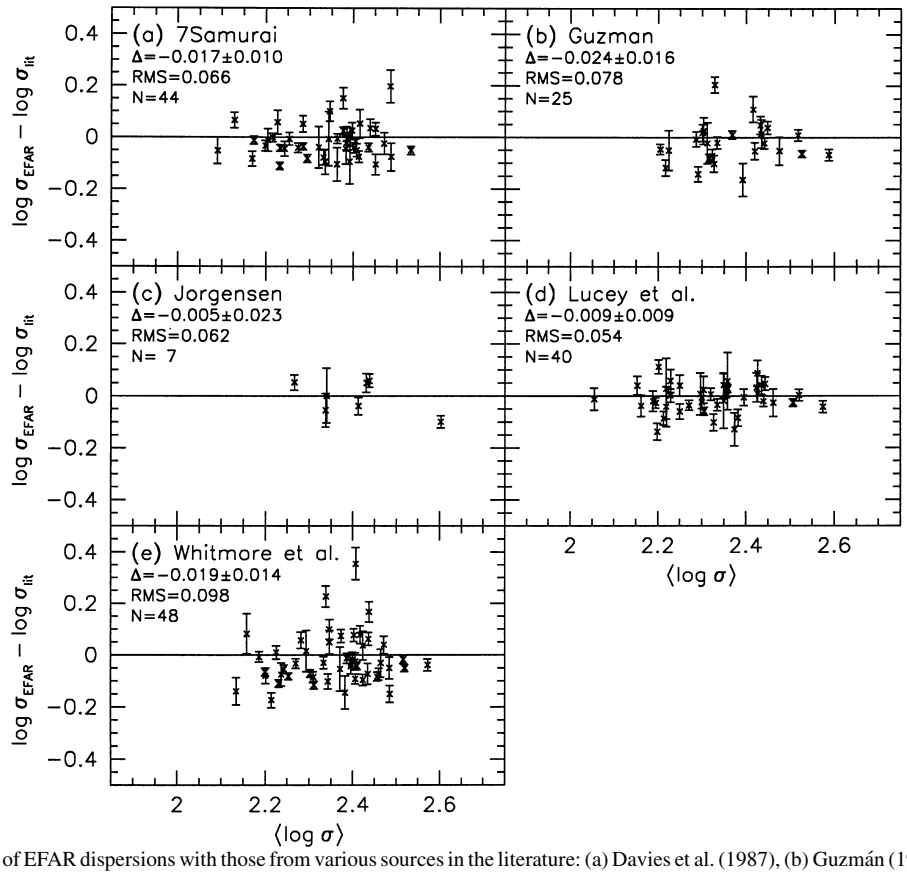


**Figure 13.** Comparisons of EFAR dispersions with those from various sources in the literature: (a) Davies et al. (1987), (b) Guzmán (1993), (c) Jørgensen (1997), (d) Lucey et al. (1997) and (e) Whitmore et al. (1985). In each case the mean difference, $\Delta = \langle \log \sigma_{\rm EFAR} - \log \sigma_{\rm lit} \rangle$, and its standard error are indicated, along with the rms scatter and the number of galaxies in the comparison.

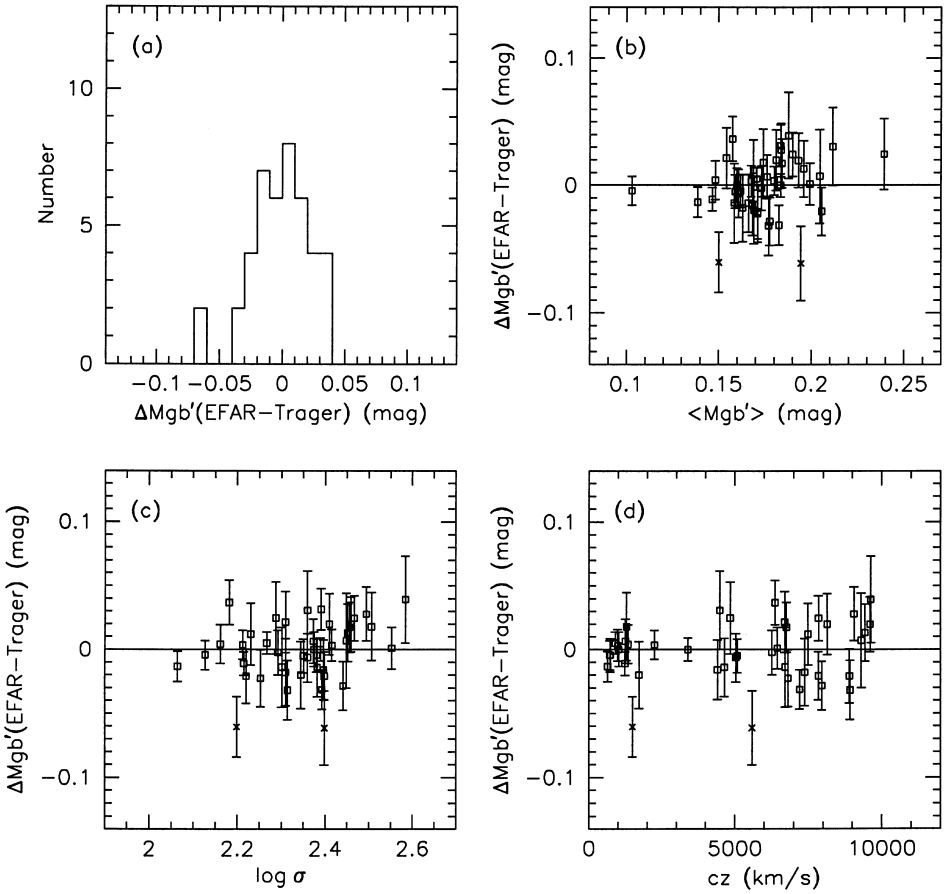


**Figure 14.** The residual differences in Mg$b'$ linestrengths from EFAR and Trager et al. (1998) *after* applying the zero-point corrections discussed in the text: (a) the distribution of residuals; (b) the residuals as a function of Mg$b'$; (c) the residuals as a function of log $\sigma$; (d) the residuals as a function of redshift. Outliers excluded from the determination of the zero-point corrections are shown as crosses.

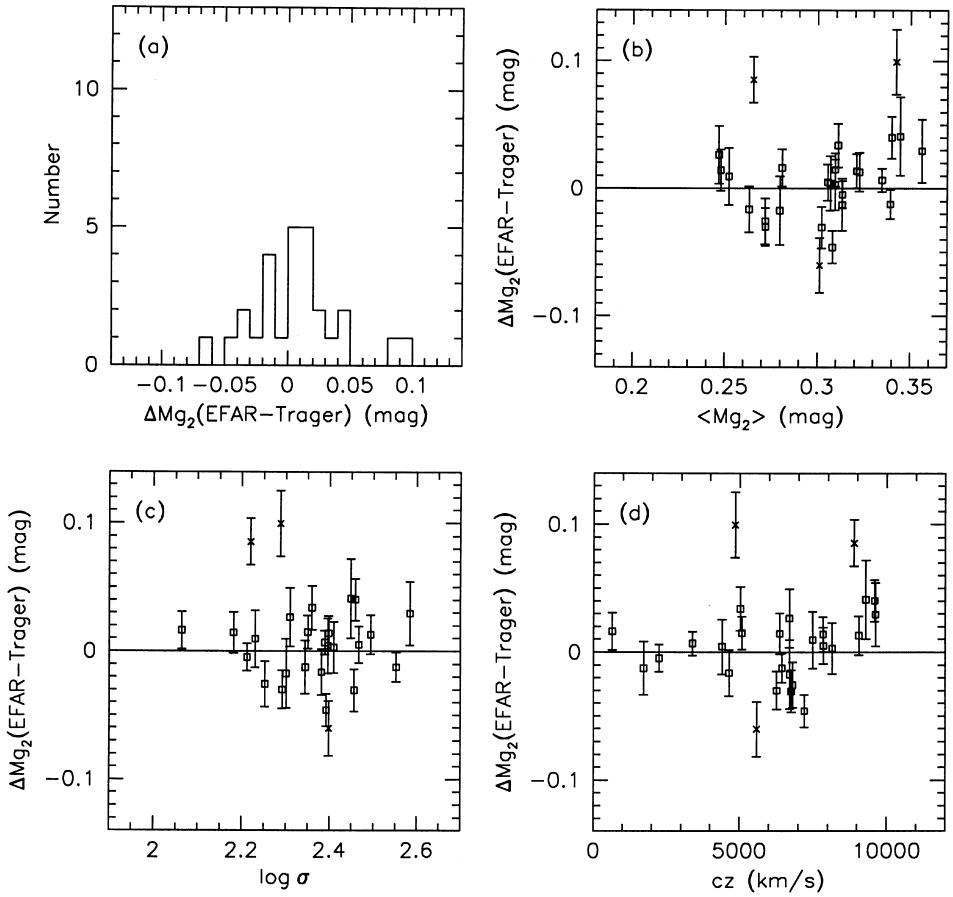


**Figure 15.** The residual differences in $Mg_2$ linestrengths from EFAR and Trager et al. (1998) *after* applying the zero-point corrections discussed in the text: (a) the distribution of residuals; (b) the residuals as a function of $Mg_2$; (c) the residuals as a function of log $\sigma$; (d) the residuals as a function of redshift. Outliers excluded from the determination of the zero-point corrections are shown as crosses.

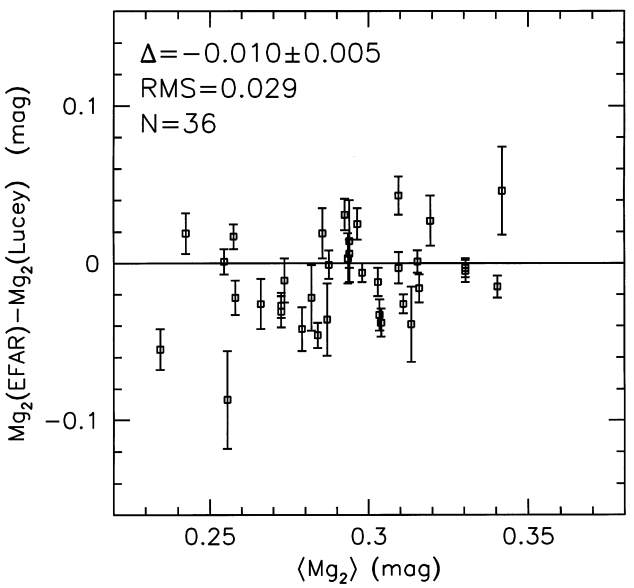


**Figure 16.** Comparisons of $Mg_2$ linestrengths obtained by EFAR and Lucey et al. (1997). The mean difference, $\Delta = Mg_2(\mathrm{EFAR}) - Mg_2(\mathrm{Lucey})$, and its standard error are indicated, along with the rms scatter and the number of galaxies in the comparison.

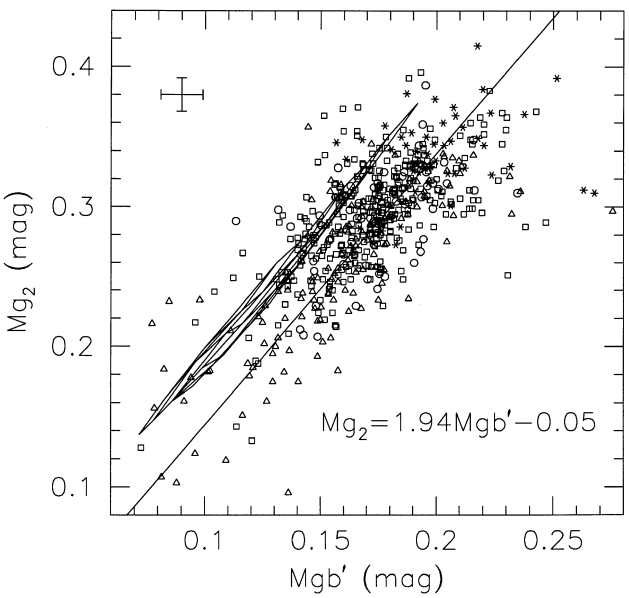


**Figure 17.** The relation between Mg$b'$ and $Mg_2$ and its maximum likelihood fit. Ellipticals are marked by circles, E/S0s by squares, cDs by asterisks and spirals by triangles. Typical estimated errors are shown in the top left corner. The relation between Mg$b'$ and $Mg_2$ as a function of age and metallicity, as predicted by Worthey (1994), is shown as the grid lying parallel to, but offset from, the data.

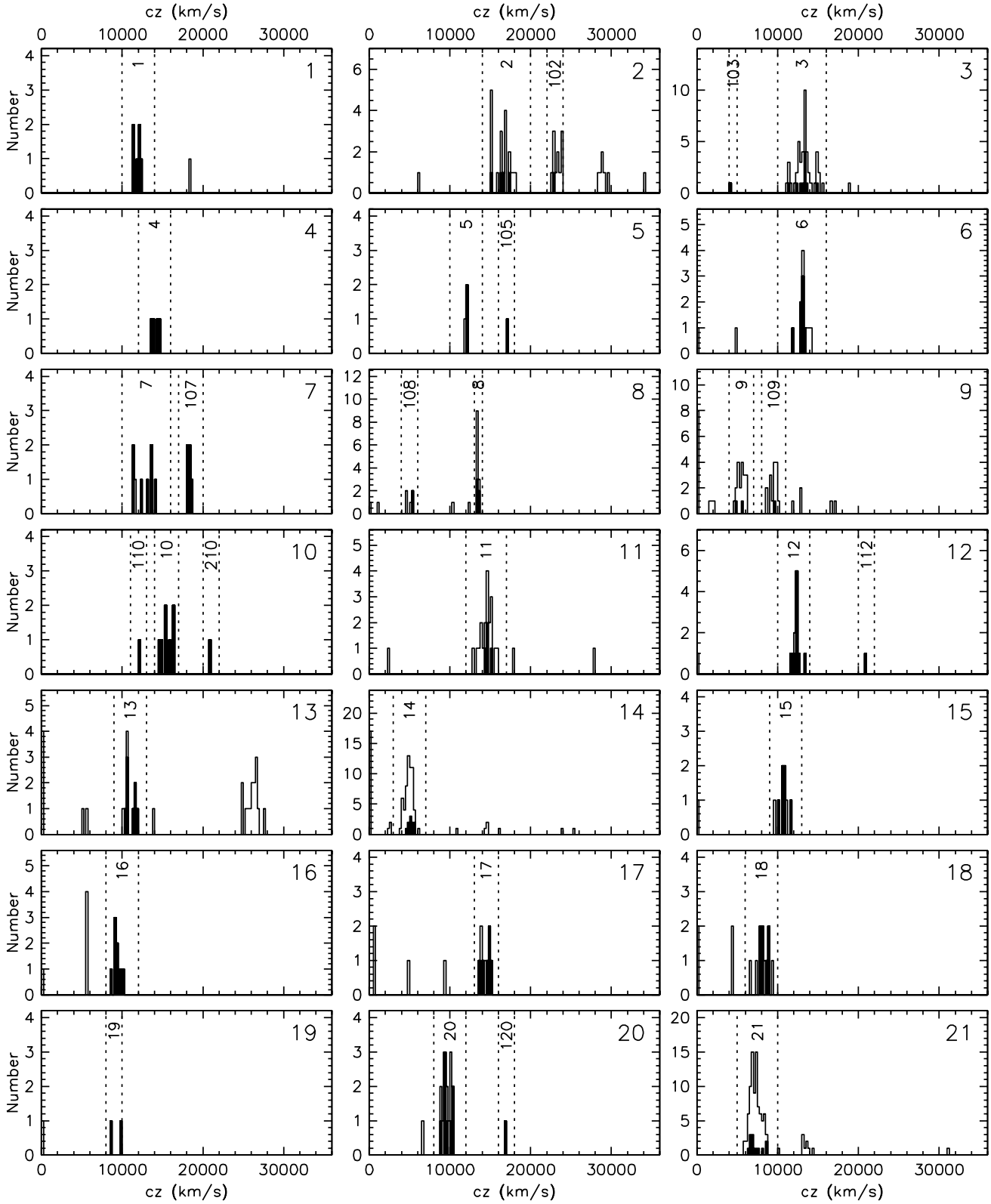


**Figure 18.** The redshift distributions of galaxies within $3\,h^{-1}$ Mpc of each nominal EFAR cluster using the EFAR and ZCAT data. Each distribution is labelled at top right by the nominal cluster ID number (CID). The solid histogram shows the distribution of EFAR galaxies; the open histogram shows the extra ZCAT galaxies. The groupings adopted have boundaries in redshift marked by dotted lines and are labelled by their cluster assignment number (CAN). Clusters without numbers and boundaries contain no EFAR galaxies.

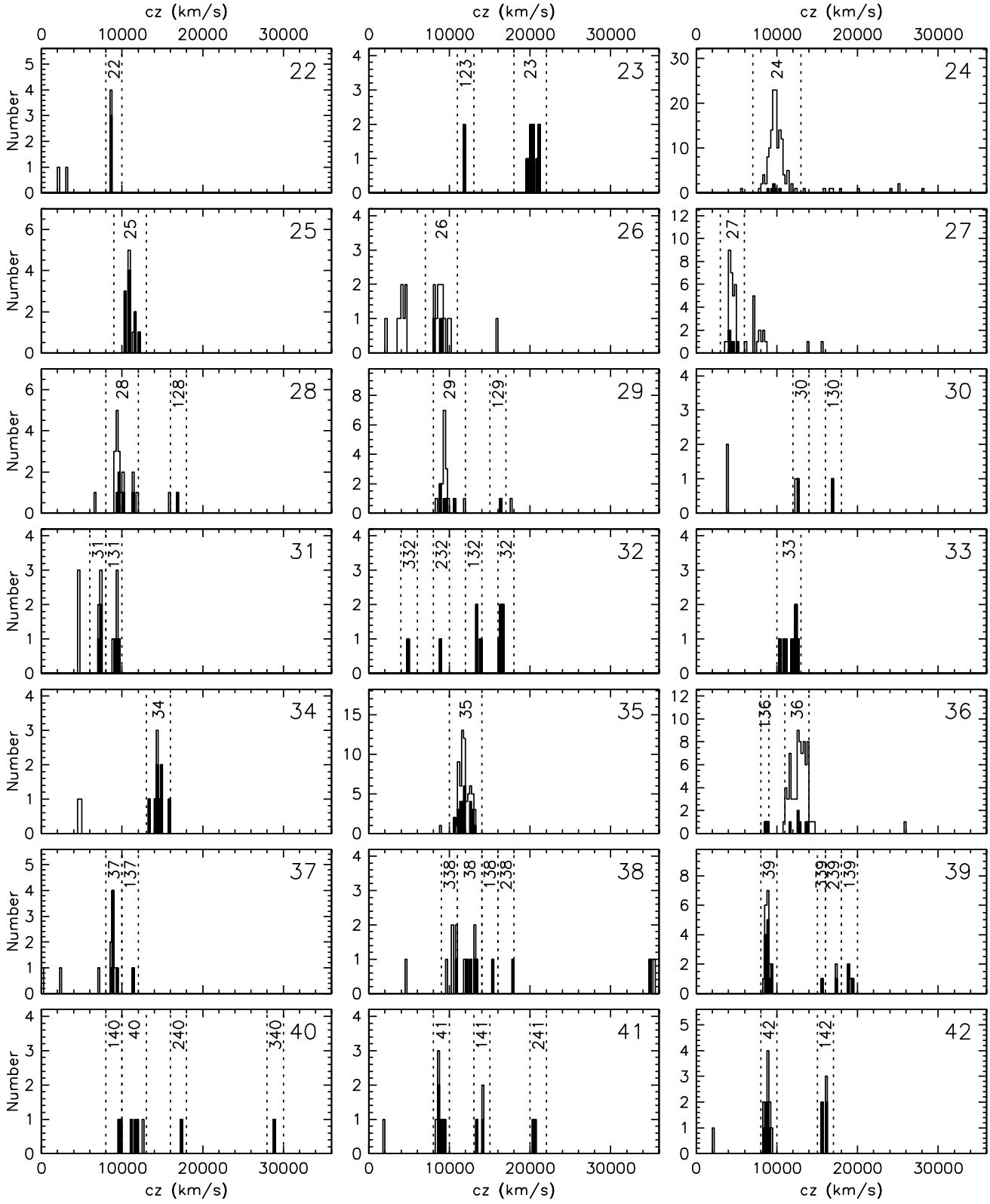


**Figure 18** – *continued*

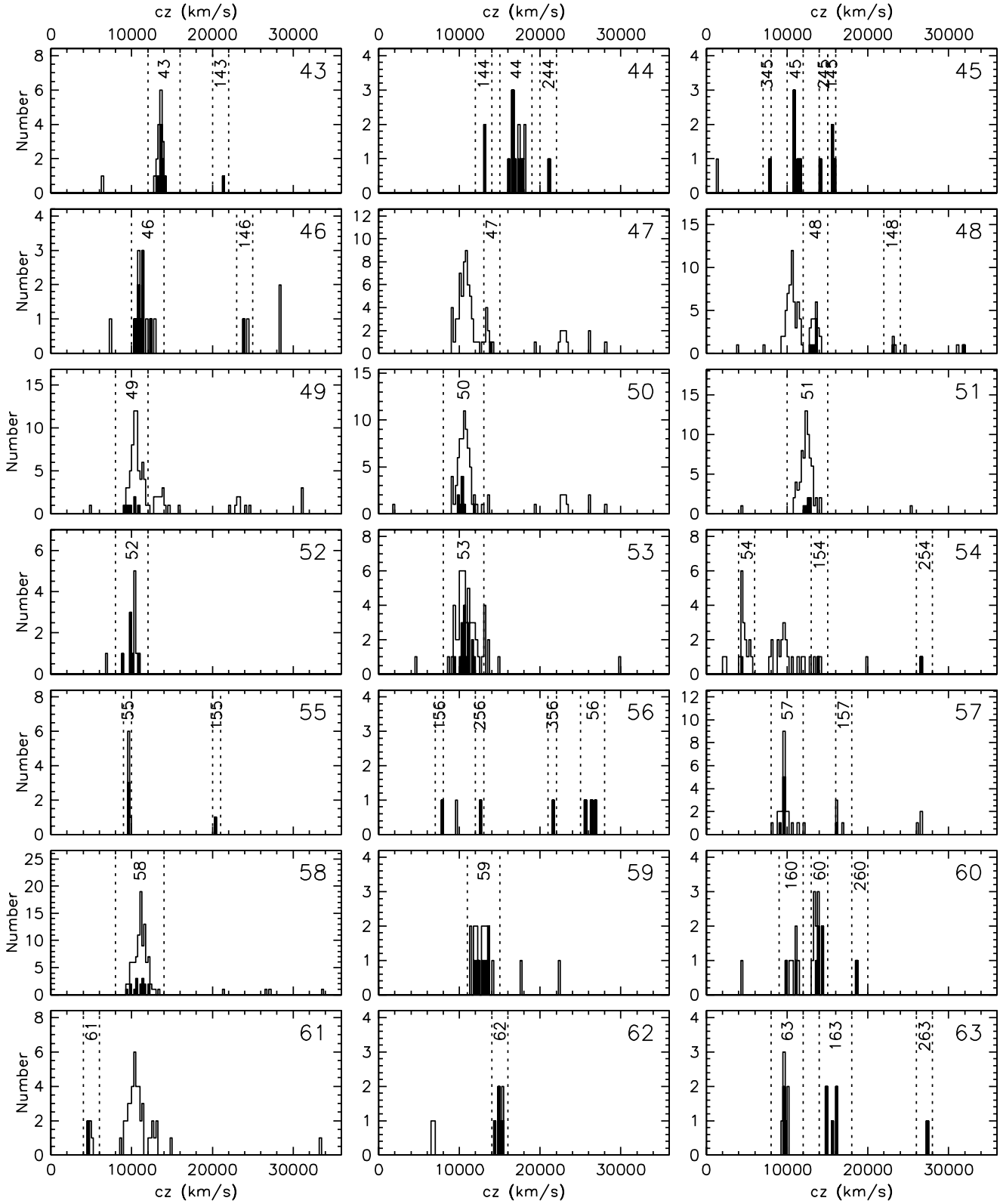


**Figure 18** – *continued*

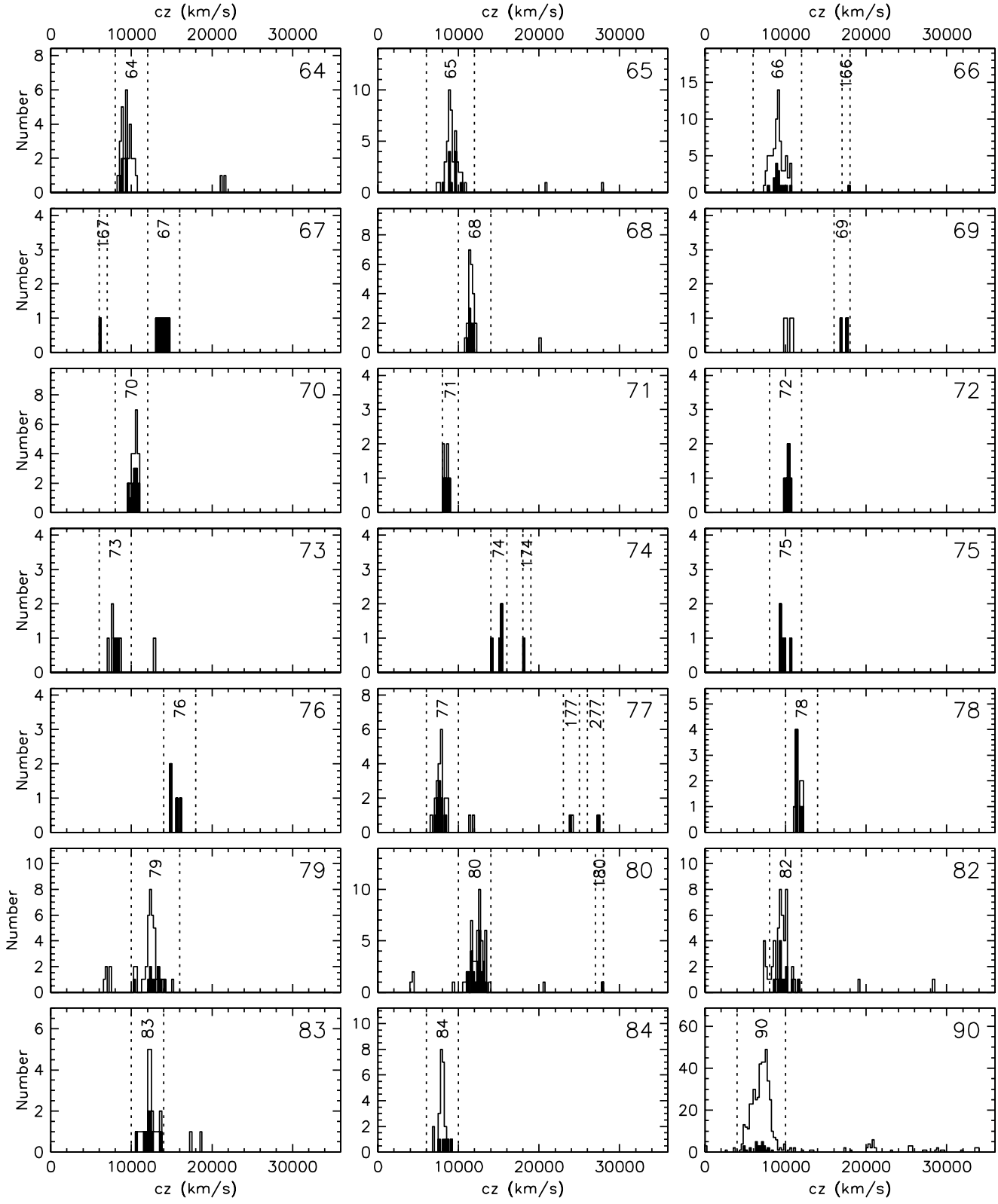


**Figure 18** – *continued*

**Table 7.** Cluster mean redshifts and velocity dispersions.

| | | EFAR | | | EFAR+ZCAT | | | | EFAR | | | EFAR+ZCAT | |
|---|---|---|---|---|---|---|---|---|---|---|---|---|---|
| CAN | $N$ | $\langle cz \rangle$ | $\sigma$ | $N$ | $\langle cz \rangle$ | $\sigma$ | CAN | $N$ | $\langle cz \rangle$ | $\sigma$ | $N$ | $\langle cz \rangle$ | $\sigma$ |
| 1 | 6 | 11888 ± 191 | 468 | 6 | 11888 ± 191 | 468 | 241 | 2 | 20440 ± 94 | 134 | 2 | 20440 ± 94 | 134 |
| 2 | 4 | 16332 ± 466 | 931 | 19 | 16454 ± 227 | 991 | 42 | 6 | 8783 ± 114 | 280 | 11 | 8856 ± 93 | 309 |
| 102 | 1 | 22837 ± 71 | — | 11 | 23340 ± 134 | 444 | 142 | 4 | 15863 ± 146 | 292 | 5 | 15917 ± 125 | 280 |
| 3 | 10 | 13168 ± 287 | 907 | 45 | 13280 ± 158 | 1060 | 43 | 9 | 13667 ± 82 | 246 | 17 | 13536 ± 81 | 332 |
| 103 | 1 | 4127 ± 18 | — | 1 | 4127 ± 18 | — | 143 | 1 | 21438 ± 20 | — | 1 | 21438 ± 20 | — |
| 4 | 4 | 14090 ± 263 | 527 | 4 | 14090 ± 263 | 527 | 44 | 8 | 16950 ± 191 | 539 | 11 | 17184 ± 191 | 633 |
| 5 | 2 | 12082 ± 8 | 11 | 3 | 11994 ± 88 | 153 | 144 | 2 | 13190 ± 23 | 33 | 2 | 13190 ± 23 | 33 |
| 105 | 1 | 17154 ± 30 | — | 1 | 17154 ± 30 | — | 244 | 1 | 21199 ± 64 | — | 1 | 21199 ± 64 | — |
| 6 | 7 | 12899 ± 183 | 484 | 11 | 13193 ± 177 | 588 | 45 | 5 | 11123 ± 143 | 320 | 5 | 11123 ± 143 | 320 |
| 7 | 7 | 12782 ± 425 | 1123 | 8 | 12625 ± 400 | 1131 | 145 | 3 | 15757 ± 109 | 188 | 3 | 15757 ± 109 | 188 |
| 107 | 5 | 18296 ± 91 | 204 | 5 | 18296 ± 91 | 204 | 245 | 1 | 14024 ± 39 | — | 1 | 14024 ± 39 | — |
| 8 | 5 | 13466 ± 49 | 109 | 12 | 13414 ± 33 | 116 | 345 | 1 | 7789 ± 36 | — | 1 | 7789 ± 36 | — |
| 108 | 2 | 5276 ± 23 | 33 | 5 | 5000 ± 136 | 303 | 46 | 9 | 11136 ± 197 | 591 | 12 | 11321 ± 208 | 719 |
| 9 | 2 | 5212 ± 376 | 531 | 19 | 5482 ± 103 | 447 | 146 | 1 | 23945 ± 21 | — | 2 | 24166 ± 221 | 313 |
| 109 | 1 | 9599 ± 22 | — | 15 | 9473 ± 126 | 486 | 47 | 1 | 13876 ± 26 | — | 9 | 13576 ± 113 | 338 |
| 10 | 7 | 15546 ± 270 | 715 | 7 | 15546 ± 270 | 715 | 48 | 7 | 13466 ± 114 | 302 | 22 | 13455 ± 78 | 364 |
| 110 | 1 | 12206 ± 50 | — | 1 | 12206 ± 50 | — | 148 | 1 | 23099 ± 71 | — | 3 | 23233 ± 134 | 231 |
| 210 | 1 | 20957 ± 12 | — | 1 | 20957 ± 12 | — | 49 | 7 | 9944 ± 247 | 653 | 64 | 10528 ± 80 | 640 |
| 11 | 4 | 14747 ± 163 | 325 | 19 | 14499 ± 179 | 782 | 50 | 9 | 10427 ± 193 | 580 | 67 | 10548 ± 89 | 730 |
| 12 | 10 | 12342 ± 142 | 448 | 11 | 12315 ± 131 | 435 | 51 | 6 | 12593 ± 127 | 312 | 69 | 12353 ± 84 | 699 |
| 112 | 1 | 20993 ± 41 | — | 1 | 20993 ± 41 | — | 52 | 6 | 9982 ± 262 | 642 | 12 | 10215 ± 146 | 504 |
| 13 | 8 | 11074 ± 213 | 603 | 10 | 10944 ± 191 | 605 | 53 | 16 | 10786 ± 149 | 598 | 49 | 10675 ± 131 | 917 |
| 14 | 10 | 5145 ± 100 | 317 | 59 | 4935 ± 61 | 471 | 54 | 1 | 4410 ± 18 | — | 16 | 4699 ± 113 | 452 |
| 15 | 6 | 10725 ± 204 | 499 | 8 | 10655 ± 214 | 606 | 154 | 1 | 13830 ± 20 | — | 3 | 13818 ± 212 | 367 |
| 16 | 9 | 9376 ± 161 | 484 | 9 | 9376 ± 161 | 484 | 254 | 1 | 26612 ± 73 | — | 1 | 26612 ± 73 | — |
| 17 | 7 | 14417 ± 196 | 519 | 9 | 14355 ± 163 | 490 | 55 | 3 | 9635 ± 39 | 68 | 7 | 9636 ± 29 | 77 |
| 18 | 7 | 8353 ± 169 | 448 | 11 | 8206 ± 232 | 770 | 155 | 1 | 20285 ± 29 | — | 1 | 20285 ± 29 | — |
| 19 | 2 | 9256 ± 511 | 723 | 2 | 9256 ± 511 | 723 | 56 | 3 | 26280 ± 339 | 587 | 3 | 26280 ± 339 | 587 |
| 20 | 8 | 9676 ± 172 | 486 | 14 | 9663 ± 126 | 472 | 156 | 1 | 7955 ± 15 | — | 1 | 7955 ± 15 | — |
| 120 | 1 | 16841 ± 15 | — | 1 | 16841 ± 15 | — | 256 | 1 | 12730 ± 18 | — | 1 | 12730 ± 18 | — |
| 21 | 13 | 7241 ± 210 | 757 | 86 | 7253 ± 72 | 663 | 356 | 1 | 21558 ± 71 | — | 1 | 21558 ± 71 | — |
| 22 | 3 | 8666 ± 28 | 48 | 4 | 8649 ± 26 | 53 | 57 | 6 | 9520 ± 107 | 263 | 22 | 9582 ± 132 | 617 |
| 23 | 9 | 20400 ± 188 | 565 | 9 | 20400 ± 188 | 565 | 157 | 1 | 16075 ± 45 | — | 4 | 16237 ± 192 | 384 |
| 123 | 2 | 11852 ± 34 | 49 | 2 | 11852 ± 34 | 49 | 58 | 16 | 10943 ± 197 | 789 | 99 | 11106 ± 79 | 781 |
| 24 | 6 | 9651 ± 204 | 499 | 137 | 9854 ± 66 | 776 | 59 | 8 | 12864 ± 242 | 683 | 16 | 12693 ± 215 | 862 |
| 25 | 10 | 10999 ± 204 | 646 | 12 | 11021 ± 172 | 596 | 60 | 5 | 13993 ± 142 | 318 | 11 | 13707 ± 119 | 393 |
| 26 | 3 | 8677 ± 297 | 514 | 12 | 8937 ± 189 | 653 | 160 | 2 | 10474 ± 651 | 921 | 6 | 10730 ± 223 | 547 |
| 27 | 5 | 4540 ± 188 | 420 | 30 | 4436 ± 65 | 355 | 260 | 1 | 18545 ± 26 | — | 1 | 18545 ± 26 | — |
| 28 | 5 | 10030 ± 363 | 813 | 17 | 9884 ± 208 | 857 | 61 | 2 | 4742 ± 16 | 11 | 5 | 4878 ± 90 | 202 |
| 128 | 1 | 16920 ± 27 | — | 1 | 16920 ± 27 | — | 62 | 5 | 14918 ± 167 | 373 | 6 | 14991 ± 154 | 378 |
| 29 | 5 | 9492 ± 339 | 759 | 18 | 9528 ± 181 | 769 | 63 | 3 | 9699 ± 92 | 159 | 7 | 9777 ± 116 | 306 |
| 129 | 1 | 16483 ± 18 | — | 1 | 16483 ± 18 | — | 163 | 5 | 15563 ± 273 | 610 | 5 | 15563 ± 273 | 610 |
| 30 | 1 | 12711 ± 19 | — | 2 | 12576 ± 135 | 191 | 263 | 1 | 27486 ± 71 | — | 1 | 27486 ± 71 | — |
| 130 | 1 | 16760 ± 14 | — | 1 | 16760 ± 14 | — | 64 | 5 | 9062 ± 154 | 345 | 28 | 9423 ± 113 | 598 |
| 31 | 3 | 7288 ± 47 | 81 | 5 | 7289 ± 31 | 69 | 65 | 11 | 9223 ± 171 | 568 | 46 | 9137 ± 97 | 659 |
| 131 | 3 | 9384 ± 171 | 296 | 6 | 9299 ± 102 | 250 | 66 | 15 | 9156 ± 178 | 689 | 73 | 9014 ± 93 | 796 |
| 32 | 5 | 16416 ± 94 | 210 | 5 | 16416 ± 94 | 210 | 166 | 1 | 17795 ± 44 | — | 1 | 17795 ± 44 | — |
| 132 | 3 | 13499 ± 144 | 250 | 3 | 13499 ± 144 | 250 | 67 | 7 | 13876 ± 215 | 570 | 7 | 13876 ± 215 | 570 |
| 232 | 1 | 8926 ± 9 | — | 1 | 8926 ± 9 | — | 167 | 1 | 6086 ± 12 | — | 1 | 6086 ± 12 | — |
| 332 | 1 | 4758 ± 9 | — | 1 | 4758 ± 9 | — | 68 | 8 | 11514 ± 97 | 273 | 22 | 11547 ± 67 | 316 |
| 33 | 7 | 11652 ± 340 | 899 | 7 | 11652 ± 340 | 899 | 69 | 2 | 17344 ± 403 | 570 | 2 | 17344 ± 403 | 570 |
| 34 | 8 | 14498 ± 265 | 749 | 9 | 14488 ± 234 | 702 | 70 | 13 | 10320 ± 109 | 392 | 23 | 10396 ± 78 | 376 |
| 35 | 27 | 11834 ± 133 | 694 | 66 | 11866 ± 78 | 630 | 71 | 4 | 8465 ± 147 | 294 | 6 | 8442 ± 113 | 278 |
| 36 | 6 | 12861 ± 309 | 757 | 69 | 12732 ± 101 | 837 | 72 | 5 | 10311 ± 136 | 305 | 5 | 10311 ± 136 | 305 |
| 136 | 2 | 8764 ± 234 | 331 | 2 | 8764 ± 234 | 331 | 73 | 3 | 8121 ± 176 | 305 | 7 | 7935 ± 194 | 514 |
| 37 | 6 | 8888 ± 81 | 199 | 8 | 8866 ± 82 | 231 | 74 | 4 | 14965 ± 267 | 534 | 4 | 14965 ± 267 | 534 |
| 137 | 1 | 11399 ± 18 | — | 1 | 11399 ± 18 | — | 174 | 1 | 18187 ± 36 | — | 1 | 18187 ± 36 | — |
| 38 | 4 | 12788 ± 280 | 559 | 6 | 12695 ± 252 | 616 | 75 | 5 | 9784 ± 233 | 521 | 5 | 9784 ± 233 | 521 |
| 138 | 1 | 15405 ± 16 | — | 1 | 15405 ± 16 | — | 76 | 4 | 15365 ± 320 | 640 | 4 | 15365 ± 320 | 640 |
| 238 | 1 | 17845 ± 27 | — | 1 | 17845 ± 27 | — | 77 | 9 | 7639 ± 124 | 373 | 20 | 7728 ± 112 | 502 |
| 338 | 1 | 10873 ± 35 | — | 5 | 10438 ± 236 | 528 | 177 | 1 | 23926 ± 12 | — | 2 | 23992 ± 66 | 93 |
| 39 | 12 | 8882 ± 69 | 238 | 18 | 8832 ± 61 | 257 | 277 | 1 | 27282 ± 13 | — | 1 | 27282 ± 13 | — |
| 139 | 3 | 19044 ± 183 | 317 | 4 | 19076 ± 133 | 266 | 78 | 6 | 11504 ± 133 | 327 | 9 | 11571 ± 136 | 408 |
| 239 | 1 | 17438 ± 55 | — | 2 | 17443 ± 5 | 7 | 79 | 10 | 12692 ± 328 | 1036 | 40 | 12441 ± 149 | 944 |
| 339 | 1 | 15651 ± 30 | — | 1 | 15651 ± 30 | — | 80 | 24 | 12331 ± 133 | 649 | 48 | 12399 ± 107 | 740 |
| 40 | 3 | 11612 ± 217 | 376 | 4 | 11846 ± 280 | 560 | 180 | 1 | 27823 ± 8 | — | 1 | 27823 ± 8 | — |
| 140 | 2 | 9806 ± 160 | 226 | 2 | 9806 ± 160 | 226 | 82 | 12 | 9771 ± 238 | 824 | 43 | 9573 ± 113 | 741 |
| 240 | 1 | 17291 ± 26 | — | 1 | 17291 ± 26 | — | 83 | 9 | 12157 ± 253 | 759 | 23 | 12252 ± 156 | 748 |
| 340 | 1 | 28973 ± 28 | — | 1 | 28973 ± 28 | — | 84 | 5 | 8345 ± 224 | 500 | 24 | 7962 ± 90 | 442 |
| 41 | 5 | 8973 ± 135 | 303 | 7 | 8848 ± 127 | 335 | 90 | 29 | 6663 ± 172 | 924 | 435 | 6942 ± 50 | 1034 |
| 141 | 2 | 13685 ± 405 | 573 | 3 | 13794 ± 258 | 447 | | | | | | | |

The fully corrected measurements of each parameter from the individual spectra are given in Table 3; the final parameters for 706 galaxies, computed as the appropriately weighted means of the individual measurements, are listed in Table 5. The median estimated errors in the combined measurements (including measurement errors and run correction uncertainties) are $\Delta cz = 20\,\mathrm{km\,s^{-1}}$, $\Delta\sigma/\sigma = 9.1$ per cent (i.e. $\Delta \log \sigma = 0.040$ dex), $\Delta \mathrm{Mg}b/\mathrm{Mg}b = 7.2$ per cent (i.e. $\Delta \mathrm{Mg}b' = 0.013$ mag) and $\Delta \mathrm{Mg}_2 = 0.015$ mag. Comparisons with redshifts and dispersions from the literature show no systematic errors. The linestrengths required only small zero-point corrections to bring them on to the Lick system.

We have assigned galaxies to physical clusters (as opposed to apparent projected clusters) by examining the line-of-sight velocity distributions based on EFAR and ZCAT redshifts, together with the projected distributions on the sky. We derive mean redshifts for these physical clusters, which will be used in estimating distances and peculiar velocities, and also velocity dispersions, which will be used to test for trends in the galaxy population with cluster mass or local environment.

The results presented here comprise the largest single set of velocity dispersions and linestrengths for early-type galaxies published to date. These data will be used in combination with the sample selection criteria of Wegner et al. (1996, Paper I) and the photometric data of Saglia et al. (1997a, Paper III) to analyse the properties and peculiar motions of early-type galaxies in the two distant regions studied by the EFAR project.

## ACKNOWLEDGMENTS

We gratefully acknowledge all the observatories that supported this project: MMC, RKM, RLD and DB were Visiting Astronomers at Kitt Peak National Observatory, while GB, RLD and RKM were Visiting Astronomers at Cerro Tololo Inter-American Observatory – both observatories are operated by AURA, Inc., for the National Science Foundation; GW and DB used MDM Observatory, operated by the University of Michigan, Dartmouth College and the Massachusetts Institute of Technology; DB and RKM used the Multiple Mirror Telescope, jointly operated by the Smithsonian Astrophysical Observatory and Steward Observatory; RPS used facilities at Calar Alto (Centro Astrofísico Hispano Alemano) and La Silla (ESO); MMC observed at Siding Spring (MSSSO); MMC, RLD, RPS and GB used the telescopes of La Palma Observatory. We thank the many support staff at these observatories who assisted us with our observations. We thank S. Sakai for doing one observing run. We also thank the SMAC team for providing comparison data prior to publication, and Mike Hudson for helpful discussions. We gratefully acknowledge the financial support provided by various funding agencies: GW was supported by the SERC and Wadham College during a year's stay in Oxford, and by the Alexander von Humboldt-Stiftung during a visit to the Ruhr-Universität in Bochum; MMC acknowledges the support of a Lindemann Fellowship, DIST Collaborative Research Grants and an Australian Academy of Science/Royal Society Exchange Program Fellowship; RPS was supported by DFG grants SFB 318 and 375. This work was partially supported by NSF Grant AST90-16930 to DB, AST90-17048 and AST93-47714 to GW, and AST90-20864 to RKM. The entire collaboration benefited from NATO Collaborative Research Grant 900159 and from the hospitality and financial support of Dartmouth College, Oxford University, the University of Durham and Arizona State University. Support was also received from PPARC visitors' grants to Oxford and Durham Universities and a PPARC rolling grant, 'Extragalactic Astronomy and Cosmology in Durham 1994–98'. IRAF is distributed by the National Optical Astronomy Observatories, which is operated by the Association of Universities for Research in Astronomy, Inc., under contract with the National Science Foundation.

## REFERENCES

Baggley G., 1996, PhD thesis, University of Oxford
Beers T. C., Forman W., Huchra J. P., Jones C., Gebhardt K., 1991, AJ, 102, 1581
Burstein D., Faber S. M., Gaskell C. M., Krumm N., 1984, ApJ, 287, 586
Colless M. M., 1987, PhD thesis, University of Cambridge
Colless M. M., Dunn A. M., 1996, ApJ, 458, 435
Colless M. M., Burstein D., Wegner G., Saglia R. P., McMahan R., Davies R. L., Bertschinger E., Baggley G., 1993, MNRAS, 262, 475
Colless M. M., Burstein D., Davies R. L., McMahan R., Jr, Saglia R. P., Wegner G., 1999, MNRAS, 303, 813 (Paper V)
Davies R. L., Burstein D., Dressler A., Faber S. M., Lynden-Bell D., Terlevich R., Wegner G., 1987, ApJS, 64, 581
Dressler A., Shectman S. A., 1988, AJ, 95, 284
Faber S. M., Jackson R. E., 1976, ApJ, 204, 668
González J. J., 1993, PhD thesis, University of California
Gorgas J., Efstathiou G., Salamanca A. A., 1990, MNRAS, 245, 217
Guzmán R., 1993, PhD thesis, University of Durham
Huchra J., Geller M., Clemens C., Tokarz S., Michel A., 1992, Bull. CDS, 41, 31
Jørgensen I., 1997, MNRAS, 288, 161
Jørgensen I., Franx M., Kjærgaard P., 1995, MNRAS, 276, 1341
Lucey J. R., Guzmán R., Steel J., Carter D., 1997, MNRAS, 287, 899
McElroy D. B., 1995, ApJS, 100, 105
Malumuth E. M., Kriss G. A., Van Dyke Dixon W., Ferguson H. C., Ritchie C., 1992, AJ, 104, 495
Saglia R. P., Bertschinger E., Baggley G., Burstein D., Colless M. M., Davies R. L., McMahan R. K., Wegner G., 1993, MNRAS, 264, 961
Saglia R. P., Burstein D., Bertschinger E., Baggley G., Colless M. M., Davies R. L., McMahan R. K.., Wegner G., 1997a, MNRAS, 292, 499 (Paper III)
Saglia R. P., Bertschinger E., Baggley G., Burstein D., Colless M. M., Davies R. L., McMahan R. K., Wegner G., 1997b, ApJS, 109, 79 (Paper IV)
Smith R. J., Lucey J. R., Hudson M. J., Steel J., 1997, MNRAS, 291, 461
Tonry J. L., Davis M., 1979, AJ, 84, 1511
Trager S. C., Worthey G., Faber S. M., Burstein D., González J. J., 1998, ApJS, 116, 1
Tripicco M. J., Bell R. A., 1995, AJ, 110, 3035
Wegner G., Colless M. M., Baggley G., Davies R. L., Bertschinger E., Burstein D., McMahan R. K., Saglia R. P., 1996, ApJS, 106, 1 (Paper I)
Whitmore B. C., McElroy D. B., Tonry J. L., 1985, ApJS, 59, 1
Worthey G., 1993, PhD thesis, University of California
Worthey G., 1994, ApJS, 95, 107
Worthey G., Faber S. M., González J. J., Burstein D., 1994, ApJS, 94, 687
Zabludoff A. I., Geller M. J., Huchra J. P., Vogeley M. S., 1993, AJ, 106, 1273

## APPENDIX A: OBSERVING DETAILS

This appendix gives further details of the instrumental configurations used on different telescopes.

MDM 2.4-m: the Mark IIIa spectrograph, with a 1.87 arcsec wide slit, was used for all runs up to the end of 1988; from 1989 this was replaced by the Mark IIIb spectrograph, which is identical except that a 1.68-arcsec slit was used (except for run 113, when the slit width was 2.36 arcsec). For runs 101–103 a 600 line $\mathrm{mm^{-1}}$ grism blazed at 4600 Å was used; for all subsequent runs, a 600 line $\mathrm{mm^{-1}}$ grism blazed at 5700 Å was employed. The slit was usually oriented north–south. Two-pixel binning perpendicular to the dispersion direction was employed to lower the readout noise.

KPNO 4-m: the RC spectrograph and grating KPC-17B (527 line $mm^{-1}$) were used with the UV Fast Camera and the TI2 CCD.

KPNO 2.1-m: the Gold spectrograph/camera and grating #240 (500 line $mm^{-1}$) were used with the TI5 CCD.

WHT 4.2-m: the blue arm of the ISIS spectrograph was used with the CCD-IPCS imaging photon counting system. Most objects were observed using the R600B grating (600 line $mm^{-1}$), but one object (J26 A, GIN = 648) was observed with the R300B grating (300 line $mm^{-1}$).

INT 2.5-m: the Intermediate Dispersion Spectrograph (IDS) and R632V grating (632 line $mm^{-1}$) were used with the 235-mm camera for all runs.

SSO 2.3-m: both runs used the blue arm of the Double Beam Spectrograph (DBS) with a 600 line $mm^{-1}$ grating. Run 130 used the Photon Counting Array (PCA), while run 132 used a Loral CCD.

MMT Blue: the 'Big Blue' spectrograph was employed with a 300 line $mm^{-1}$ grating (blazed at 4800 Å in first order) and the Reticon detector. The MMT image stacker gave two 2.5-arcsec circular apertures separated by 36 arcsec.

MMT Red: the MMT Red Channel was used with a 600 line $mm^{-1}$ grating (blazed at 4800 Å) and the $800 \times 800$ TI CCD binned by two pixels perpendicular to the dispersion. The slit was $1.5 \times 180$ $arcsec^2$, but heavily vignetted in the outer 30 arcsec in one direction.

Calar Alto 2.2-m: the Cassegrain Boller & Chivens slit spectrograph with grating #7 (60 Å $mm^{-1}$) was used in combination with the TEK#6 CCD.

ESO 3.6-m: the MEFOS fibre feed and the Boller & Chivens spectrograph were used. MEFOS has 58 2.6 arcsec diameter fibres (29 for targets and 29 for sky) positioned within a 1°-diameter field at prime focus. The detector was a Tektronix TK512CB CCD (ESO#32).

CTIO 4-m: the ARGUS 24-object fibre spectrograph was used. ARGUS has a 50-arcmin field at the $f/2.8$ prime focus. Each of the 24 arms holds two 1.9 arcsec diameter fibres which lie 36 arcsec apart on the sky; one arm is positioned on the target and the other on sky. The fibres feed a thermally and mechanically isolated bench spectrograph with a 510 mm focal length Schmidt blue collimator and a 229 mm focal length Schmidt camera. A Reticon II $1200 \times 400$ CCD detector was used with grating KPGL #3.

This paper has been typeset from a TEX/LATEX file prepared by the author.